

1-1-2007

## Development of seat shock isolation systems

Erik Wolf

*University of Nevada, Las Vegas*

Follow this and additional works at: <https://digitalscholarship.unlv.edu/rtds>

---

### Repository Citation

Wolf, Erik, "Development of seat shock isolation systems" (2007). *UNLV Retrospective Theses & Dissertations*. 2780.

<http://dx.doi.org/10.25669/ap94-f6mj>

This Dissertation is protected by copyright and/or related rights. It has been brought to you by Digital Scholarship@UNLV with permission from the rights-holder(s). You are free to use this Dissertation in any way that is permitted by the copyright and related rights legislation that applies to your use. For other uses you need to obtain permission from the rights-holder(s) directly, unless additional rights are indicated by a Creative Commons license in the record and/or on the work itself.

This Dissertation has been accepted for inclusion in UNLV Retrospective Theses & Dissertations by an authorized administrator of Digital Scholarship@UNLV. For more information, please contact [digitalscholarship@unlv.edu](mailto:digitalscholarship@unlv.edu).

DEVELOPMENT OF SEAT SHOCK ISOLATION SYSTEMS

by

Erik Wolf

Bachelor of Science in Engineering  
University of Nevada, Las Vegas  
2000

Master of Science in Engineering  
University of Nevada, Las Vegas  
2004

A dissertation submitted in partial fulfillment  
of the requirements for the

**Doctor of Philosophy Degree in Mechanical Engineering**  
**Department of Mechanical Engineering**  
**Howard R. Hughes College of Engineering**

**Graduate College**  
**University of Nevada, Las Vegas**  
**December 2007**

UMI Number: 3302367

### INFORMATION TO USERS

The quality of this reproduction is dependent upon the quality of the copy submitted. Broken or indistinct print, colored or poor quality illustrations and photographs, print bleed-through, substandard margins, and improper alignment can adversely affect reproduction.

In the unlikely event that the author did not send a complete manuscript and there are missing pages, these will be noted. Also, if unauthorized copyright material had to be removed, a note will indicate the deletion.

**UMI**<sup>®</sup>

---

UMI Microform 3302367

Copyright 2008 by ProQuest LLC.

All rights reserved. This microform edition is protected against unauthorized copying under Title 17, United States Code.

ProQuest LLC  
789 E. Eisenhower Parkway  
PO Box 1346  
Ann Arbor, MI 48106-1346



**Dissertation Approval**  
The Graduate College  
University of Nevada, Las Vegas

November 16, 2007

The Dissertation prepared by

Erik J. Wolf

**Entitled**

Development of Seat Shock Isolation Systems

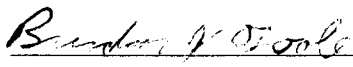
is approved in partial fulfillment of the requirements for the degree of

Doctor of Philosophy in Mechanical Engineering

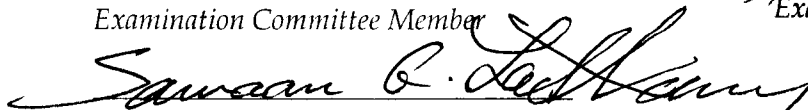
  
Examination Committee Chair

  
Dean of the Graduate College

  
Examination Committee Member

  
Examination Committee Member

  
Examination Committee Member

  
Graduate College Faculty Representative

## ABSTRACT

### **Development of Seat Shock Isolation Systems**

by

Erik J. Wolf

Dr. Douglas Reynolds, Examination Committee Chair  
Professor of Mechanical Engineering  
University of Nevada, Las Vegas

A numerical model has been created to predict the behavior of seat shock isolation systems exposed to mine blast loading. The model is a two dimensional, five degree-of-freedom, rigid body, mass-spring-damper approximation of the seat system and human occupant. The outputs of the model are the positions, velocities, and accelerations of the system masses, the forces of the connecting elements, such as the seat cushion force, the load limiter force, the spinal force, and the Dynamic Response Index (DRI) based on the pelvic z-axis acceleration. The model has been calibrated with drop tower test data collected by the Army Research Laboratory in Aberdeen, Maryland. The model and test results agree within 6% for z-axis acceleration, spine load, and DRI

Two conceptual seat shock isolation systems have been designed using the numerical model, and their components have been assembled and partially tested in the UNLV laboratory. Both designs use air-pneumatic seat cushion technology. For force limiting, one design uses coil rope spring isolators and the other uses an 8896-N (2000-lb<sub>f</sub>) honeycomb panel force limiter. Both designs are sized to fit in current U.S. military vehicle envelopes. The numerical model predicts the following performance indicators

when the seat designs are exposed to a peak acceleration input of 395 g's with a duration of 5 ms, which is typical of mine blast exposure levels. The following results were obtained: (a) design with honeycomb force limiter - peak z-axis pelvic acceleration was  $191 \text{ m/s}^2$ , spine load was 5344 N, and Dynamic Response Index was 13.1 and (b) design with cable rope spring - peak z-axis pelvic acceleration was  $179.2 \text{ m/s}^2$ , spine load was 5368 N, and Dynamic Response Index was 13.1. These levels are acceptable according to Army and NATO recommendations for the survivability of seated crewmembers exposed to a mine blast.

## TABLE OF CONTENTS

ABSTRACT .....	iii
LIST OF FIGURES .....	viii
LIST OF TABLES .....	xi
ACKNOWLEDGMENTS .....	xii
<b>CHAPTER 1 INTRODUCTION .....</b>	<b>1</b>
1.1 Characterization of Mine Blast Threat .....	2
1.2 Energy Absorbers .....	2
1.3 Seat Cushions .....	4
1.4 Air Bladder Concept.....	5
1.5 Mathematical Models .....	6
1.6 Seat System Configurations.....	7
<b>CHAPTER 2 INJURY ASSESSMENT .....</b>	<b>9</b>
2.1 Abbreviated Injury Scale.....	9
2.2 Foot, Ankle, Leg, and Knee Injury Criteria.....	11
2.3 Pelvis/Spinal Injury Criteria .....	13
2.4 Head Injury Criteria .....	17
2.5 Neck Injury Criteria .....	20
2.6 Chest Injury Criteria .....	21
2.7 Abdominal Injury Criteria .....	23
2.8 Mine Blast Injury Criteria .....	24
2.9 Testing and Evaluation Injury Criteria .....	25
<b>CHAPTER 3 MODELING .....</b>	<b>27</b>
3.1 Equations .....	28
3.1.1 Constraint Equations .....	28
3.1.2 Force Balance Equations .....	31
3.1.2.1 M <sub>1</sub> – Seat Pan .....	31
3.1.2.2 M <sub>2</sub> – Legs.....	31
3.1.2.3 M <sub>3</sub> – Pelvis.....	32
3.1.2.4 M <sub>4</sub> – Upper Torso .....	33
3.1.3 System Equations .....	33
3.2 Inputs .....	34
3.3 Force Limiters .....	34
3.3.1 Rope Springs .....	35

3.3.2 Honeycomb Isolators .....	36
3.4 Seat Cushion Model .....	39
3.5 Human Body Model .....	40
3.6 Restraint Forces .....	41
3.7 Solution Technique .....	42
3.7.1 Assumptions and Limitations .....	44
<b>CHAPTER 4 PNEUMATIC SEAT CUSHION DEVELOPMENT .....</b>	<b>45</b>
4.1 Seat Cushion Description .....	45
4.2 Seat Cushion Modeling .....	45
4.3 Seat Cushion Parameter Identification .....	50
4.3.1 Volume Testing .....	51
4.3.2 Force - Compression Testing .....	51
4.3.3 Damping Estimation .....	55
4.4 Seat Cushion Shock Performance .....	56
<b>CHAPTER 5 MODEL VALIDATION .....</b>	<b>62</b>
5.1 Model Comparisons .....	64
5.1.1 Damping Constants .....	71
<b>CHAPTER 6 MODEL RESULTS .....</b>	<b>73</b>
6.1 Forces and Accelerations .....	73
6.2 Displacements .....	79
6.3 Occupant Weight .....	84
<b>CHAPTER 7 SUMMARY OF RESULTS, CONCLUSIONS, AND RECOMMENDATIONS .....</b>	<b>86</b>
7.1 Numerical Model Validation .....	86
7.2 Numerical Model Results .....	87
7.3 General Conclusions.....	89
7.4 Recommended Seat Design.....	90
7.5 Ongoing Research.....	92
7.6 Recommendations .....	93
<b>BIBLIOGRAPHY .....</b>	<b>95</b>
<b>APPENDIX 1 FORCE LIMITER COMPARISON PLOTS.....</b>	<b>98</b>
<b>APPENDIX 2 POSITION COMPARISON PLOTS.....</b>	<b>105</b>
<b>APPENDIX 3 INPUT COMPARISON PLOTS .....</b>	<b>115</b>
<b>APPENDIX 4 OCCUPANT WEIGHT COMPARISON PLOTS.....</b>	<b>122</b>
<b>APPENDIX 5 DERVIATION OF DYNAMIC RESPONSE INDEX .....</b>	<b>127</b>

VITA.....	130
-----------	-----

## LIST OF FIGURES

Figure 1	Typical Injury Risk Curves .....	10
Figure 2	Shock Motion Terminology .....	12
Figure 3	Shock Input Tolerance Levels for a Standing Stiff-Legged Man .....	12
Figure 4	Shock Input Tolerance Levels for a Seated Man .....	13
Figure 5	DRI Mass-Spring-Damper System .....	14
Figure 6	Spinal Injury Rate as a Function of DRI for Aircraft Seat Ejection Events ....	16
Figure 7	Duration and Magnitude of Vertical Acceleration (Eiband).....	18
Figure 8	Average Acceleration and Corresponding HIC Times for Cadaver Head Impacts and Human Volunteer Interactions with an Air Bag .....	19
Figure 9	AIS Injury Rating Versus Normalized Chest Deflection.....	22
Figure 10	Comparison of AIS $\geq 4$ Probability for Left- and Right-Side Impacts .....	23
Figure 11	Recommended Injury Criteria for Landmine Testing by the U.S. Army.....	25
Figure 12	Model Schematic.....	28
Figure 13	Free Body Diagram .....	29
Figure 14	Wire Rope Spring Force-Deflection Characteristics.....	36
Figure 15	Honeycomb Panel Force-Deflection Characteristics .....	38
Figure 16	Drawing of Inflatable, Low-Density, Open-Cell Foam Shock Attenuating Seat Core.....	46
Figure 17	Foam Compression Test Results .....	52
Figure 18	Air Bladder Pressure Test Results.....	53
Figure 19	Foam - Air System Test Results.....	53
Figure 20	Air Cushion Force Comparison .....	54
Figure 21	Thor III Hybrid Anthropomorphic Dummy Positioned on an Air Cushion....	56
Figure 22	Platform Accelerations .....	52
Figure 23	Platform Velocities.....	52
Figure 24	Platform Positions .....	53
Figure 25	Measured Pelvis x-Axis Acceleration for 30-in. and 50-in Drops .....	59
Figure 26	Measured Pelvis z-Axis Acceleration for 30-in. and 50-in Drops .....	60
Figure 27	Measured z-Axis Spine Load for 30-in. and 50-in. Drops .....	60
Figure 28	Calculated z-Axis DRI Values for 30-in. and 50-in. Drops .....	61
Figure 29	Model Comparison of x-axis Pelvis Acceleration, 30 in. drop .....	66
Figure 30	Model Comparison of z-axis Pelvis Acceleration, 30 in. drop .....	67
Figure 31	Model Comparison of Spine Load, 30 in. drop.....	67
Figure 32	Model Comparison of DRI, 30 in. drop .....	68
Figure 33	Model Comparison of x-axis Pelvis Acceleration, 50 in. drop .....	69
Figure 34	Model Comparison of z-axis Pelvis Acceleration, 50 in. drop .....	70
Figure 35	Model Comparison of Spine Load, 50 in. drop.....	70
Figure 36	Model Comparison of DRI, 50 in. drop .....	71

Figure 37	50 inch drop force limiter comparison, Pelvis x-axis acceleration .....	75
Figure 38	50 inch drop force limiter comparison, Pelvis z-axis acceleration .....	75
Figure 39	50 inch drop force limiter comparison, Spine Load.....	76
Figure 40	50 inch drop force limiter comparison, DRI.....	76
Figure 41	Pelvis Acceleration, z-axis, Bladder + Honeycomb Force Limiter .....	78
Figure 42	Pelvis Acceleration, z-axis, Bladder + Spring .....	79
Figure 43	50 inch drop, Pelvis Position x-Axis.....	81
Figure 44	50 inch drop, Pelvis Position z-Axis.....	81
Figure 45	50 inch drop, Pelvis Position $\theta$ -Axis.....	82
Figure 46	50 inch drop, Bladder Compression.....	82
Figure 47	50 inch drop, Spring Compression.....	83
Figure 48	50 inch drop, Honeycomb Compression.....	83
Figure 49	Prototype Seat Design with Coil Rope Springs .....	91
Figure 50	Prototype Seat Design with Honeycomb Panel Force Limiters.....	92
Figure A1-1	30 Inch Drop, X-axis Pelvic Acceleration .....	99
Figure A1-2	30 Inch Drop, Z-axis Pelvic Acceleration .....	99
Figure A1-3	30 Inch Drop, Spine Load .....	100
Figure A1-4	30 Inch Drop, DRI .....	100
Figure A1-5	40 Inch Drop, X-axis Pelvic Acceleration .....	101
Figure A1-6	40 Inch Drop, Z-axis Pelvic Acceleration .....	101
Figure A1-7	40 Inch Drop, Spine Load .....	102
Figure A1-8	40 Inch Drop, DRI .....	102
Figure A1-9	50 Inch Drop, X-axis Pelvic Acceleration .....	103
Figure A1-10	50 Inch Drop, Z-axis Pelvic Acceleration .....	103
Figure A1-11	50 Inch Drop, Spine Load .....	104
Figure A1-12	50 Inch Drop, DRI .....	104
Figure A2-1	30 Inch Drop, Pelvic X-axis Position .....	106
Figure A2-2	30 Inch Drop, Pelvic Z-axis Position .....	106
Figure A2-3	30 Inch Drop, Pelvic $\theta$ -axis Position .....	107
Figure A2-4	30 Inch Drop, Bladder Compression .....	107
Figure A2-5	30 Inch Drop, Spring Compression .....	108
Figure A2-6	30 Inch Drop, Honeycomb Compression .....	108
Figure A2-7	40 Inch Drop, Pelvic X-axis Position .....	109
Figure A2-8	40 Inch Drop, Pelvic Z-axis Position .....	109
Figure A2-9	40 Inch Drop, Pelvic $\theta$ -axis Position .....	110
Figure A2-10	40 Inch Drop, Bladder Compression .....	110
Figure A2-11	40 Inch Drop, Spring Compression .....	111
Figure A2-12	40 Inch Drop, Honeycomb Compression .....	111
Figure A2-13	50 Inch Drop, Pelvic X-axis Position .....	112
Figure A2-14	50 Inch Drop, Pelvic Z-axis Position .....	112
Figure A2-15	50 Inch Drop, Pelvic $\theta$ -axis Position .....	113
Figure A2-16	50 Inch Drop, Bladder Compression .....	113
Figure A2-17	50 Inch Drop, Spring Compression .....	114
Figure A2-18	50 Inch Drop, Honeycomb Compression .....	114
Figure A3-1	Pelvis X-axis Acceleration, Bladder Only .....	116
Figure A3-2	Pelvis Z-axis Acceleration, Bladder Only .....	116

Figure A3-3	Spine Load, Bladder Only .....	117
Figure A3-4	Dynamic Response Index, Bladder Only .....	117
Figure A3-5	Pelvis X-axis Acceleration, Bladder + Rope Spring .....	118
Figure A3-6	Pelvis Z-axis Acceleration, Bladder + Rope Spring .....	118
Figure A3-7	Spine Load, Bladder + Rope Spring .....	119
Figure A3-8	Dynamic Response Index, Bladder + Rope Spring .....	119
Figure A3-9	Pelvis X-axis Acceleration, Bladder + Honeycomb Isolator .....	120
Figure A3-10	Pelvis Z-axis Acceleration, Bladder + Honeycomb Isolator .....	120
Figure A3-11	Spine Load, Bladder + Honeycomb Isolator .....	121
Figure A3-12	Dynamic Response Index, Bladder + Honeycomb Isolator .....	121
Figure A4-1	Pelvis X-axis Acceleration, 80% Occupant Weight .....	123
Figure A4-2	Pelvis Z-axis Acceleration, 80% Occupant Weight.....	123
Figure A4-3	Spine Load, 80% Occupant Weight.....	124
Figure A4-4	Dynamic Response Index, 120% Occupant Weight.....	124
Figure A4-5	Pelvis X-axis Acceleration, 120% Occupant Weight .....	125
Figure A4-6	Pelvis Z-axis Acceleration, 120% Occupant Weight.....	125
Figure A4-7	Spine Load, 120% Occupant Weight.....	126
Figure A4-8	Dynamic Response Index, 120% Occupant Weight.....	126

## LIST OF TABLES

Table 1	Abbreviated Injury Scale Codes .....	8
Table 2	Lumbar Spine Tolerance Levels Recommended by the U.S. Army .....	14
Table 3	Landmine Injury Criteria Proposed by Axelsson .....	22
Table 4	Landmine Injury Criteria Proposed by Alem et. al. ....	22
Table 5	Model Mass Description.....	27
Table 6	Human Body Model Parameters .....	41
Table 7	Seat Belt Spring Constants .....	42
Table 8	Seat Cushion Inflated Volumes .....	51
Table 9	Air Cushion Test Results.....	57
Table 10	Drop Tower Testing Initial Conditions .....	62
Table 11	Seat Cushion Constants .....	63
Table 12	Human Body Geometry.....	64
Table 13	0.762m (30 in) Drop Model Validation Results .....	66
Table 14	1.27m (50 in) Drop Model Validation Results .....	68
Table 15	Seat Cushion Bottom Damping Constants .....	72
Table 16	Seat Cushion Back Damping Constants .....	72
Table 17	30 inch Drop Model Predictions.....	74
Table 18	40 inch Drop Model Predictions.....	74
Table 19	50 inch Drop Model Predictions.....	74
Table 20	50 inch Drop Model Predictions, 80% Occupant Weight .....	85
Table 21	50 inch Drop Model Predictions, 120% Occupant Weight .....	85
Table 22	Model Predictions for Recommended Seat Designs .....	91

## ACKNOWLEDGMENTS

I would like to thank the members of my committee and the rest of the shock seat project team for assisting me with the completion of this project. I would especially like to thank Dr. B.J Landsberger for spending a great deal of time instructing me in the mysterious ways of product design and for helping me develop the computer model.

I must also express my sincere appreciation for Dr. Douglas Reynolds, who has been my advisor for eight years and three college degrees. He has been a true mentor for me, both professionally and personally, has been instrumental in shaping my life. While I am looking forward to the next steps in my career away from the university, I will miss his expert council.

My co-workers at UNLV have given a lot to me and to this project, but none more than Mr. Trevor Wilcox. He and I have bounced ideas off each other daily and gotten our hands dirty in the machine shop on many occasions. Trevor is an top notch engineer and an even better friend.

Lastly, I would like to mention my wife Amanda, who has cheered me on and supported me through many late nights. Anyone who has pursued a doctoral degree will understand the commitment and hard work their family dedicates to the effort. Amanda and I have been through many trials, but her love and support have never faltered. Thank you sweetheart, we made it.

## CHAPTER 1

### INTRODUCTION

Military ground vehicles operating in hostile environments are subjected to a wide variety of threats. Prominently featured among these dangers is the use of explosive devices to injure personnel and disrupt convoys. Anti-vehicle landmines, which are inexpensive to manufacture, can be easily concealed and detonated in a wide variety of ways and are a common form of explosives employed by the enemy. Even though vehicle armoring techniques have proven effective in reducing the penetration of shrapnel into the vehicle interior [1], the acceleration/shock energy that is associated with a mine blast is still transmitted through the vehicle structure to the vehicle occupants. This transmitted energy can cause potentially lethal injuries. Often, vertebrae in the spine or other bones in the lower extremities are fractured [2]. Soft tissues, such as the aortal artery, bladder, and spleen, may also be torn or ruptured. Head, brain, and neck injuries are also common. Additionally, a land mine strike that prevents a soldier from continuing the fight can be just as life threatening as one that kills outright. In order to provide total protection from a land mine event, a method is required to reduce the acceleration/shock energy transmitted to the vehicle operators through the seat.

This study will address modeling techniques, system component characterization, and test methodology used to develop a seat system capable of protecting an occupant from land-mine scale accelerations input at the vehicle floor.

## 1.1 Characterization of the Mine Blast Threat

The energy transmitted to the vehicle from a mine blast can vary widely in magnitude and duration. It is a function of many factors [3], such as the amount of explosive charge, type of soil, depth of burial of the mine, location of the mine relative to the vehicle, and vehicle properties (mass, material properties, undercarriage geometry). Although mines may be oriented in any spatial axis, in practice most mines are directed upwards from beneath the vehicle. Additionally, while the resulting pressure wave is hemispherical, the largest portion of blast energy exists predominately in the vertical (z-axis) direction. The standard method for quantifying the level of the transmitted force that is harmful to the vehicle occupant is to measure the acceleration of the vehicle cabin floor. Information provided to the research team by the Army Research Laboratory identified acceleration pulses ranging from  $2000 \text{ m/s}^2$  to over  $4000 \text{ m/s}^2$  in magnitude, roughly triangular in shape, and of a period ranging from 5ms to 10ms as typical of mine blast loading on a vehicle floor. Despite these extreme levels, published research indicates that it may be possible to devise a vehicle seat that could significantly increase the level of survivability from a land mine event.

## 1.2 Energy Absorbers

The design of seats systems for the mitigation of shock energy began with fixed wing and rotary aircraft. These seats were made to protect pilots and passengers in the event of a crash. The methods used to reduce the transmitted shock are varied, but a common feature to all is an energy absorbing (EA) device. An EA device can be a separate component or may be a part of the seat structure, and its purpose is to dissipate energy via

plastic deformation. This deformation requires some motion of the seat relative to the vehicle interior. The distance through which the seat must move is termed the “stroke length”. Each seat design then becomes a trade-off between the level of transmitted energy and the position of the seat occupant inside the vehicle. A US Army Aviation Systems Command report [4] gives examples of several different types of EA devices. This list includes wires or straps bending around dies, tubes that crush, invert, or fold on themselves, a rolling torus, metal rods or cables in tension, and a pulley system that deforms its housing.

Some seat designs have made use of direct deformation of the seat structures as opposed to external devices. This is the case with the V-22 Osprey [5]. The troop seats in the main cabin are connected to the walls with deformable brackets. The FAA and NASA developed a similar system for aircraft passenger seats in the early eighties [6] which used composite tubes to replace some the seat understructure.

The amount of energy attenuation provided by EA devices can sometimes be adjusted to the weight of the seat occupant. This is usually performed prior to installation in the case of a Fixed Load Energy Absorber (FLEA) or as an adjustment made by the seat occupant when entering the vehicle in the case of Variable Load Energy Absorbers (VLEA). Labun and Rapaport [7] have created a system that performs this function automatically, termed a “third generation” energy absorber for helicopter crash seats, which they call an ASAVLEA (Acceleration-Sensing Automatic VLEA). They also recommend using a Variable Profile Energy Absorber (VPEA) with a “notched” profile of load vs. stroke in order to reduce dynamic overshoot and obtain the required attenuation while reducing the overall stroking distance. Richards and Podob [8] in

subsequent work evaluated a working seat system with a VPEA, achieving promising results.

A different approach to these passive EA devices is attempting to actively control the motion. One example is the Volvo Safety Ride Down system for passenger cars [9]. The system basically consists of electronically controlled hydraulic dampers. Volvo states that these shock absorbers can be adjusted every two milliseconds to provide optimum shock performance. While this type of technology has not been applied to the extreme case of mine blast loading, it may be possible in the future. The limiting factor with regards to landmines is the speed of the event, approximately 5 ms for the initial blast. No currently marketed systems were found that had response times capable of dealing with a landmine blast.

### 1.3 Seat Cushions

Many EA seat systems are a collection of components that provide an overall level of protection. While the bulk of the energy dissipation is usually attributed to an EA device, such as those previously discussed, it is also important to consider the role of the seat cushion. The seat cushion is a required part of the seat system, if for no other reason than to provide some level of comfort for the occupant. Given this fact, it would be beneficial if the cushion could add to the total energy absorbing mechanism. In the past, seat cushions have been treated as a necessary evil in terms of shock acceleration. Research on aircraft seat ejection systems demonstrated that a seat with a foam-filled cushion often performed poorer than when no foam-filled seat cushion was used [10]. The foam-filled cushions used in these tests normally contained high-density foams, which were

necessary to support the weight of the seat occupant. These seat cushions were stiff and had limited compressibility before they became solid, allowing high acceleration levels to reach the seat occupant. In some cases, the seat cushion generated an amplification of the acceleration measured at the seat occupant interface. This was due to the buildup of input energy during the time it took to compress the cushion before solid impact with the occupant.

In spite of these initial, discouraging results, some research indicates that a different type of seat cushion could be effective in the reduction of acceleration levels. In 2001, Naasz [11] presented a paper in which a lumped parameter model of an EA seat and occupant was developed. Here, the seat cushion was treated as an additional mass-spring-damper between the seat pan and occupant pelvis. An experiment was conducted with six different typical aircraft seat cushions (fabric over foam) in a drop cage test facility to show the impact of the cushion on lumbar loads. The results showed that seat cushions can reduce these loads, but usually at the expense of stroking distance. Other seat cushion material designs, such as the air-pneumatic cushion discussed later in the document, can effectively utilize the stroke length inherent to the seat cushion and may greatly reduce the level of the transmitted acceleration as well as lumbar loads.

#### 1.4 Air Bladder Concept

A new seat cushion concept is being investigated at UNLV that uses an encapsulated air bladder with low density foam. This cushion has a bottom and a back section. A few of the possible advantages to using this type of seat cushion are:

- The cushion thickness adds stroke length for acceleration reduction.

- The flexible air bladder will create an even force distribution on occupant.
- Air cushions have the physical properties of low initial stiffness and high final stiffness under compression, similar to an energy absorbing device.
- The air cushion proposed has a bottom and back section, providing protection in the front to back and vertical directions.
- The force transmitted to the occupant by an air cushion is rate dependant on the input acceleration at the seat pan, due to damping caused by internal air movement from the bottom to the back section of the cushion.
- The air cushion will have limited spring back.
- The air cushion may also have enhanced ride-comfort when exposed to rough road conditions over a traditional foam cushion.

### 1.5 Mathematical Models

Several mathematical models have been developed to simulate the response of seat systems to shock inputs. While many complex, finite element models have been created for seat systems and human occupants, it is often practical to use more simple methods to approximate the seat-human body interaction. The analytical models most prominent in the literature are single-axis rigid-body models that use springs and dampers to approximate seat system components. Many models have been used in connection with off-road vehicles. One example of a rigid body model for seat systems was created by Choy and Wereley [12]. This model was used to predict the response of a seat system with magnetorheological damper for off-road vehicles. A unique feature of this model was a separate mass-spring-damper connected to the upper torso to model the human

viscera. Another model that was developed by Naasz [11] for helicopter seats is a five-component, single-axis, mass- spring- damper system. The seat cushion is represented by a mass with a linear spring and damper connected to the seat pan. An additional spring and damper used to model the occupant buttocks is attached to the top of the seat cushion mass.

The rigid body models available in the literature are restrained to single-axis vertical motion. Input energy from road vibration or land mine events is assumed to be mostly present in the vertical direction; therefore, the reduction of acceleration in the vertical direction has been the target for current seat system designs. While this may be generally true, angular deflections of the body in the seat can lead to energy being transferred into the horizontal (eyes-forward) direction. This can result in significant errors in the prediction of the vertical axis acceleration values.

Finite element models are available to create full, three-dimensional seat system models. These models often require the use of very expensive commercial software. They are often cumbersome to modify, calculation intensive, and require very long run times to achieve a system response for a time interval of only a few milliseconds.

## 1.6 Seat System Configurations

A two-dimensional rigid-body model developed during this project that simulates a seat shock isolation system with a human occupant is presented in Chapter 3. Three configurations of the seat shock isolation system using the air bladder concept were investigated:

- Seat shock isolation system with only a seat cushion air bladder present in the seat pan;
- Seat shock isolation system with a seat cushion air bladder present in the seat pan and cable rope springs used to support the seat pan; and
- Seat shock isolation system with a seat cushion air bladder present in the seat pan and a traditional force limiter installed beneath the seat pan.

Cable rope springs were selected because they will result in minimum “spring-back” after they have been fully compressed. Aluminum honeycomb panels were selected for the load limiter because they result in a simple load limiter configuration. They can also be used to validate the effectiveness of a load limiter. Honeycomb panels have well documented force–deflection curves that are relatively flat over 80-90% of the thickness of the panel.

## CHAPTER 2

### INJURY ASSESSMENT

Before any mine blast attenuating seat system can be designed, vehicle occupant injury criteria must be specified. Injury criteria define numerical relationships between measurable engineering parameters that define specified loads to various parts of the human body and the potential for injuries these loads may cause [2]. These criteria are necessary to specify acceptable shock levels that the body can experience without causing serious injuries. These acceptable shock levels then become the design goals for the seat system. Injury criteria that will be covered in this section include the following body areas: (1) foot, ankle, and leg; (2) pelvis and spinal column; (3) head and neck; and (4) chest and abdomen. Even though the mine blast attenuating seat system that will be recommended by this study will be designed to only reduce the potential for vertical compressive spine injuries, the other potential injury modes are presented to give a fairly complete overview of the different injury modes that vehicle occupants can experience when exposed to a mine blast.

#### 2.1 Abbreviated Injury Scale

When assessing injury potential, the threshold limit defines the cutoff number that exposure must be below for a particular injury metric. It is also useful to know how the

potential for injury approaches the upper limit and how severe the injury might be. Often, a risk curve is generated for medical data to quantify the risk potential and severity of an injury below the threshold value. Figure 1 gives examples of typical risk curves that can be applied to spinal injury. The particular curve selected corresponds to an injury severity coding, which is given in Table 1. Several of the injury metrics presented in the following sections refer to the AIS scale when describing the severity of potential injury when the threshold limit is reached.

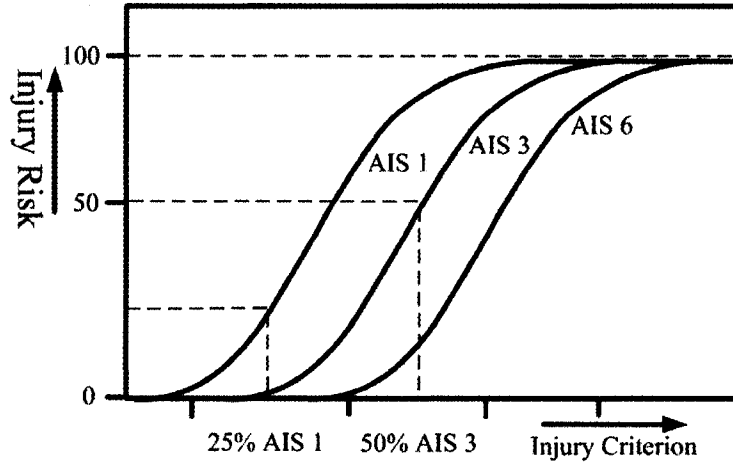


**Figure 1** Typical Injury Risk Curves

**Table 1** Abbreviated Injury Scale Codes

<b>AIS Code</b>	<b>Injury Description</b>
1	Minor
2	Moderate
3	Serious
4	Severe
5	Critical
6	Maximum (currently treatable)
9	Unknown

## 2.2 Foot, Ankle, Leg, and Knee Injury Criteria

A study completed by Hirsch [13] and also reported by Axelsson et. al. [14] indicates that, for shock pulses similar to the one shown in Figure 2 that have a duration of less than 10 ms, the tolerance limit for the potential onset of foot/ankle/leg injuries for a stiff-legged standing man is a peak velocity change ( $V_{\max}$  in Figure 2) of 10 ft/s (3 m/s) for the structure supporting the foot. Figure 3 shows the tolerance levels presented by Hirsch and Axelsson et. al. for a stiff-legged standing man to shock motion directed into the foot /ankle. When the shock pulse duration is greater than 10 ms the tolerance limit increases to a maximum peak velocity change of 40 ft/s (12 m/s). This typically corresponds to an average acceleration (Figure 2) of 10 g's (98 m/s<sup>2</sup>). Figure 3 indicates that foot/ankle/leg fractures can occur when the foot/ankle tolerance limit is exceeded. A report prepared for the army by Coltman et. al. [2] recommended that a peak shock force of 1,700 lb<sub>f</sub> (7562 N) to the foot/ankle is a realistic criterion for the onset of foot/ankle/leg injuries. This report also refers to the Federal Motor Vehicle Safety Standard 208 which specifies a maximum shock load of 2,250 lb<sub>f</sub> (10008 N).

A criterion was presented to the US Army by Coltman et. al. to specify the permissible peak force to the knee from a shock load. The following equations are the femur injury criterion (FIC) that defines the permissible peak knee load to a shock input to the knee:

$$\begin{aligned} F(\text{kN}) &= 23.14 - 0.71 * T(\text{ms}) && \text{for } T < 20\text{ms} \\ F(\text{kN}) &= 9.90 && \text{for } T > 20\text{ms}. \end{aligned} \tag{1}$$

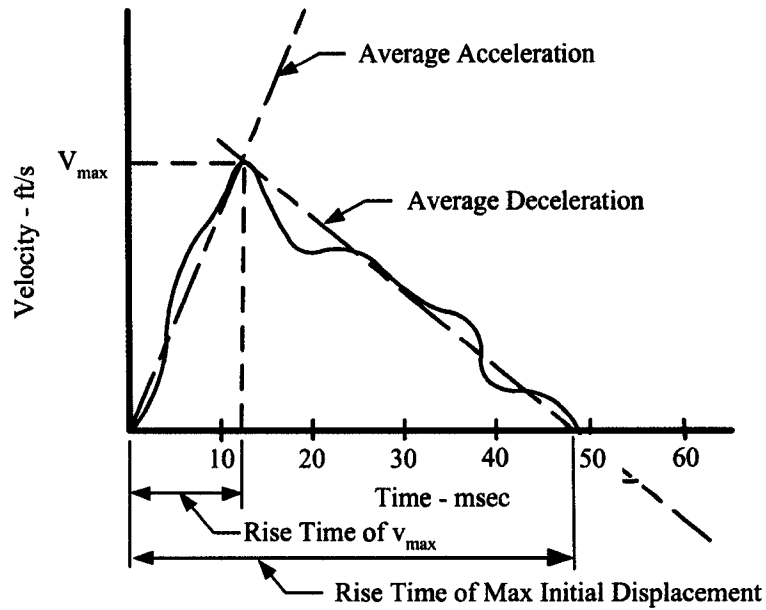


Figure 2 Shock Motion Terminology for Figures 3 and 4 [13], 1964

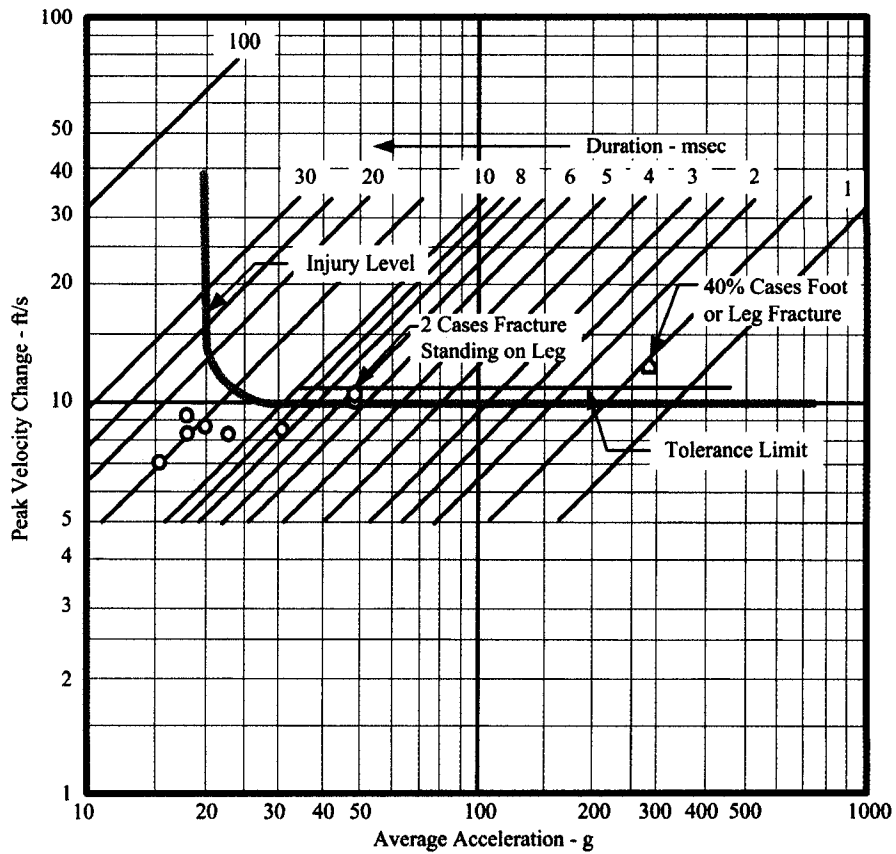


Figure 3 Shock Input Tolerance Levels for a Standing Stiff-Legged Man [13], 1964

### 2.3 Pelvis/Spinal Injury Criteria

A study completed by Hirsch [13] and also reported by Axelsson [14] et. al. indicates that, for shock pulses similar to the one shown in Figure 2 that have a duration of less than 20 ms, the tolerance limit for the potential onset of pelvis/spine injuries for a man sitting in an upright position is a peak velocity change ( $V_{max}$  in Figure 2) of 20 ft/s (4.5 m/s) for the seat structure supporting the pelvis. When the shock pulse duration is greater than 20 ms the tolerance limit increases to a maximum peak velocity change of 60 ft/s (18.3 m/s). This typically corresponds to an average acceleration (Figure 4) of 15 g's (147 m/s<sup>2</sup>). Figure 4 indicates that spinal injuries can occur when the pelvis/spine tolerance limit is exceeded.

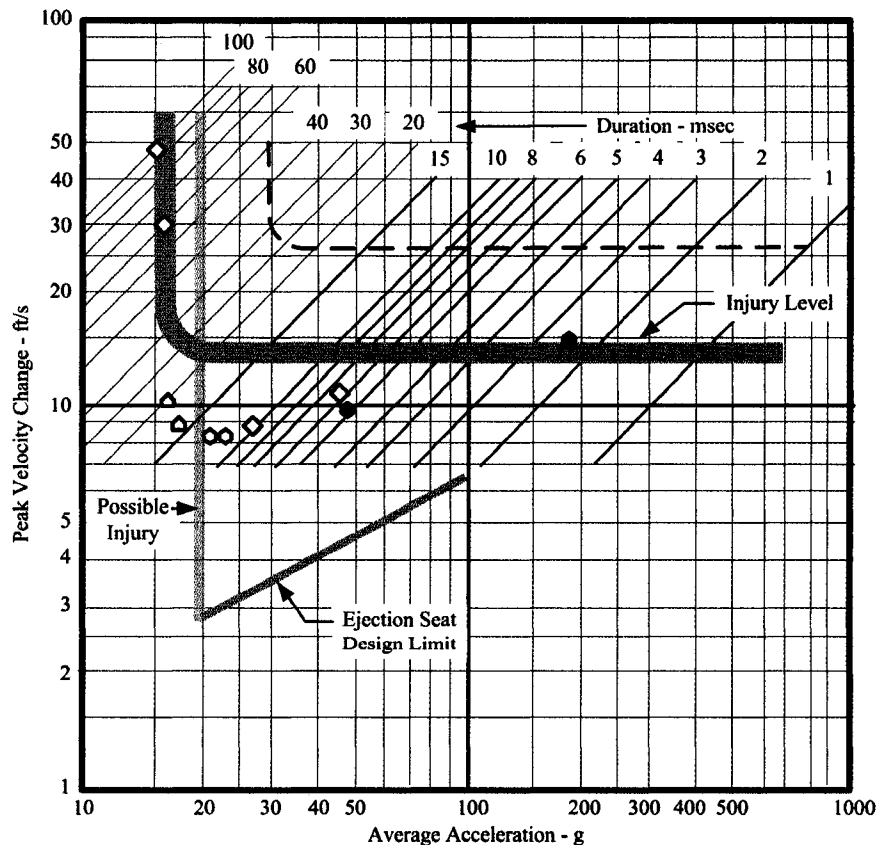


Figure 4 Shock Input Tolerance Levels for a Seated Man [13], 1964

The Dynamic Response Index (DRI) was developed to predict the probability of thoracolumbar-spine fracture injury during ejection seat use [13, 14, 15]. The DRI uses a simple mass-spring-damper system (Figure 5) with base excitation to predict the response of an aircrew member subjected to abrupt vertical acceleration during seat ejection. The equation of motion is given by Equation 2:

$$\frac{d^2 \ddot{\alpha}(t)}{dt^2} + 2\zeta\omega_n \frac{d\ddot{\alpha}(t)}{dt} + \omega_n^2 \ddot{\alpha}(t) = \ddot{n}(t) \quad (2)$$

where:

- $\ddot{\alpha}(t)$  = deflection of the seat system (in., m)
- $\zeta$  = damping ratio (dimensionless)
- $\omega_n$  = resonance frequency (rad/s)
- $\ddot{n}(t)$  = acceleration of seat supporting the pelvis (in./s<sup>2</sup>, m/s<sup>2</sup>).

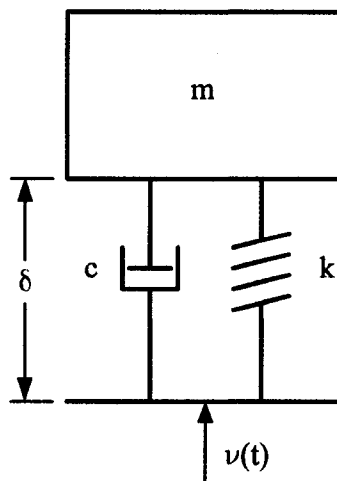


**Figure 5** DRI Mass-Spring-Damper System

A derivation of Equation (2) is presented in Appendix 5. DRI is representative of the maximum dynamic compression of the vertebral column. The DRI model assesses the response of the human body to transient acceleration-time profiles. The equation for computing the DRI is:

$$\text{DRI} = \frac{w_n^2 \delta_{\max}}{g} \quad (3)$$

where:

$\delta_{\max}$  = maximum deflection of the seat system (in., m).

The DRI value is obtained by solving equation (2) for a known seat acceleration signal,  $a(t)$ , for the case where  $w_n$  equals 52.9 rad/s (8.4 Hz),  $\phi$  equals 0.224, and  $g$  is the acceleration of gravity (386 in./s<sup>2</sup>, 9.8 m/s<sup>2</sup>). The solution to equation (2) gives  $\delta_{\max}$  (in., m), the maximum displacement of the system. This is used in equation (3) to determine the DRI value. Figure 6 shows a plot of the spinal injury rate (%) as a function of DRI [13, 18]. A DRI value equal to 16 corresponds to a 1% risk of a detectable fracture to the spine based on operational experiences.

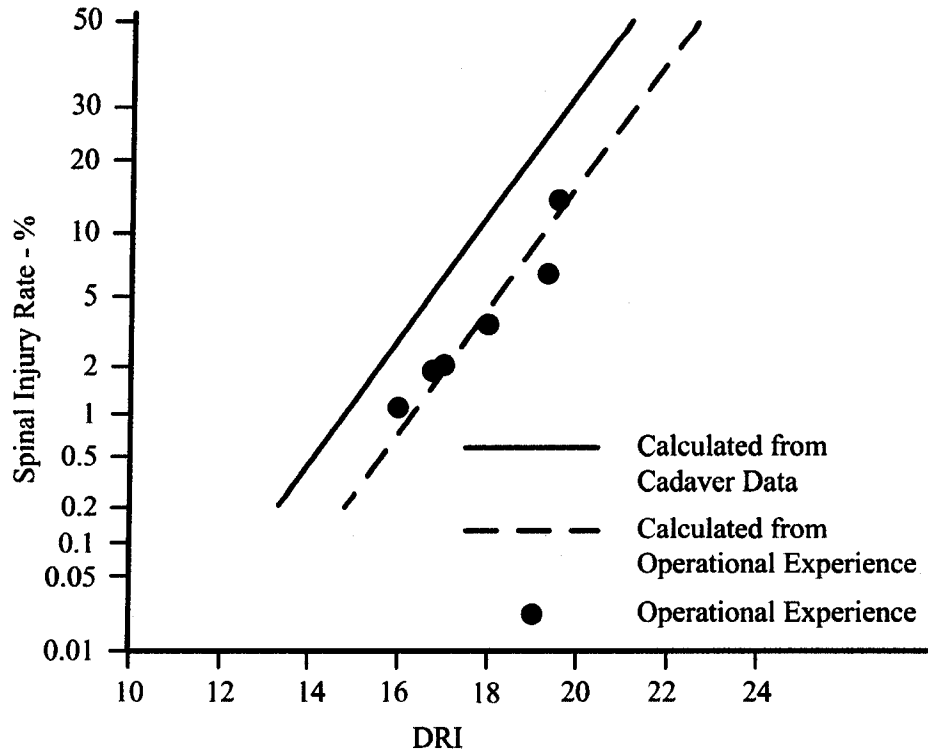


**Figure 6** Spinal Injury Rate as a Function of DRI for Aircraft Seat Ejection Events [18], 2000

Federal Aviation Regulation 29 requires the axial compression force measured between the pelvis and lumbar spine not to exceed 1,500 lb (6,672 N) to be considered safe [18]. Table 2 lists the lumbar spine tolerance levels recommended by the US Army.

**Table 2** Lumbar Spine Tolerance Levels Recommended by the U.S. Army

Vehicle Occupant Size (Percentile)	Lumbar Load Tolerance (lb)
5 <sup>th</sup> Female	1,281
50 <sup>th</sup> Female	1,610
50 <sup>th</sup> Male	2,065
95 <sup>th</sup> Male	2,534

The Eiband criterion is used to predict the potential for whole body injuries associated with exposure to whole body shock events [16, 17, 18]. The information shown in Figure 3, for a standing stiff legged man, is based on both animal and human experiments by the National Aeronautic and Space Administration. The figure is most reliable for predicting injury potential for long-term shock events. Figure 7 (see next page) suggests that the vertical peak acceleration for short-term shock inputs to the pelvis should not exceed 15 g's.

Another report prepared by the US Army [19] indicates that forward (longitudinal) pelvic acceleration exceeding 40 g's ( $392 \text{ m/s}^2$ ) for more than 7 ms or lateral (transverse) or upward (vertical) pelvic accelerations exceeding 23 g's ( $225 \text{ m/s}^2$ ) for more than 7 ms are considered to cause immediate and complete incapacitation for military tasks. Lumber spine bending moments in excess of 10,932 in.-lb<sub>f</sub> (1235 N-m) in forward flexion, 3,276 in.-lb<sub>f</sub> (370 N-m) in rearward extension, and 5,976 in.-lb<sub>f</sub> (675 N-m) in lateral bending, regardless of duration, are predicted to cause immediate and complete incapacitation for military tasks.

#### 2.4 Head Injury Criteria

Head injury assessment is based on head accelerations [18]. Peak levels which exceed 150 g's ( $1,471 \text{ m/s}^2$ ) for more than 2 ms are expected to cause a concussion with immediate and complete incapacitation for military tasks. The Head Injury Criterion (HIC) is used to assess the potential for head injuries associated with exposure to sudden shocks. The HIC is calculated by Equation (4).

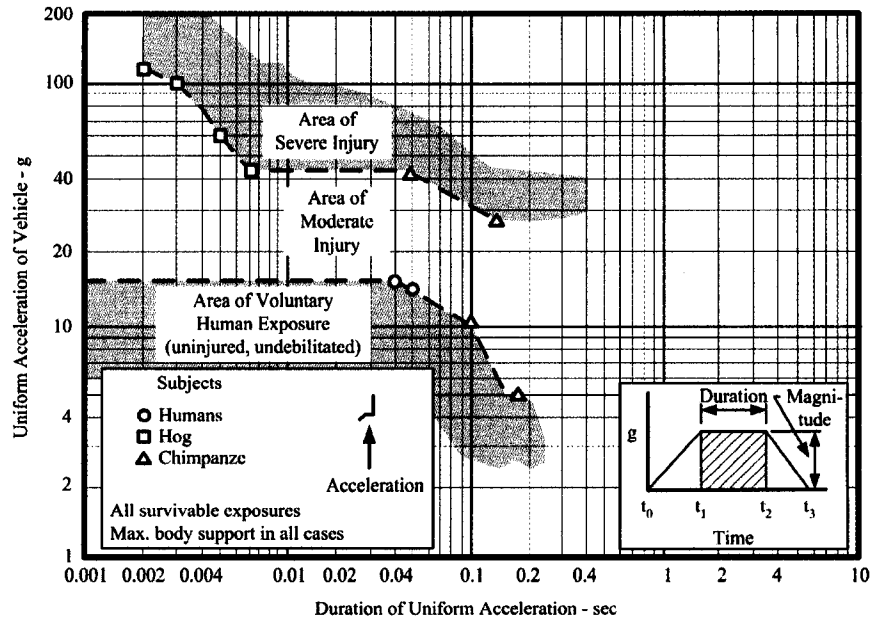


**Figure 7** Duration and Magnitude of Vertical Acceleration (Eiband) [18], 2000

$$HIC = (t_2 - t_1) \frac{1}{t_2 - t_1} \int_{t_1}^{t_2} a(t) dt \quad (4)$$

where:

$t_1, t_2$  = the initial and final times during which HIC attains a maximum value

$a(t)$  = the resultant acceleration measured at the head's center of gravity [18].

FMVSS 208 sets a maximum allowable HIC value of 1,000 [2]. It also specifies that the time interval between  $t_1$  and  $t_2$  shall not exceed 36 ms. Studies suggested that a reduction in HIC from 1000 to 800 would result in an estimated reduction of 21.7% in the risk of skull fractures [18]. The maximum HIC value of 1000 set by FMVSS 208 corresponds to a 16% risk of life threatening brain injuries [18]. The HIC duration should be limited to 15 ms or less for the calculation of the HIC value for a given head acceleration-time

history. Figure 8 is a plot for an average acceleration and corresponding HIC times for cadaver head impacts and human volunteer interaction with an air bag [18].

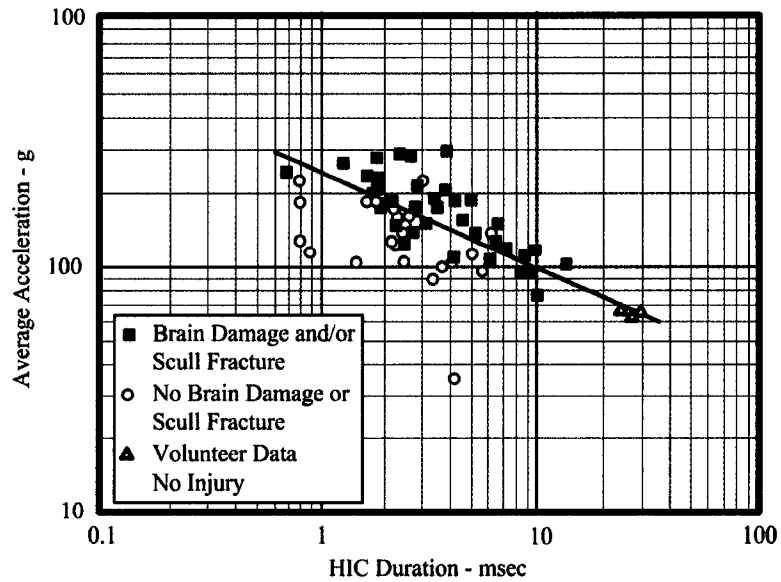


**Figure 8** Average Acceleration and Corresponding HIC Times for Cadaver Head Impacts and Human Volunteer Interactions with an Air Bag [18], 2000

Two other criteria can be used to evaluate the potential for head injuries. According to a hypothesis developed by Holburn [21] and reported by Coltman [2], shear stresses induced by head rotation can produce concussions. Coltman also reported that Kornhauser [22] proposed a relationship between damaging rotational head velocity and damaging rotational head acceleration. The relationship is:

$$\frac{d\alpha}{dt} = \frac{d^2\alpha/dt^2}{\omega_n} \tag{5}$$

where:

$d\theta/dt$  = the damaging rotational velocity (rad/s)

$d^2\theta/dt^2$  = the damaging rotational acceleration (rad/s<sup>2</sup>)

$\omega_n$  = the resonance frequency of rotation of the brain.

The second criterion for assessing the potential for head injuries is the Severity Index (SI). It was proposed by Gadd [23] and reported by Coltman [2]. The severity index, SI, is given by:

$$SI = \int_{t_1}^{t_2} a^n(t) dt \quad (6)$$

where:

$a(t)$  = the acceleration as a function of time

$n$  = the weighting factor greater than 1, and  $t$  is the time.

The exponent  $n$  is 2.5 for facial and head impacts. A severity index of 1,000 was proposed by Gadd [23] for danger-to-life threshold from head injuries in frontal impacts. Severity index values exceeding 600 produced concussion in head impacts sustained by U.S. Army aircrew members in aircraft accidents [2].

## 2.5 Neck Injury Criteria

The likelihood of neck injury involves the neck axial ( $F_z$ ) and shear ( $F_x$ ) forces and neck bending moments ( $M_x$  and  $M_y$ ). Neck bending moments in excess of 1680 in.-lb

(190 N-m) in forward flexion, 504 in.-lb (57 N-m) in rearward extension, and 924 in.-lb (104 N-m) in lateral bending, regardless of duration, are predicted to cause immediate incapacitation for military tasks [18]. The Neck Injury Criterion (NIC) is given by [18]:

$$\text{NIC} = \frac{F_z}{F_{zn}} + \frac{M_y}{M_{yn}} \quad (7)$$

where:

$F_z$  = upper neck axial force (N)

$M_y$  = moment about occipital condyle (N-m)

$F_{zn}$  = axial force critical value (N)

$M_{yn}$  = moment critical value (N-m)

## 2.6 Chest Injury Criteria

Chest injury is assessed based on the resultant chest acceleration, measured at the center of gravity of the upper torso of the mannequin. Resultant chest accelerations greater than 70 g's (686 m/s<sup>2</sup>) are likely to cause serious thoracic injury when the acceleration pulse time interval is greater than 3 ms [24]. Dillon et. al. [20] suggests that chest accelerations of 40 g's (392 m/s<sup>2</sup>) sustained for more than 7 ms can have a high risk of thoracic trauma and are scored as complete and immediate incapacitation for military. Latest studies showed that a 40% of maximum chest compression corresponded to a 50/50 chance of the occupant sustaining AIS 4 or greater chest injury. AIS is the Abbreviated Injury Scale and was developed as a comprehensive system for rating injuries by types and severity that would be acceptable to physicians, engineers, and

researchers working in automotive crash investigations. Also, it was shown that an impact producing a peak viscous response (the product of the velocity of deformation times the instantaneous compression) of 1.3 m/s had a 50/50 chance of inducing thoracic injury of AIS 4 or greater. An impact producing a peak viscous response of 2 m/s had a 50/50 chance of inducing cardiac rupture. Figure 8 shows the relationship between AIS injury rating and normalized chest deflections [2].

The thoracic trauma index (TTI) has been proposed as the human tolerance criterion [18]. The TTI is given by:

$$TTI = \frac{1}{2}(G_R + G_{LS}) \quad (8)$$

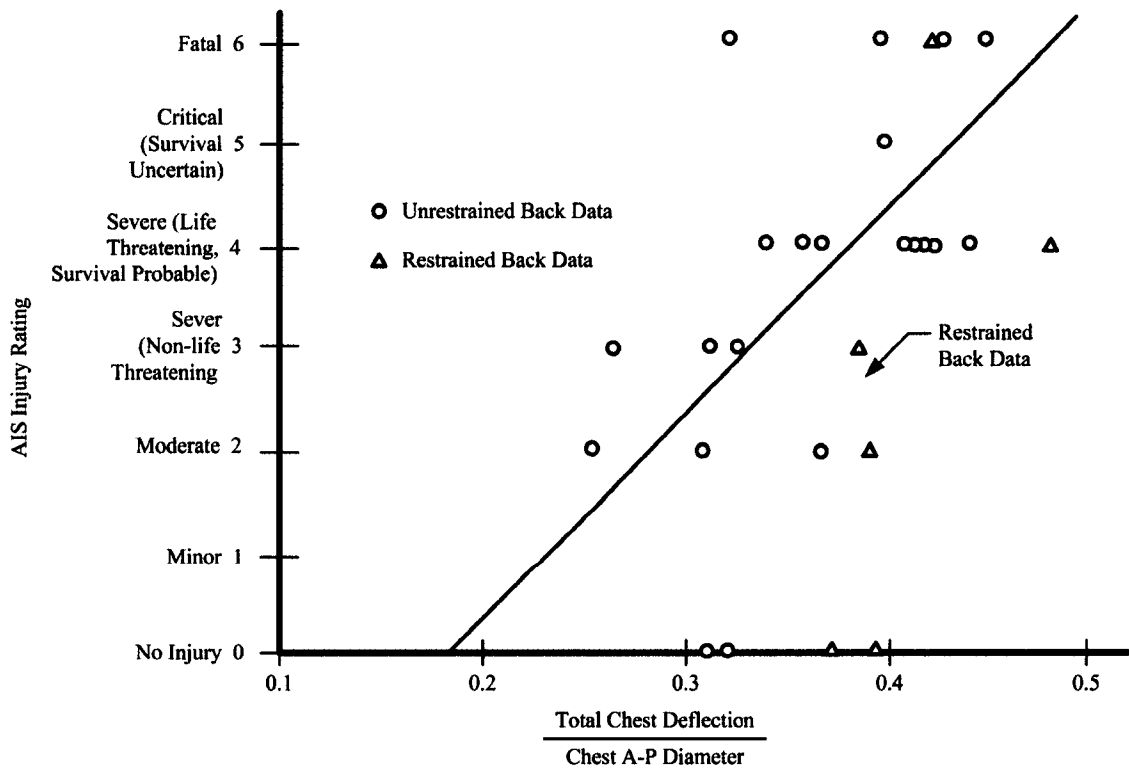


**Figure 9** AIS Injury Rating Versus Normalized Chest Deflection [4], 1989

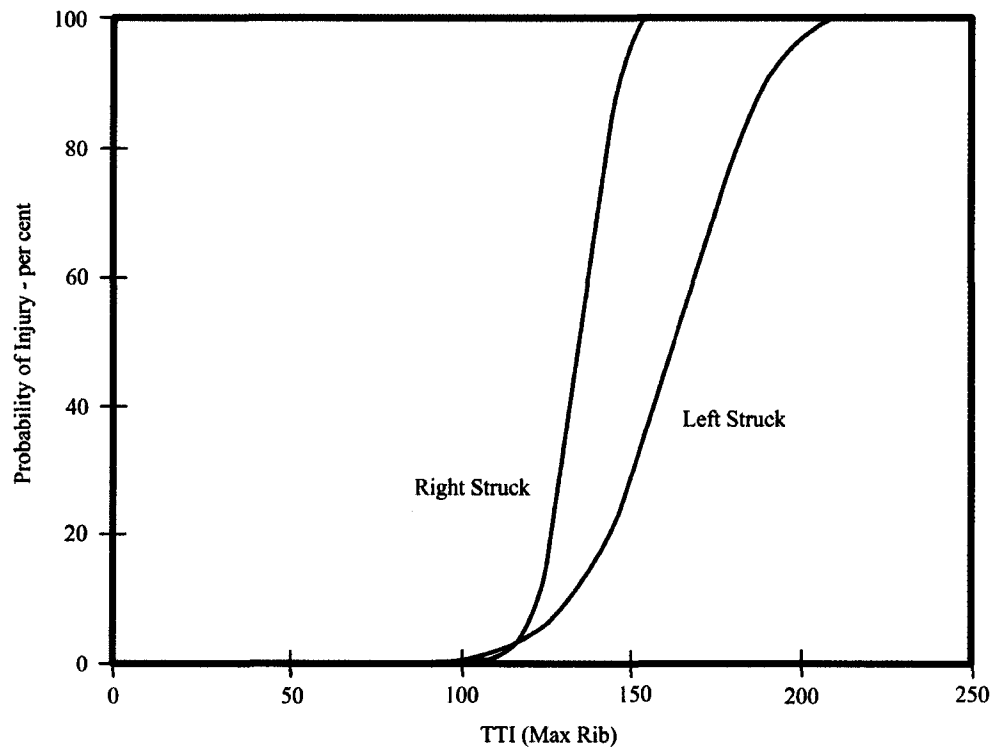


**Figure 10** Comparison of AIS  $\geq 4$  Probability for Left- and Right-Side Impacts [4], 1989

$G_R$  is the greater of the peak accelerations of either the upper or lower rib in g's, and  $G_{LS}$  is the lower spine peak acceleration in g's. Figure 10 shows a comparison of AIS  $\geq 4$  probability for left- and right-side impacts [2].

### 2.7 Abdominal Injury Criteria

Studies have shown that the liver is the most commonly injured abdominal organ. Lau and Viano found that a viscous response of 1.4 m/s had a 50/50 chance of causing severe laceration of the liver (AIS equal to or greater than 5) in the fore/aft direction [2].

## 2.8 Mine Blast Injury Criteria

Table 3 gives a summary of landmine injury criteria proposed by Axelsson [14]. Table 4 gives a summary of landmine injury criteria proposed by Alem et. al. [25]. Figure 11 gives a summary of the recommended injury criteria for vehicles exposed to landmines that is presented in the U.S. Army's Occupant Crash Protection Handbook for Tactical Ground Vehicles [18].

**Table 3** Landmine Injury Criteria Proposed by Axelsson.

Body Part	Type of Load	Tolerance Value
Brain	$HIC = (t_2 - t_1) \left[ \frac{1}{t_2 - t_1} \int_{t_1}^{t_2} a(t) dt \right]^{2.5}$	1,000
Neck	Compression	250-900 lb
	Tension	250-750 lb
	For-Aft Shear	250-700 lb
Chest	Serious Thoratic Injury	60 g's
Lumbar Spine	Vertical Direction	1,500-1,800 lb
Seat Design Limit	Vertical Direction	< 14.5 g's

**Table 4** Landmine Injury Criteria Proposed by Alem et. al.

Foot/Ankle Shock Acceleration	Average Acceleration < 10 g's or Maximum Velocity Change < 3 m/s
Pelvis/Spine Shock Acceleration	Average Acceleration < 15 g's or Maximum Velocity Change < 4.5 m/s
	DRI < 16

Hybrid III Simulant Response Parameter	Symbol (units) <sup>a</sup>	SAE Filter	Assessment Reference Values <sup>b</sup>
Head resultant acceleration Head injury criterion	A (G) HIC	CFC 1000 (1650 HZ)	150 G @ 2 msec. 750, ~ 5 % risk of brain injury for $t_2 - t_1 < / = 15$ ms *
Chest resultant acceleration	A (G)	CFC 180 (300 HZ)	60 G @ 3 ms, 40 G @ 7 ms
Pelvis forward acceleration Pelvis lateral acceleration Pelvis vertical acceleration	Ax (G) Ay (G) Az (G)	CFC 180 (300 HZ)	40 G @ 7 ms 23 G @ 7 ms 23 G @ 7 ms
Seat (Pelvis) forward DRI Seat (Pelvis) lateral DRI Seat (Pelvis) vertical DRI	DRI - x (G) DRI - y (G) DRI - z (G)	CFC 180 (300 HZ)	35, 40, 46 Gx (low, med, high risks) 14, 17, 22 Gy (low, med, high risks) 15, 18, 23 Gz (low, med, high risks)
Neck shear force Neck axial compressive force Neck axial tensile force	Fx or Fy (N) - Fz (N) + Fz (N)	CFC 1000 (1650 HZ)	1100 N (45 ms), 1500 N (25-35 ms), 3100N (0 ms) 1100 N (30 ms), 4000 N (0 ms) * 1100 N (45 ms), 2900 N (35 ms), 3300 N (0 ms)
Neck lateral moment Neck forward flexion moment Neck rearward extension moment	Mx (N-m) + My (N-m) - My (N-m)	CFC 600 (1000 HZ)	105 N-m 190 N-m 57 N-m
Lumbar spine shear force  Lumbar spine axial compression force Lumbar spine axial tension force	Fx or Fy (N)  - Fz (N) + Fz (N)	CFC 1000 (1650 HZ)	<sup>b</sup> 3800 N (45 ms), 5200 N (25-35 ms), 10700 N (0 ms)  3800 N (30 ms), 6673 N (0 ms)  <sup>c</sup> 3800 N (45 ms), 10200 N(35 ms), 12700 N (0 ms)
Lumbar spine lateral moment Lumbar spine flexion moment Lumbar spine extension moment	Mx (N-m) + My (N-m) - My (N-m)	CFC 1000 (1650 HZ)	675 N-m 1235 N-m 370 N-m
Femur or Tibia axial compression force	Fz (N)	CFC 600 (1000 HZ)	7562 N (10 ms), 9074 N (0 ms)
Tibia axial compressive force combined with Tibia bending moment	F (N) M (N-m)	CFC 600 (1000 HZ)	F / Fc - M / Mc < 1 Where: Fc = 35,584 N and Mc = 225 N-m
<sup>a</sup> x = Longitudinal, y = Lateral, z = Vertical <sup>b</sup> Exceeding values indicates a moderate to high risk of major injury <sup>c</sup> Approximately 3.4 times neck force values * Recommended deviations to referenced values. DRI = Dynamic Response Index; CFC = Channel Frequency Class			

Reference: Chapter 6, "Physical Testing and Data Analysis", of Final Report entitled, "Protection of Wheeled Vehicle Occupants from Landmine Effects", Land Systems Div; U.S. Army Aberdeen Test Center

**Figure 11 Recommended Injury Criteria for Landmine Testing by the U.S. Army [18], 2000**

## 2.9 Testing and Evaluation Injury Criteria

The definitive document that summarizes the injury criteria to be used for the purposes of design and evaluation of vehicle protection systems was recently published by the North Atlantic Treaty Organization [25]. The technical committees involved with this report thoroughly investigated the vehicle and occupant interaction during a land mine strike from the perspective of body mechanics, vehicular structural behavior, and experimental measurements. The goal of this study was to recommend test methodology

for the evaluation of vehicle protection systems. It is the recommendation of the authors of this report that the Dynamic Response Index (DRI) be the sole evaluation standard for protection against thoraco-lumbar spine injury. Their decision is based on the fact that only the DRI model accounts for the acceleration duration at the pelvis and has been validated with medical data. For the calculation of DRI, the NATO committee recommends using the z-axis pelvic acceleration measured by an anthropomorphic test device (ATD) placed on the vehicle seat. The variability of test results has been shown to be at a minimum for this measurement location. When this technique is used, a tolerance level of 17.7 for DRI will correspond to a 10% risk (AIS 2+) spinal vertebrae injuries. This DRI threshold is only valid for spine inclinations of less than or equal to 5 degrees. Further misalignment of the spine with the input force direction may lead to a greater potential for injury at the same DRI level, but no supporting data is available to quantify the increase.

For the purposes of this project, DRI was used to evaluate seat system performance, and other values, such as pelvic accelerations and spinal loading, are reported for completeness.

## CHAPTER 3

### MODELING

To efficiently determine the performance of seat system components and to assist with the development of seat concepts, a multi-dimensional computer model has been created. This numerical model, written for Matlab, is a five-degree-of-freedom mass-spring-damper (MCK) representation of seat system components and a human crewmember. A model schematic is shown in Figure 12. Table 5 lists the physical characteristics of the masses in Figure 12. Figure 13 shows a free body diagram representation of the model.

**Table 5 Model Mass Description**

<b>Component</b>	<b>Description</b>	<b>Mass (kg)</b>
0	Cabin floor	$\infty$
1	Seat pan	20
2	Legs	12
3	Pelvis	8.18
4	Upper torso	34.52

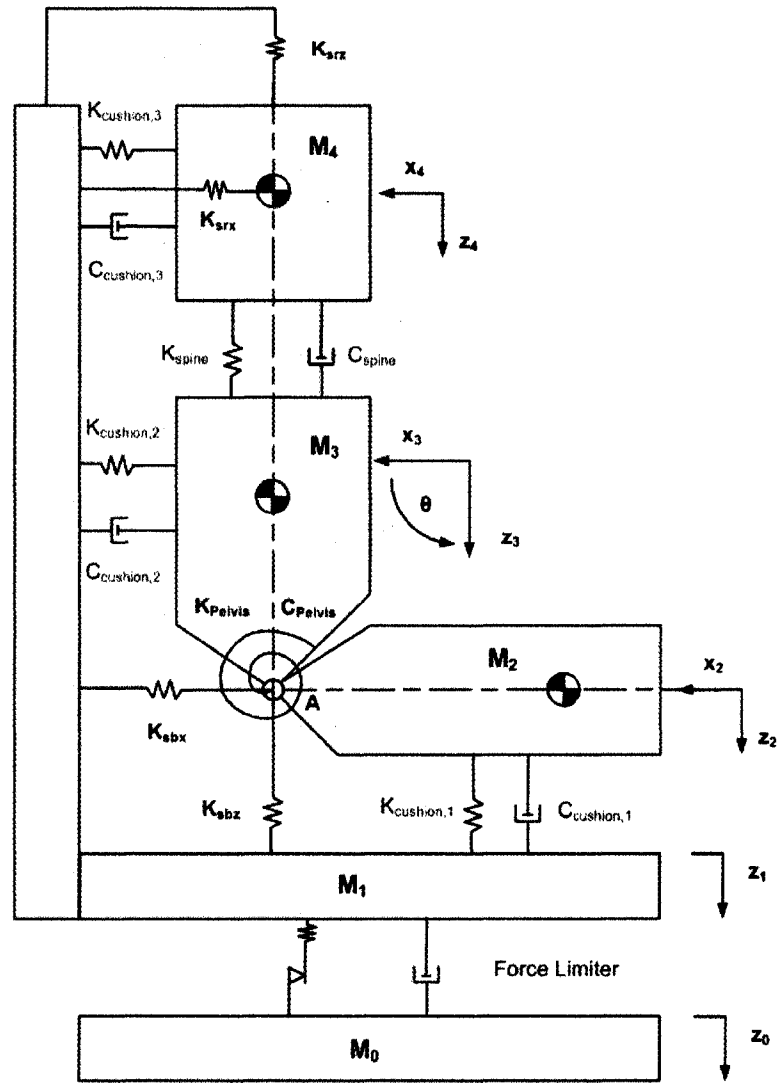


Figure 12 Model schematic

### 3.1 Equations

#### 3.1.1 Constraint equations

As shown in Figure 12, the inertial reference frame for all system masses is a right handed coordinate system with the z-axis positive downward and the x-axis positive to the left. The pelvis mass ( $M_3$ ) is allowed to rotate about the pin joint ( $\theta$ -axis)

representing the hip in a positive counter clockwise fashion. All coordinates zero points are set to coincide with the statically undeflected positions of the springs.

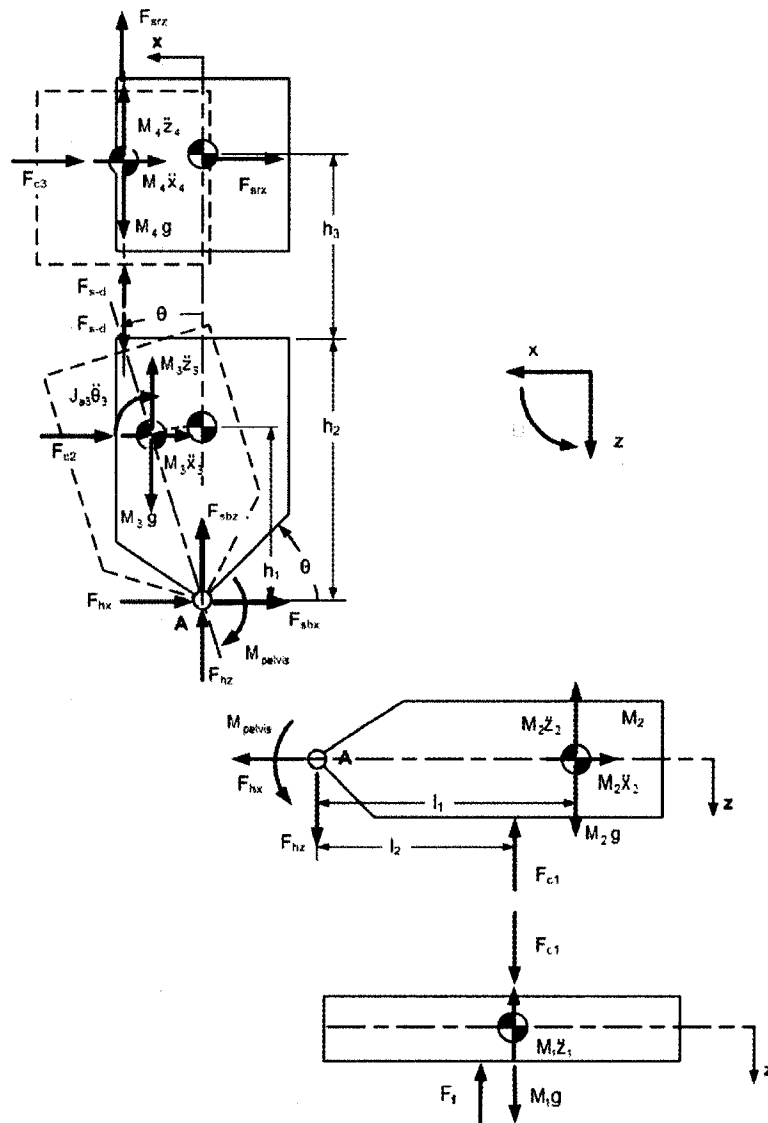


**Figure 13 – Free Body Diagram**

In order to relate the motion of the center of gravity (c.g.) of the pelvis mass ( $M_3$ ) to the motion of the c.g. of the legs ( $M_2$ ), the following constraint equations were applied.

$$x_3 = x_2 + h_1 \sin(\theta) \quad (9)$$

$$x_3 = x_2 + \theta h_1 \cos(\theta) \quad (10)$$

$$x_3 = x_2 + \theta h_1 \cos(\theta) - (\theta)^2 h_1 \sin(\theta) \quad (11)$$

$$z_3 = z_2 + h_1(1 - \cos(\theta)) \quad (12)$$

$$z_3 = z_2 + \theta h_1 \sin(\theta) \quad (13)$$

$$z_3 = z_2 + \theta h_1 \sin(\theta) + (\theta)^2 h_1 \cos(\theta) \quad (14)$$

The motion of the upper torso ( $M_4$ ) is related to the motion of c.g. of the pelvis mass ( $M_3$ ) plus the pelvis rotation. In the x-axis, the motion of the upper torso and spine attachment point on the top of the pelvis are equal. In the z-axis, the position of the spine attachment point on the pelvis must be calculated to determine the spring and damping forces of the spine. The constraint equations that relate the x-axis motion of the  $M_4$  and the z-axis motion of spinal attachment point of  $M_3$  to the motion of the c.g. of the legs ( $M_2$ ) are listed below.

$$x_4 = x_2 - h_2 \sin(\theta) \quad (15)$$

$$x_4 = x_2 + \theta h_2 \cos(\theta) \quad (16)$$

$$x_4 = x_2 + \theta h_2 \cos(\theta) - (\theta)^2 h_2 \sin(\theta) \quad (17)$$

$$z_{3,top} = z_2 + h_2(1 - \cos(\theta)) \quad (18)$$

$$z_{3,top} = z_2 + \theta h_2 \sin(\theta) \quad (19)$$

$$z_{3,top} = z_2 + \theta h_2 \sin(\theta) + (\theta)^2 h_2 \cos(\theta) \quad (20)$$

### 3.1.2 Force balance equations

Newtonian force balance equations for Figure 13 result in a system of non-linear differential equations. The resulting equations are given below.

#### 3.1.2.1 $M_1$ – Seat Pan

$$\sum F_{z1} = -M_1 z_1 + F_{cl} + F_{fl} + M_1 g = 0 \quad (21)$$

where:

$F_{fl}$  = force limiter reaction force, see section 3.3 (N)

$F_{cl}$  = seat cushion force, see section 3.4 (N).

#### 3.1.2.2 $M_2$ – Legs

$$\sum F_{z2} = -M_2 z_2 - F_{cl} + F_{hz} + M_2 g = 0 \quad (22)$$

$$\sum F_{x2} = -M_2 x_2 + F_{hx} = 0 \quad (23)$$

$$\sum M_A = M_2 z_2 l_1 - M_2 g l_1 + F_{cl} l_2 + M_{pelvis} = J_{a2} \theta = 0 \quad (24)$$

where:

$F_{cl}$  = seat cushion bottom force (N)

$F_{hx}$  = reaction force at hip in x-axis (N)

$F_{hz}$  = reaction force at hip in z-axis (N)

$g$  = acceleration due to gravity (9.81 m/s<sup>2</sup>)

$M_{pelvis}$  = hip joint rotational spring and damper moment (N-m)

$J_{a2}$  = rotational inertia of the mass of the legs about the hip pin.

The legs are constrained to translational motion only.

### 3.1.2.3 $M_3$ – Pelvis

$$\sum F_{z3} = -M_3 z_3 - F_{hz} - F_{sbz} + F_{s-d} + M_3 g = 0 \quad (25)$$

$$\sum F_{x3} = -M_3 x_3 - F_{c2} - F_{hx} - F_{sbx} - F_{c3} - M_4 x_4 - F_{srx} = 0 \quad (26)$$

$$\sum M_A = -J_{a3} \theta - (M_3 z_3 - M_3 g) h_1 \sin(\theta) - M_3 x_3 h_1 \cos(\theta) - F_{c2} h_1 + F_{s-d} h_2 \sin(\theta) + (F_{c3} + F_{srx})(h_2 \cos(\theta) + h_3 - z_4) - K_{pelvis} \theta - C_{pelvis} \dot{\theta} = 0 \quad (27)$$

where:

$F_{sbz}$  = lap belt spring force in z-axis (N)

$F_{sbx}$  = lap belt spring forces in x-axis (N)

$F_{srx}$  = shoulder belt spring forces in x-axis (N)

$F_{s-d}$  = spring force (N) and damping force (N) in the spine (see Equation 28)

$$F_{s-d} = K_{spine} (z_4 - z_{3,top}) + C_{spine} (\dot{z}_4 - \dot{z}_{3,top}) \quad (28)$$

$F_{c2}$  = cushion back force on pelvis (N)

$F_{c3}$  = cushion back reaction force on upper torso (N)

$J_{a3}$  = moment of inertia of the legs about the hip pin (kg-m<sup>2</sup>)

$K_{\text{pelvis}}$  = hip spring constant (N/m)

$C_{\text{pelvis}}$  = hip damping constant (N-s/m).

### 3.1.2.4 $M_4$ – Upper Torso

$$\sum F_{z4} = -M_4 z_4 + M_4 g - F_{s-d} - F_{srz} = 0 \quad (29)$$

where:

$F_{srz}$  = shoulder restraint force in the z direction (N).

### 3.1.3 System equations

When the geometric constraints are applied, hip pin reaction forces are eliminated, and the equations are rearranged to solve for accelerations, they become:

$$z_1 = \frac{1}{M_1} (-F_{fl} + F_{cl} + M_1 g) \quad (30)$$

$$z_2 = \frac{1}{M_2 + M_3} \begin{pmatrix} -M_3 (\theta h_1 \sin(\theta) + (\theta)^2 h_1 \cos(\theta)) \\ -F_{c1} + (M_2 + M_3)g - F_{sbz} + F_{s-d} \end{pmatrix} \quad (31)$$

$$x_2 = \frac{1}{M_2 + M_3 + M_4} \begin{pmatrix} -M_3 (\theta h_1 \cos(\theta) - (\theta)^2 h_1 \sin(\theta)) \\ -M_4 (\theta h_2 \cos(\theta) - (\theta)^2 h_2 \sin(\theta)) \\ -F_{c2} - F_{c3} - F_{s-bx} - F_{srx} \end{pmatrix} \quad (32)$$

$$\theta = \frac{1}{J_{a3}} \begin{pmatrix} -M_3 z_3 h_1 \sin(\theta) - M_3 x_3 h_1 \cos(\theta) + M_3 g h_1 \sin(\theta) \\ -F_{c2} h_1 + F_{s-d} h_2 \sin(\theta) - K_{\text{pelvis}} (\theta) - C_{\text{pelvis}} (\dot{\theta}) \\ -(F_{c3} + F_{srx})(h_2 \cos(\theta) + h_3 - z_4 + z_2) \end{pmatrix} \quad (33)$$

$$z_4 = \frac{1}{M_4} (M_4 g - F_{s-d} - F_{sz}) \quad (34)$$

These five equations define the motion of the seat system and can be solved numerically for any known input (see solution method).

### 3.2 Inputs

The input to the model is the acceleration of the vehicle floor. Any well-defined acceleration profile may be used. The form of the input signal is defined as a text file, with evenly spaced samples of the cabin floor acceleration profile. The program was originally designed to be used with test data that was taken in units of g's and will convert the input file to units of  $m/s^2$  automatically. The time step of the input values must be sufficiently small so that the changes in the signal in between values can be assumed to be linear. A time step of 0.00002 seconds was used for typical mine blast inputs. Graphical representations of the input profiles used in this research are shown in Chapter 4.

### 3.3 Force Limiters

The seat pan was modeled as a one-dimensional element that only moved in the z direction. One of three types of connections was used between the vehicle floor (input) and the seat pan. The first connection type was a rigid connection where the motion of the seat pan follows that of the floor. The second two types of connections were rope

springs and honeycomb force limiters. These connections were energy absorbing (EA) elements.

### 3.3.1 Rope Springs

Four wire cable rope springs, attached in parallel, was one of the connection types between the vehicle floor and seat pan that was investigated. The force of the spring was determined by the compression distance between the seat pan and the vehicle floor along with a small amount of damping force based on the relative velocity between the floor and seat pan. Any spring type may be used as long as the force response is known as a function of deflection and an estimation of the damping constant can be made. Manufacturer's data (Figure 14) was used to determine the following equations:

$$F_1 = ropeScale \left( \begin{array}{l} -74359785.2 \delta_{rs}^4 + 14003416.8 \delta_{rs}^3 \\ -1037449.5 \delta_{rs}^2 + 51636.2 \delta_{rs}^1 \end{array} \right) \quad (35)$$

$$\delta_{rs} = z_1 - z_0 \quad (36)$$

$$F_2 = F_1 \frac{(1 + 1000 L_{rs})}{1000 L_{rs}} \quad (37)$$

$$C_{rs} = 2 \zeta_{rs} \sqrt{\left( \frac{F_2}{\delta_{rs} * M_1} \right)} M_1 \quad (38)$$

$$F_3 = C_{rs} (z_0 - z_1) \quad (39)$$

$$F_{fl} = F_2 + F_3 \quad (40)$$

where:

RopeScale = the number of isolators used

$\delta_{rs}$  = the absolute deflection of the rope spring (m)

$\zeta_{rs}$  = the damping ratio of the rope spring (assumed to be 0.3).

The exponential equation for  $F_2$  was used to prevent the isolator from assuming negative displacements as it became completely compressed. The forces produced by the rope spring in tension are assumed to be the negative of the compression forces (ie.  $F_1 = -F_1$  if  $\delta_{rs}$  is negative).

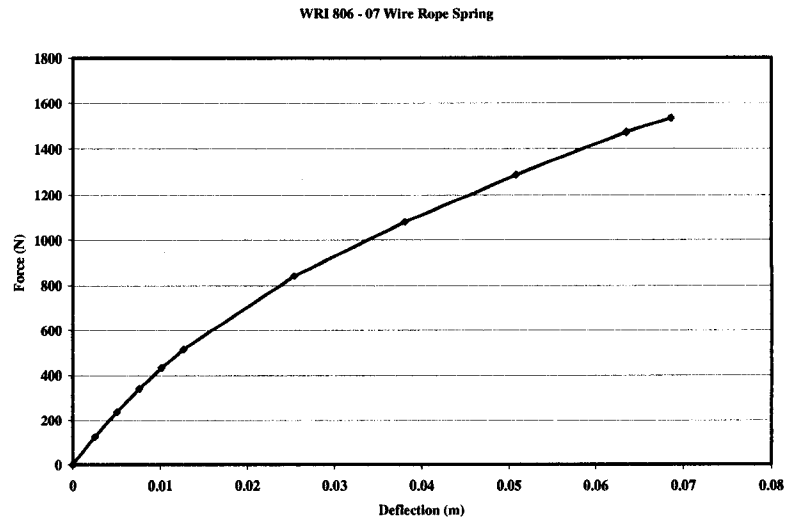


**Figure 14** Wire Rope Spring Force-Deflection Characteristics

### 3.3.2 Honeycomb isolators

A crushable aluminum honeycomb panel is a second type of connection between the vehicle floor and seat pan that was investigated. The panel has a linear load-deflection curve and uses a spring and a damper to transmit force from the floor to the seat pan. If the total force of the spring and damping element exceed a specified threshold, the

honeycomb material will buckle and the load will be limited. Figure 12 represents the honeycomb isolator by a force limiting element with a small spring on top and a damping element connected between the floor and seat pan. Since the spring on top of the force limiter is a mathematical tool used to create the restoring force and is not an actual physical part, its length should be very small (5 mm) and its stiffness should be very high (20000000 N/m). When the force in the spring and damper exceed the specified load level, the spring length is recalculated to provide a force equal to the load limit level, and the thickness of the honeycomb material is reduced accordingly. The spring must have a high stiffness so that it is never fully compressed. In the model code, a similar exponential equation to the one used for the rope spring is used to prevent negative spring lengths. This continues until the honeycomb is nearly totally compressed, and then the spring force is multiplied in a similar fashion to the rope spring isolator to prevent the floor from passing through the seat pan. Figure 15 is the force deflection curve for a 0.762m (3.5in) panel with an 8896N (2000lbf) load limit which was used for model predictions. The equations used to determine the honeycomb behavior are given below.

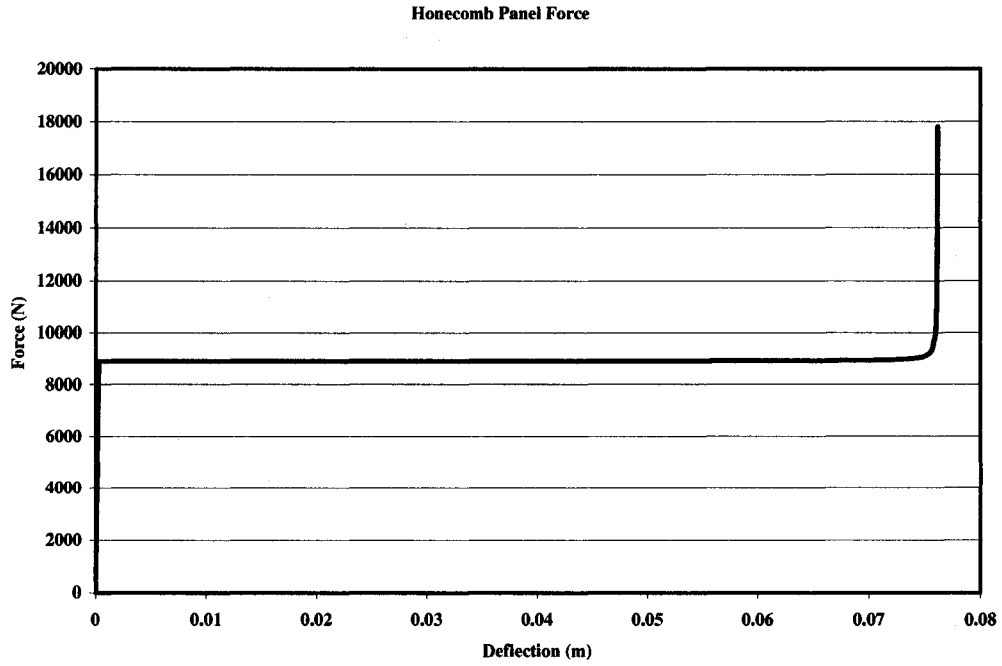


**Figure 15 Honeycomb Panel Force Deflection Characteristics**

$$\delta_{\text{spring}} = (z_0 - z_1) - \delta_{\text{fl}} + L_{\text{fl}} + L_{\text{spring}} \quad (41)$$

$$K_{\text{hc}} = K_{\text{hc0}} \frac{1 + 1000 \delta_{\text{spring}}}{1000 \delta_{\text{spring}}} \quad (42)$$

$$F_{\text{fl}} = K_{\text{hc}} (L_{\text{spring}} - \delta_{\text{spring}}) + C_{\text{hc}} (z_1 - z_0) \quad (43)$$

where:

$\delta_{\text{spring}}$  = the dynamic spring length (m)

$\delta_{\text{fl}}$  = the dynamic force limiter length (m)

$L_{\text{spring}}$  = the original force limiter spring length (m)

$L_{\text{fl}}$  = the original force limiter length (m)

$K_{\text{hc0}}$  = the original stiffness values of the force limiter spring (N/m)

$K_{hc}$  = exponentially treated stiffness to prevent negative spring lengths (N/m)

$C_{hc}$  = the damping constant of the honeycomb material (N-s/m).

If  $F_{fl}$  is greater than the force limit, the length of the spring is recalculated so that  $F_{fl}$  is equal to the load limit level until the force limiter is fully compressed (see Equations 44 and 45).

$$\delta_{spring} = \frac{L_{lim}}{K_{hc}} - \frac{C_{hc}}{K_{hc}} (z_1 - z_0) - L_{spring} \quad (44)$$

$$\delta_{fl} = z_0 - z_1 + \delta_{spring} + (L_{spring} + L_{fl0}) \quad (45)$$

where:

$L_{lim}$  = the activation force of the load limiter (N).

This new length is reinserted to Equation 41 and Equations 42 and 43 are recalculated.

### 3.4 Seat Cushion Model

The seat cushion in this model has a bottom and a back section. A specific seat cushion design using foam and air is discussed in Chapter 4; however, the model program can accept any type of cushion provided that the force-deflection performance on the cushion with a human occupant is known. The forces applied by the cushion can be approximated by using a spring and a damper. In this case, the forces on the occupant from the cushion bottom ( $F_{c1}$ ) and the cushion back ( $F_{c2}$  and  $F_{c3}$ ) become:

$$F_{c1} = K_{cushion,1} (z_0 - z_1) + C_{cushion,1} (\dot{z}_0 - \dot{z}_1) \quad (46)$$

$$F_{c2} = K_{cushion,2} (x_3) + C_{cushion,2} (\dot{x}_3) \quad (47)$$

$$F_{c3} = K_{cushion,3} (x_4) + C_{cushion,3} (\dot{x}_4) \quad (48)$$

where:

$K_{cushion}$  = the stiffness of the cushion (N/m)

$C_{cushion}$  = the damping constant of the cushion (N-s/m).

The values of stiffness and damping may differ between the bottom and back sections and can be non-linear. See Chapter 4 for an example of non-linear performance that has been modeled.

### 3.5 Human Body Model

Masses 2, 3 and 4 represent the human body. The physical parameters of the human body components are given in Table 6. The rotational stiffness  $K_{pelvis}$  and damping  $C_{pelvis}$  values in Figure 12 represent the hip joint. The stiffness  $K_{spine}$  and damping  $C_{spine}$  values associated with the spring and damper between the pelvis and upper torso represent the spine.

The selection of the physical parameters of the three masses and the spring and damper defining the spine was based on a MCK representation of the human body developed by Cheng [5] for use in modeling helicopter seat cushions. Cheng's two-mass model is a semi-definite system with a resonance frequency (52.9 rad/sec) and damping ratio (0.224) equal to that of the DRI model.

**Table 6** Human Body Model Parameters

<b>Component</b>	<b>Mass</b>	<b>K (N/m)</b>	<b>C (N*s/m)</b>
Legs	12		
Pelvis	8.18	8065.2	513.7
Upper Torso	34.52	96600	818.8

The lower torso mass recommended by Cheng is divided into a pelvis mass and leg mass connected by a pin joint. The pelvis is free to rotate about the pin, but the legs are constrained to move in two dimensions (up-down or forward-back). The assumption of purely translational motion for the legs was derived from observation of recorded video test data (see chapter 5, model validation). The mass distribution between the pelvis and legs is based on nominal human body data obtained from Clauser [26]. The rotational spring and damper that act on the pelvis at the hip joint were given values corresponding to a resonance frequency of 5 Hz. The linear spring and damper between the pelvis and upper torso represent the spine. The addition of the spring and damping forces are indicative of spine/lumbar load.

### 3.6 Restraint Forces

The restraint forces holding the human body model are generated by the lap belt and the shoulder restraints. For the purposes of this model, four separate seat belts were created using linear springs, one acting in the z direction and one acting in the x direction for both the pelvis (lab belt) and the upper torso (shoulder restraint). The seat belts forces are only applied when the springs are in tension. When the seat belts are slack, no forces

are applied. The following equations quantify the forces from these springs in terms of system spatial variables.

$$F_{sbx} = K_{sbx} x_2 \quad (49)$$

$$F_{sbz} = K_{sbz} (z_2 - z_1) \quad (50)$$

$$F_{srz} = K_{srz} x_4 \quad (51)$$

$$F_{srz} = K_{srz} (z_4 - z_1) \quad (52)$$

The following table summarizes the values used for the spring constants.

**Table 7** Seat Belt Spring Constants

Spring	K (N/m)
$K_{sbz}, K_{srz}$	100,000
$K_{sbx}, K_{sbz}$	50,000

### 3.7 Solution Technique

The system of differential equations defined by Equations 30-34 is highly non-linear. Therefore, it is not possible to solve these equations, using analytic closed form solution techniques. A finite differencing, marching solution was chosen to solve the equations in terms of the known input acceleration of the floor. The floor motion is considered to be unchanged by the presence of the seat and occupant, so the velocity and position of the floor may be determined by numerical integration using:

$$z_0(i+1) = z_0(i) + z_0(i+1) \Delta t \quad (53)$$

$$z_0(i+1) = z_0(i) + z_0(i+1) \Delta t \quad (54)$$

where:

$\Delta t$  = the numerical solution time step (s).

After the acceleration, velocity, and position of the floor are fully defined, they are used to create spring and damper forces in the element that connects the floor to the seat pan, which in turn start the motion of the seat system. In the marching solution method, the acceleration of each mass is solved for using a propagation of forces through the system. The acceleration of a system mass is solved for in terms of input forces, generated by springs and dampers, at the (i+1) time step and all other forces at the current (i) time step. An example equation for the solution of the acceleration of  $M_1$  is:

$$z_1(i+1) = \frac{1}{M_1} (-F_{fl}(i+1) + F_{c1}(i) + M_1 g) \quad (55)$$

The forces generated by the motion of the  $M_0$  are transmitted to  $M_1$  by the spring and damper between them ( $F_{fl}$ ) and are resisted by the spring and damper between  $M_1$  and  $M_2$  ( $F_{c1}$ ). The velocity and position of  $M_1$  are found using Equations 59 and 60. This motion is then used to calculate cushion compression forces,  $F_{c1}(i+1)$ , and the process repeats for each mass above  $M_1$ . The order of coordinate marching for each time step is:

$$\begin{aligned}
&M_0(z) - M_1(z) - M_2(z) - M_3(\theta) + M_3(z) - \\
&M_4(z) \rightarrow M_3(x) + M_4(x) + M_2(x)
\end{aligned}
\tag{56}$$

### 3.7.1 Assumptions and Limitations

The marching solution is a fast and very flexible technique for determining the system dynamics. Stability of the solution technique required that the acceleration, velocity and displacement changes be small compared to the time step. That is, the frequency of the time step must be much higher than any significant frequency content of the physical dynamics. Non-zero initial conditions may be specified as required.

The modeling of the human body as a collection of rigid masses is an approximation for the behavior of the real human body. While it is generally believed that the human body acts as a somewhat rigid mass when exposed to shock accelerations, it is known that there is significant absorption of energy in the tissues and muscles of the body. The rigid body model used here will have a tendency to over predict accelerations and forces, especially when seat masses impact with the human body masses. A method for correcting the system responses to better reflect a flexible human body will be discussed in Chapter 5.

## CHAPTER 4

### PNEUMATIC SEAT CUSHION DEVELOPMENT

Extensive testing at the University of Nevada, Las Vegas Center for Mechanical and Environmental Technology laboratory has been performed to determine the physical parameters of the air pneumatic seat cushion. Validation of the shock performance of the seat cushion was done at the Army Research Laboratory on a drop tower test machine. The results of these experiments will be summarized in this chapter.

#### 4.1 Seat Cushion Description

The seat cushion air bladder was constructed utilizing a specially configured air-filled, low-density, open-cell foam structure that was encapsulated in an impermeable outer covering (Figure 16). The air-filled, low-density, open-cell foam structure allows air to flow from the seat bottom to the seat back. This enables the seat bottom to deflect over 90 percent of its original thickness before it starts to become infinitely stiff.

#### 4.2 Seat Cushion Modeling

The numerical model used to describe this seat cushion was created to predict the force-deflection performance of the cushion foam and the compression of the air inside the cushion separately. The total response of the cushion is determined by adding the

force generated by the foam and the force generated by the compression of the air in parallel. The foam and air forces are non-linear functions of the compression of the cushion.

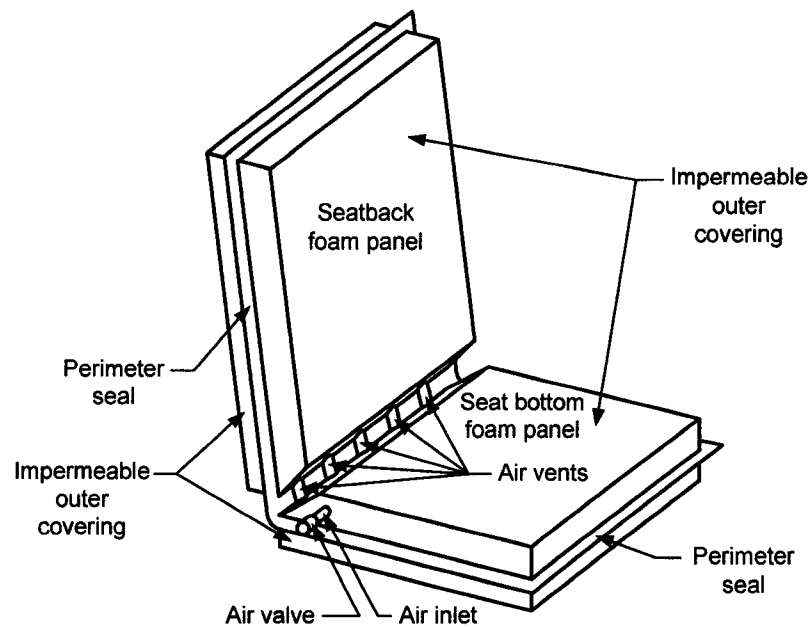


**Figure 16** Drawing of Inflatable, Low-Density, Open-Cell Foam Shock Attenuating Seat Core

The response of the air is determined using an isentropic compression equation.

$$P_{\text{cush}} = P_{\text{atm}} \left( \frac{V_1}{V_2} \right)^{\gamma} - P_{\text{atm}} \quad (57)$$

where:

$V_1$  = the total volume of the seat cushion (m)

$V_2$  = the reduced volume of the cushion during compression (m)

$P_{atm}$  = atmospheric pressure (101325 Pa).

When the seat cushion bottom is compressed, the cross-sectional perimeter of the cushion surface does not fold, but remains constant. The volume of the back section of the seat cushion expands in a linear fashion when the seat bottom is initially compressed until it is fully stretched, after which it ceases to expand further. This results in an initial reduction in the amount of pressure increase in the cushion during the beginning of the compression cycle. When these effects are accounted for, the pressure equation for the cushion becomes:

$$P_{cush} = \left( P_{atm} \left( \frac{V_1}{V_1 - EF \{ V_0 - [(L_{leg} + \delta_{cush})^2 \delta_{cush}] \}} \right)^y - P_{atm} \right) \quad (58)$$

where:

$P_{cush}$  = internal cushion pressure (Pa)

EF = the expansion factor, a ratio representing the expansion of the seat cushion back to the compression of the bottom. (0.58)

$V_1$  = the original air cushion volume the air cushion (m<sup>3</sup>)

$V_0$  = the original seat cushion bottom volume (m<sup>3</sup>)

$L_{leg}$  = the length of the leg contacting the seat cushion (m)

$\delta_{\text{cush}}$  = the z-axis compression of the cushion bottom (m).

The value of  $\delta_{\text{cush}}$  is set to zero if the distance between the occupant and the seat pan is greater than the original seat cushion thickness to prevent expansion of the cushion bottom and negative internal pressures.

The foam response is calculated from test data. The test data was fit with an exponential function:

$$F_{\text{foam}} = \frac{4.448}{(1.005 - \epsilon)^{2.7}} \quad (59)$$

where:

$\epsilon$  = the cushion compression divided by the original thickness (cushion strain).

This equation gives the foam force in units of Newtons.

The damping of the seat cushion is variable and depends on the rate of the seat cushion compression. If the seat cushion bottom compression is high (greater than 0.5 m/s), the compression of the air dominates and damping forces related to bulk flow of the air inside the cushion are small. For this case, the damping coefficient is lowered to 0.10. For recovery and all lower rate compressions, the damping ratio is 0.30. For the seat back, the damping ratio is assumed to be constant. The friction of the legs against the seat cushion bottom increases the damping constant and this increase is linearly related to the input acceleration magnitude. Because the damping forces for the x-axis include frictional forces, the occupant and the seat back are forced to remain in contact at all times. The seat belts maintain this contact. The pressure force applied by the cushion to

the occupant acts in the negative x-direction (pushing the occupant into the seat belt) at all times. The damping forces are directional with velocity. A typical equation used to determine the damping constant for the seat cushion is shown here.

$$C_{\text{cush}} = 2\zeta \sqrt{\frac{70050}{M_2 + M_3}} (M_2 + M_3) \quad (60)$$

The constant value (70070 N/m) in the equation is based on an average stiffness throughout the cushion stroke. The values used for each damping ratio and the corresponding damping coefficients are tabulated in Chapter 5

With regards to the numeric model described in Chapter 3, the forces of the cushion bottom on the legs in the z-axis and the x-axis are given by the following:

$$F_{c1} = 2P_{\text{cush}} \text{Area}_{\text{seat}} + F_{\text{foam}} + C_{\text{cush}} (z_2 - z_1) \quad (61)$$

$$F_{c2} = 2 * P_{\text{cush}} * \text{Area}_{\text{pelvis}} + F_{\text{foam},2} + C_{\text{cush,back}} * (x_3) \quad (62)$$

where:

$P_{\text{cush}}$  = the cushion pressure, see Equation 58 (Pa)

$F_{\text{foam},2}$  = foam generated force, see Equation 63 (N).

$$F_{\text{foam},2} = \frac{4.448}{\left(1.005 - \frac{x_3}{\text{cushionback, org}}\right)^{2.7}} \quad (63)$$

where

cushionback,org = the original thickness of the cushion back section (m).

Similarly, the cushion force on the upper mass in the x direction is:

$$F_{c3} = 2 * P_{\text{cush}} * \text{Area}_{\text{torso}} + F_{\text{foam},3} + C_{\text{cush,back}} * (x_4) \quad (64)$$

The foam force on the upper torso is calculated by:

$$F_{\text{foam},3} = \frac{1}{\left(1.005 - \frac{x_4}{\text{cushionback, org}}\right)^{2.7}} * 4.448 \quad (65)$$

### 4.3 Seat Cushion Parameter Identification

A series of three tests was performed on the seat cushion: (1) a dunk tank volume test, (2) a force compression test and (3) a damping characterization test.

#### 4.3.1 Volume testing

The seat cushion was dunked in a water tank while fully inflated to estimate its volume. The results of this test are summarized in Table 8.

**Table 8** Seat Cushion Inflated Volumes

<b>Seat Cushion Part</b>	<b>Approximate Dimensions (m)</b>	<b>Measured Volume (m<sup>3</sup>)</b>
Back	0.610 x 0.457 x 0.092	0.016
Bottom	0.457 x 0.457 x 0.092	0.026
Whole	N/A	0.041

#### 4.3.2 Force- compression testing

The seat cushion underwent low speed compressions on a Material Test Systems hydraulic tensile test machine. The seat cushion bottom was placed between an oversized aluminum plate on the bottom and a human seat form made from MDF fiberboard. The human form was approximately the shape of the contact area of a person sitting on the air cushion and had a surface area of 0.108 m<sup>2</sup>. The test was run at the maximum speed of the test machine (0.05m of compression per second) and data was collected from the machine's load cell, as well as, a pressure sensor mounted on the fill tube of the air bladder. The internal pressure of the cushion at the start of the test was 0 psig. The same procedure was repeated with the bottom of the seat cushion separated entirely from the back to determine the response of the foam alone. The foam only test data compared to the exponential fit estimation (Equation 46) is shown in Figure 17.

### Bladder Foam Curve Fit

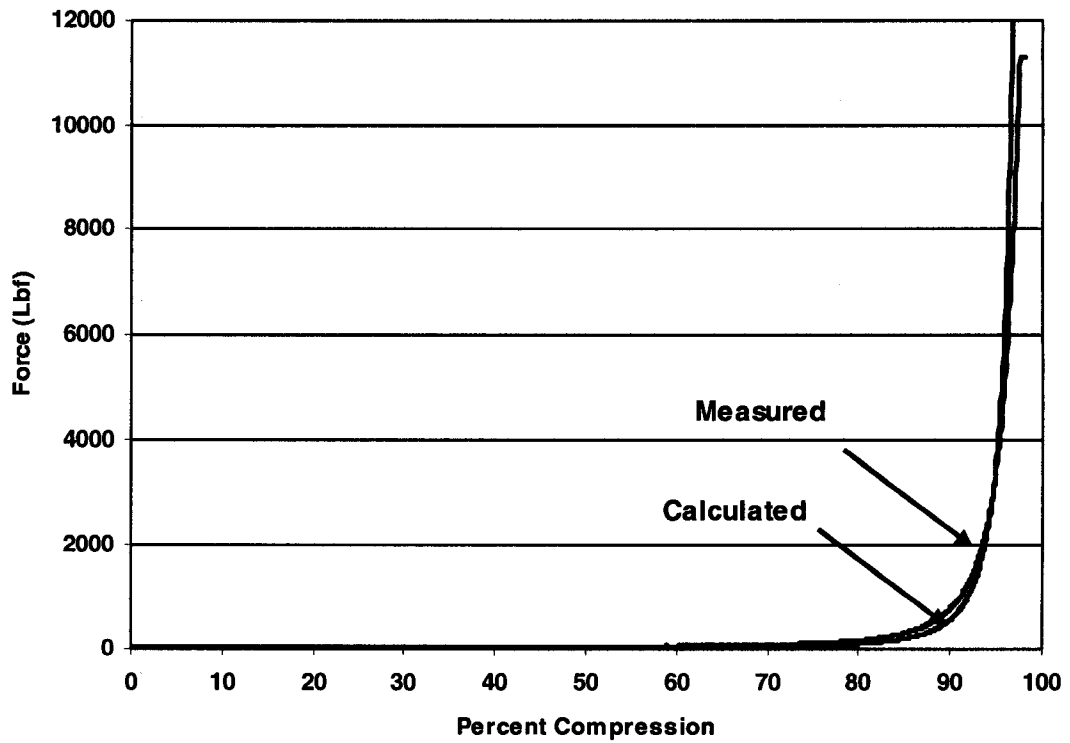


**Figure 17** Foam Compression Test Results

Figure 18 shows the air pressure sensor data plotted against the predicted results of Equation 57. The foam and air forces were treated as parallel springs. Figure 19 shows the results associated with adding the foam and air pressure results

### Air Bladder Pressure Comparison

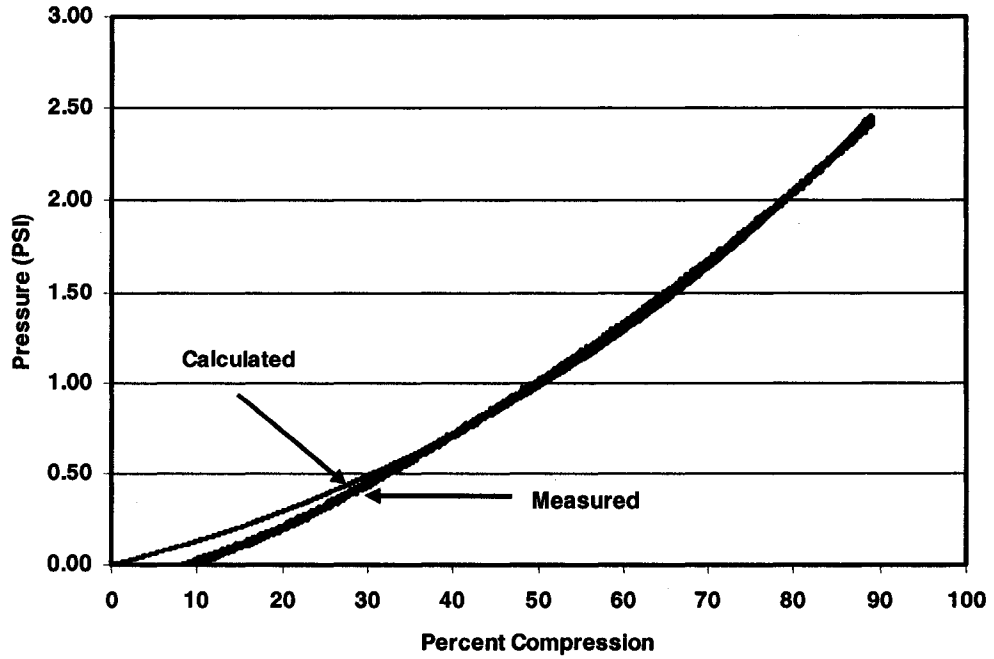


Figure 18 Air Bladder Pressure Test Results

### Air Bladder Test Data

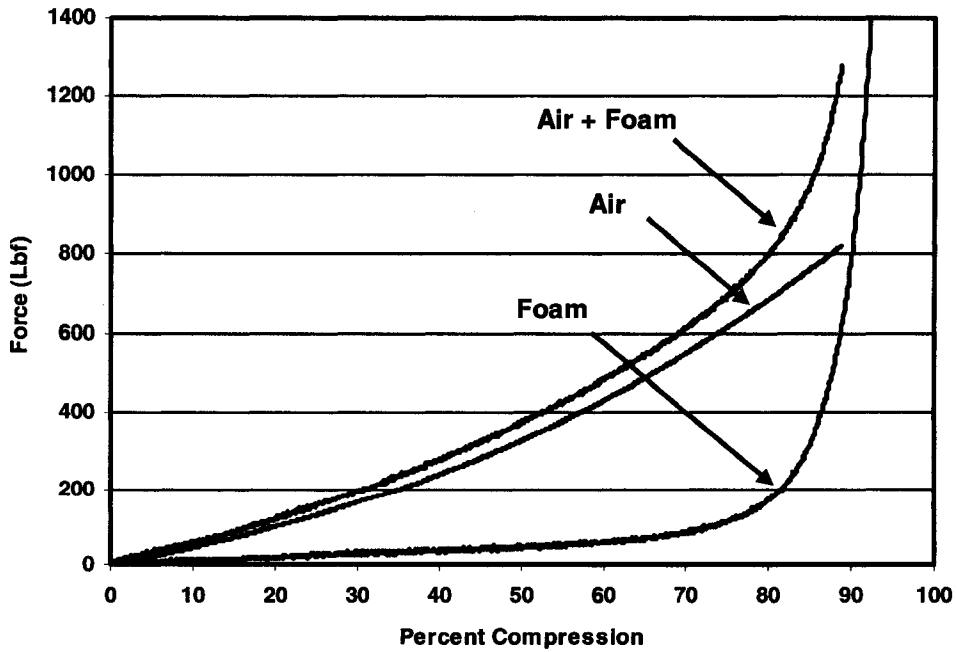
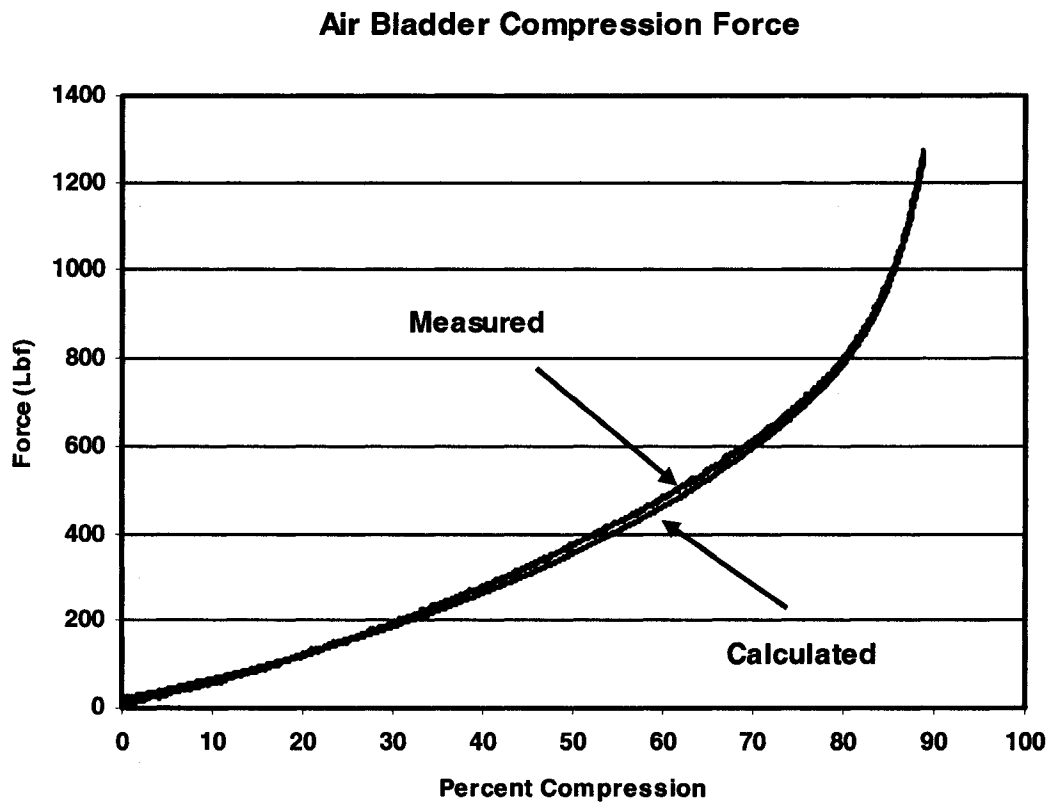


Figure 19 Foam – Air System Test Results

The Air + Foam curve represents the compressive force measured by the test machine load cell on a closed cushion system. The Air curve is derived from the pressure sensor data from the same test multiplied by 2 times the surface area of the seat form. The Foam curve is a load cell force measurement from a separate test on a cushion opened to the atmosphere. Figure 20 shows a comparison between predicted results and measured data for the cushion force.



**Figure 20** Air Cushion Force Comparison

### 4.3.3 Damping Estimation

The damping ratio of the cushion was experimentally determined using the half power point method. The air cushion was placed on top of a electro-dynamic shaker system with a 150 lb mass on top. This system can be represented as a base input, single-degree-of-freedom mass-spring-damper system. The input accelerometer was mounted to the shaker base and the response accelerometer was mounted to the top of the mass. A random excitation input ( $0.962 \text{ (m/s}^2\text{)}^2\text{/Hz}$ , 1-50 Hz) was used and the real part of the transfer function was plotted as a function of frequency. The half-power points occurred at the maximum and minimum of this plot. The resonance frequency was read from the zero-crossing between the half-power points. The damping ratio of the air cushion was determined by the frequencies at which the half power points occur by using the formula:

$$\xi = \frac{1}{2} * \frac{\left(\frac{\omega_2}{\omega_1}\right)^2 - 1}{\left(\frac{\omega_2}{\omega_1}\right)^2 + 1} \quad (59)$$

Test results showed that  $\omega_1 = 3.13 \text{ (rad/sec)}$ ,  $\omega_2 = 6.56 \text{ (rad/sec)}$ . The air cushion had a resulting damping ratio of 0.31 and a resonance frequency of 5.3 Hz.

#### 4.4 Seat Cushion Shock Performance

Mine blast testing of vehicle structures is incredibly expensive and difficult to repeat, so the Army has elected to use drop tower tests to down select seat concepts for further evaluation. Drop tower tests were conducted with the air bladder seat cushion at the U.S. Army Research Laboratory in Adelphi, Maryland, on May 18, 2006. A Thor III Hybrid anthropomorphic dynamic dummy was placed on an air bladder seat cushion, see Figure 21. Two drop heights were used: (a) 30 in. (76.2 cm) and (b) 50 in. (127.0 cm).

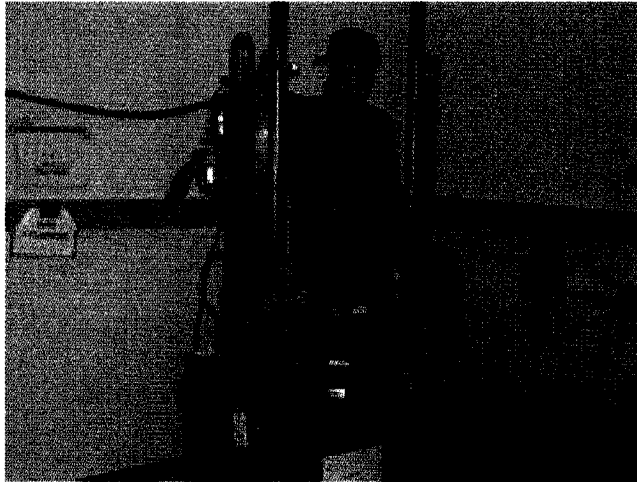


**Figure 21** Thor III Hybrid Anthropomorphic Dummy Positioned on an Air Cushion

The platform input acceleration into the underside of the air bladder seat cushion is shown in Figure 22. Figures 23 and 24 show the derived velocity and position of the drop tower platform. The 40 inch drop plotted on the graph was created by averaging the 50 inch and 30 inch drops acceleration curves, centered at the same peak accelerations occur, and is reported here for reference in Chapter 6.

The resulting measured pelvis accelerations in the z-direction (vertical) and x-direction (front-back) are shown in Figures 25 and 26. The resulting measured spine load in the z-direction is shown in Figure 27, and the resulting calculated DRI in the z-direction is shown in Figure 28. The injury prediction results are collected in Table 9. The measured z-axis peak spine load for a peak shock acceleration value of 395 g's (3,871 m/s<sup>2</sup>) associated with the 50 inch drop with the air bladder seat cushion alone was 1,574 lb<sub>f</sub> (7,000 N), which is slightly higher than the Army recommended maximum value of 1,500 lb (6,672 N). The measured z-axis peak acceleration value was 33.2 g's (326 m/s<sup>2</sup>), which is greater than the recommended maximum value of 23 g's (225.5 m/s<sup>2</sup>). The z-axis DRI value calculated from the measured acceleration values was 16, which is less than the maximum DRI value of 17.7 recommended by NATO.

**Table 9** Air Cushion Test Results

<b>Drop Height (m)</b>	<b>Peak Z Axis Input Acceleration (m/s<sup>2</sup>)</b>	<b>Peak X Axis Pelvic Acceleration (m/s<sup>2</sup>)</b>	<b>Peak Z Axis Pelvic Acceleration (m/s<sup>2</sup>)</b>	<b>Peak Spine Load (N)</b>	<b>Dynamic Response Index</b>
0.762	1132.5	74.0	242.8	-6191.9	15.1
1.27	3905.6	215.5	324.9	-6946.1	16.0
Tolerance Lim	N/A	N/A	225.5	-6672.0	17.7

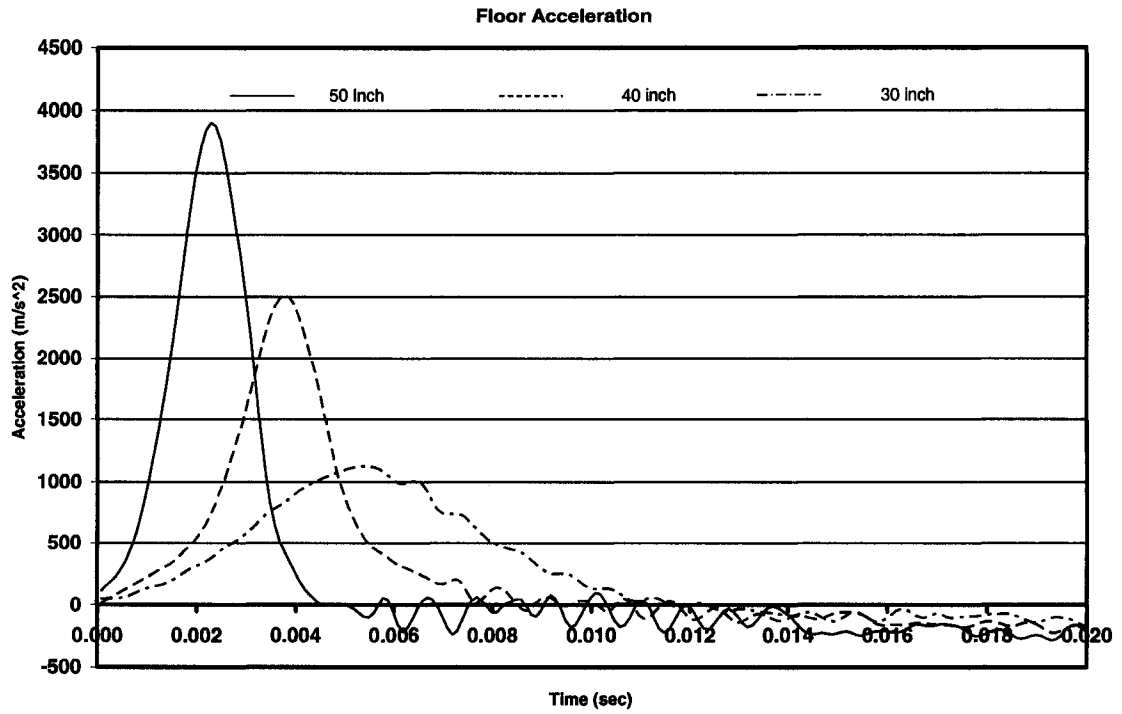


**Figure 22** Platform Accelerations for 30 in. (76.2 cm), 40 in. (101.6 cm), and 50 in. (127.0 cm) Drop Heights

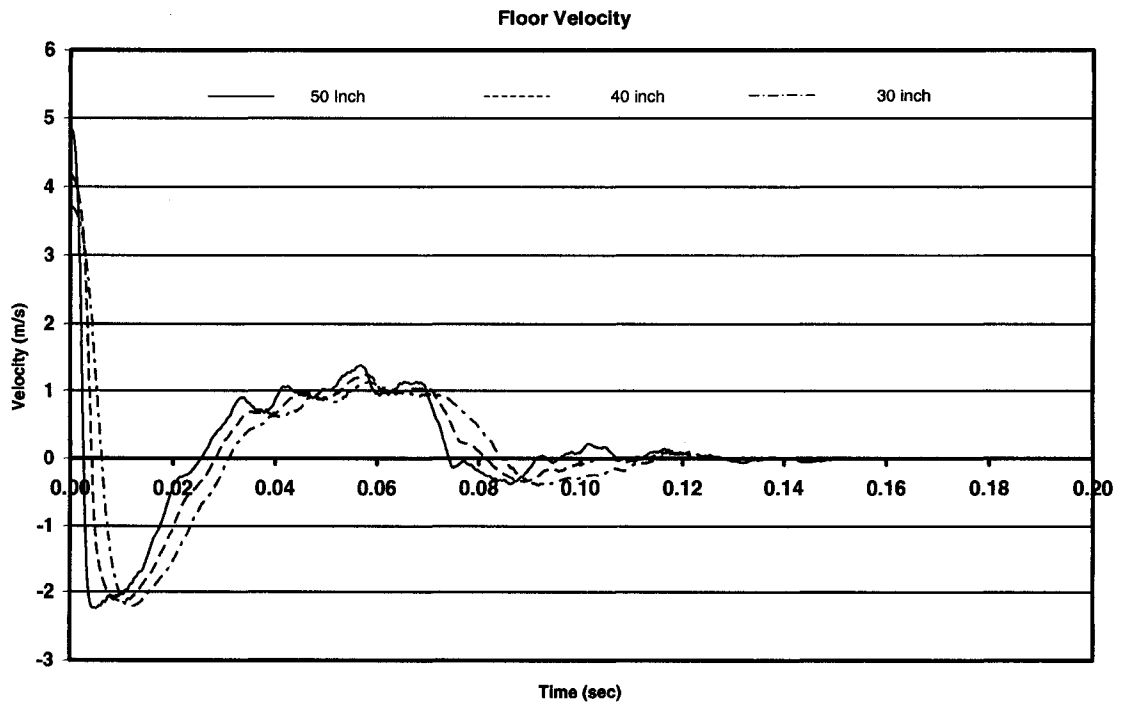


**Figure 23** Platform Velocities

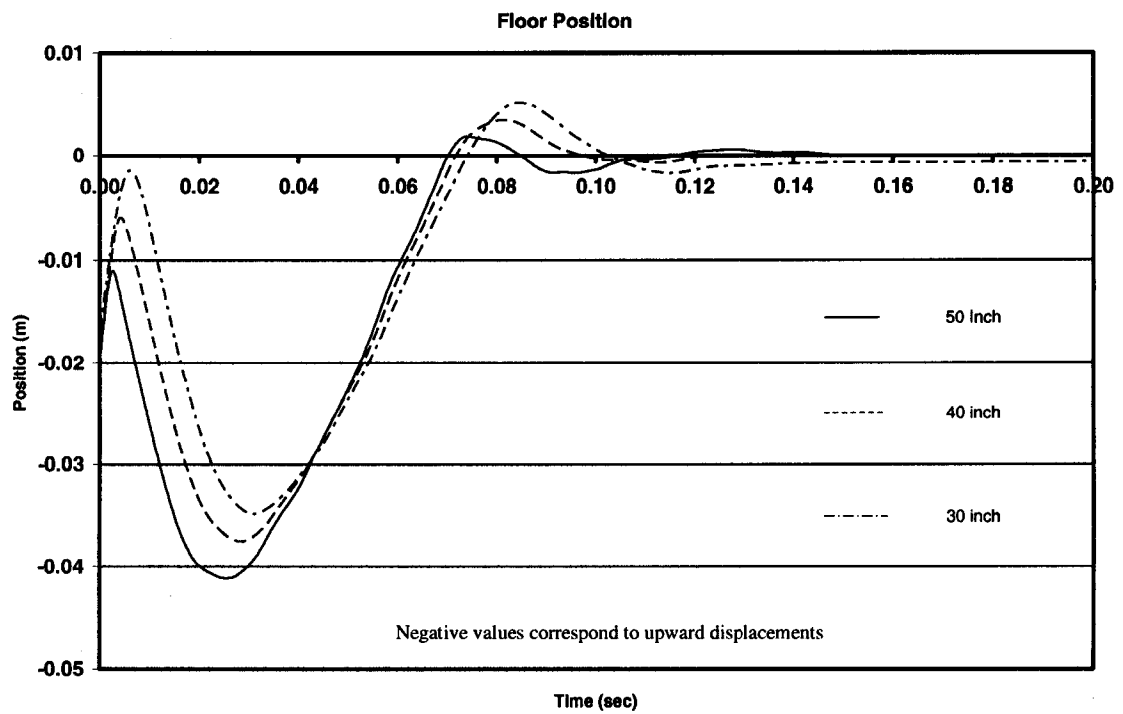


**Figure 24** Platform Positions

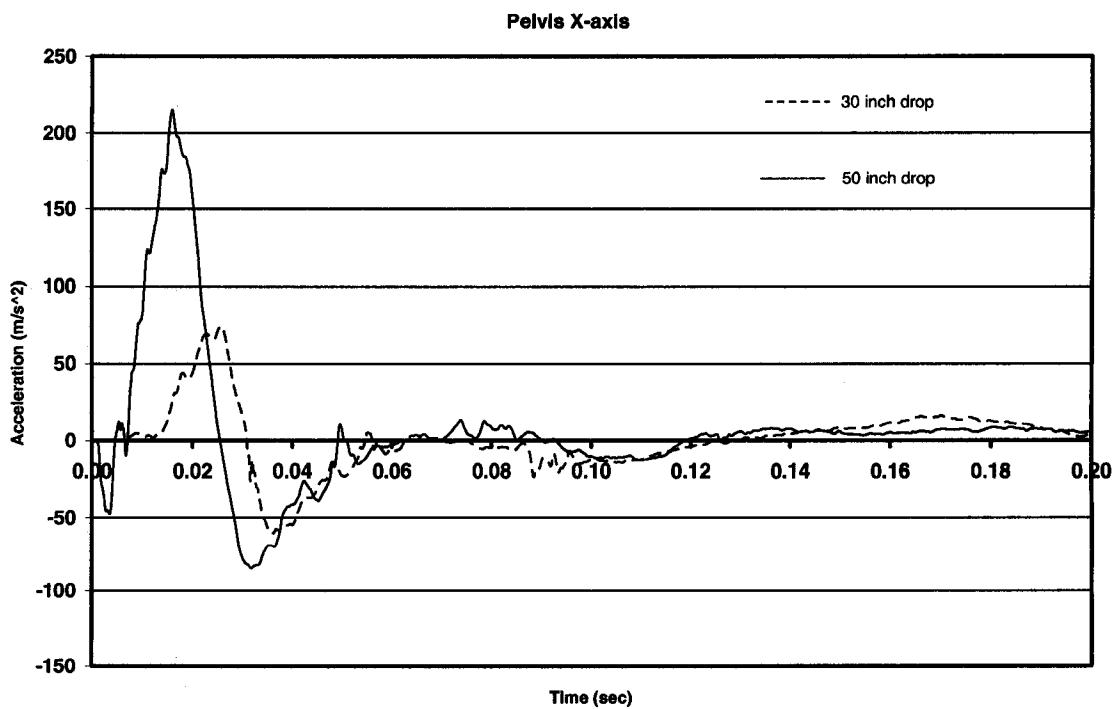


**Figure 25** Measured Pelvis x-Axis Acceleration for 30-in. and 50-in Drops

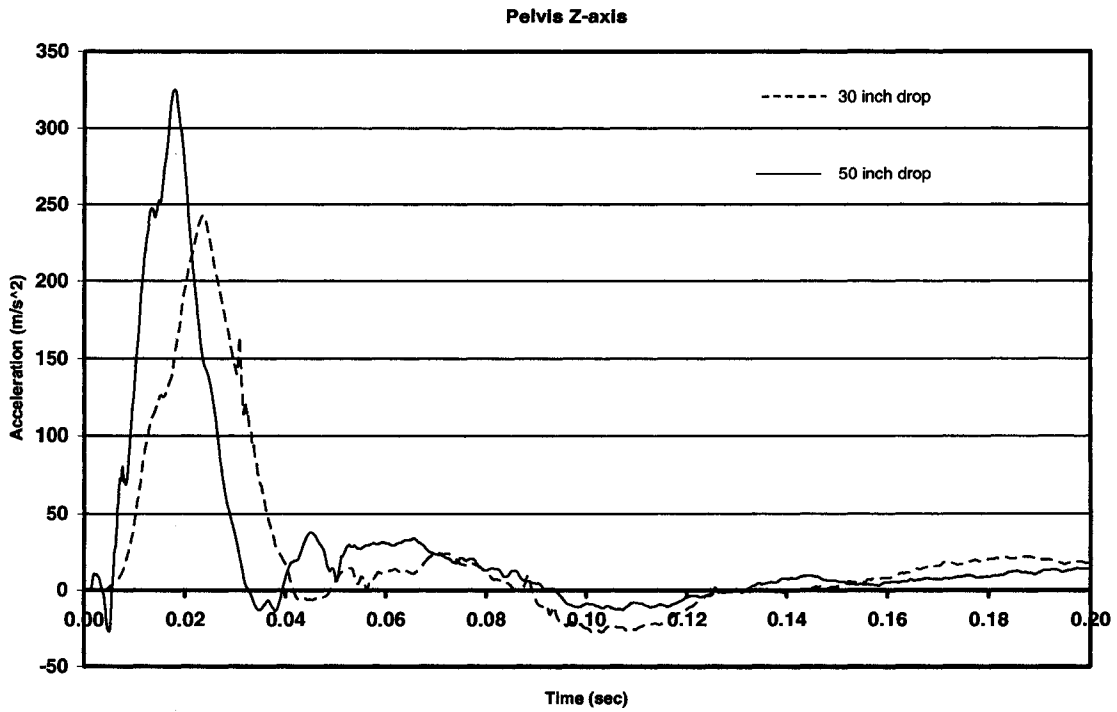


**Figure 26** Measured Pelvis z-Axis Acceleration for 30-in. and 50-in Drops

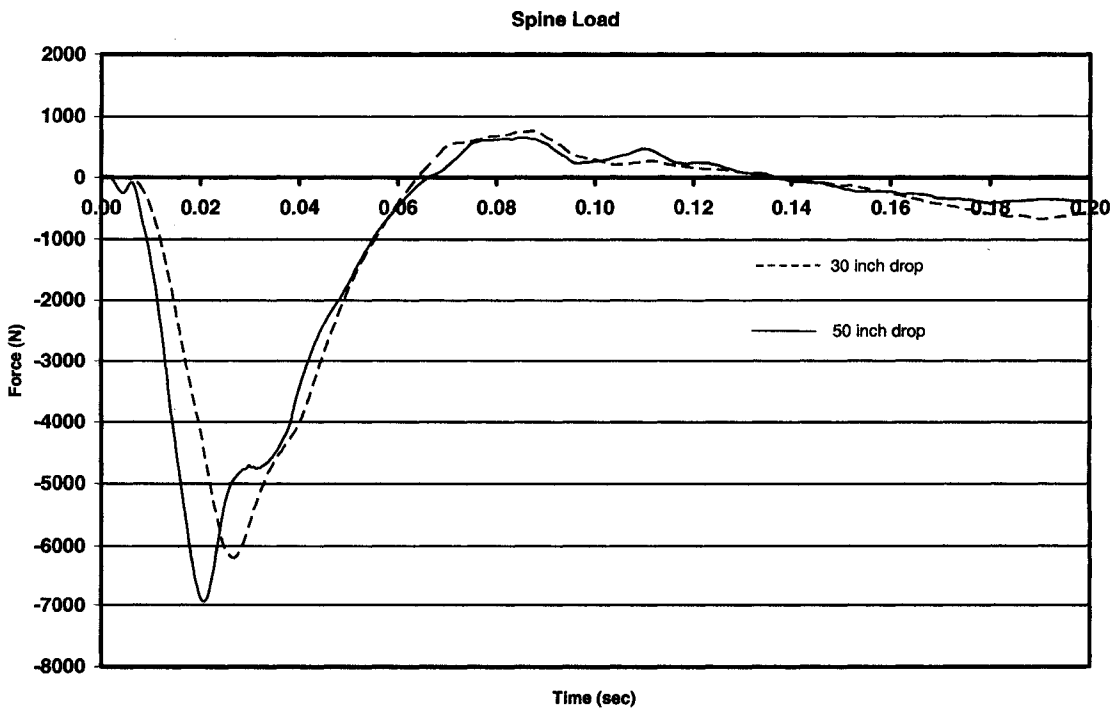


**Figure 27** Measured z-Axis Spine Load for 30-in. and 50-in. Drops

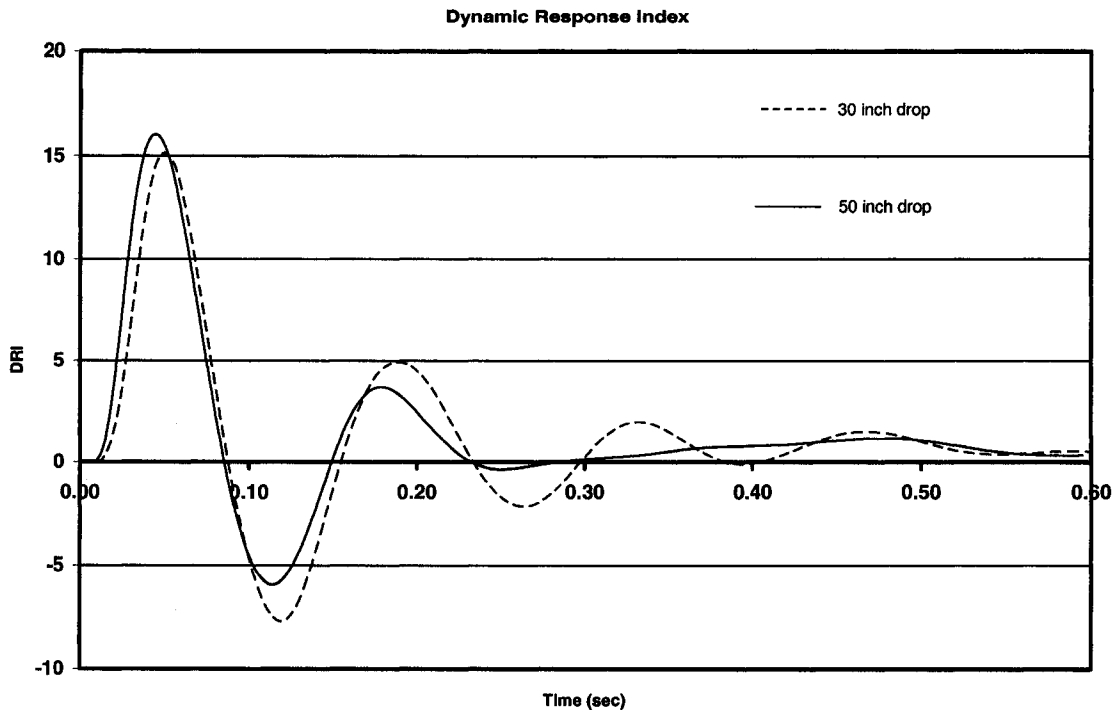


**Figure 28** Calculated z-Axis DRI Values for 30-in. and 50-in. Drops

## CHAPTER 5

### MODEL VALIDATION

The ARL test results for the 0.762 m (30 in) and 1.27 m (50 in) drops discussed in Chapter 4 were used to calibrate the numerical model. These drop tower test results with the air cushion between the ATD and a rigid seat pan were the only two data sets that were available to the UNLV research team. The model was set up to run with the seat pan and seat air bladder directly attached to the vehicle floor, and the initial conditions were applied to all masses in accordance with the velocity reached after falling from the specified drop heights. Table 10 summarizes the initial conditions that were used. The platform (floor) acceleration data supplied by ARL contained free fall acceleration values collected prior to the time of impact. Acceleration values prior to the time of impact were eliminated from the acceleration data. The simulation began at the first time step after the platform impacted the inertia base of the drop tower.

**Table 10** Drop Tower Testing Initial Conditions

<b>Drop Height (meters / inches)</b>	<b>Initial Velocity (m/s)</b>
1.27 / 50	4.85
1.02 / 40	4.17 **
0.76 / 30	3.73

\*\* The 40 inch drop is a numerical calculation and not an actual test point

Contact surface areas between the seat cushion and the human occupant were not available from the test data. The values selected were based on visual observation of test video recordings and measurements of the seat cushion. Table 11 gives the seat cushion geometric properties and the contact areas that were common to all test runs. Table 12 gives some of the model constants related to the geometry of the human body components selected for the model (refer to Figure 12, Chapter 3).

**Table 11** Seat Cushion Constants

<b>Constant</b>	<b>Description</b>	<b>Value</b>
cushMaxZ	Un-deflected cushion bottom thickness	3.625 in (0.092 m)
cushMaxX	Un-deflected cushion back thickness	3.625 in (0.092 m)
vol0	Total original Cushion Volume	2510 in <sup>3</sup> (0.041 m <sup>3</sup> )
volBot0	Volume of un-deflected seat cushion bottom	1174.5 in <sup>3</sup> (0.019 m <sup>3</sup> )
SeatArea	Contact area of occupant bottom and seat cushion	324 in <sup>2</sup> (0.209 m <sup>2</sup> )
backArea	Contact area of occupant upper back and seat cushion back	216 in <sup>2</sup> (0.139 m <sup>2</sup> )
pelvisArea	Contact area of occupant lower back and seat cushion back	216 in <sup>2</sup> (0.139 m <sup>2</sup> )
gamma	Ratio of specific heats for air	1.4

**Table 12 Human Body Geometry**

Constant	Description	Value
$M_2$	Leg mass	12 kg
$M_3$	Pelvis mass	8.18 kg
$M_4$	Upper torso mass	32.52 kg
$J_{A_{mass3}}$	Mass moment of inertia of pelvis about point A	1.65 Kg-m <sup>2</sup>
L1	distance point A to c.g. legs	0.45 m
L2	distance point A to cushion bottom force	0.30 m
L3	length of leg-seat interface	0.60 m
H1	distance point A to c.g. pelvis	0.15 m
H2	distance point A to top of pelvis	0.20 m
H3	distance top of pelvis to c.g. upper torso	0.30 m

### 5.1 Model Comparisons

The x- and z-axis of the dummy pelvis accelerometer were compared to the x- and z-axis accelerations of  $M_3$  from the model. The z-axis of the dummy spine load cell was compared to the spring + damping force between  $M_3$  and  $M_4$ . Information provided by the Army Research Laboratory indicated that the Thor III ATD has an attenuation factor of approximately 30% from input values, meaning a z-axis acceleration of 100 g's at the dummy seated surface would register as 70 g's at the dummy pelvic accelerometer. This is likely due to flexibility of the ATD's materials and the sensor mountings. The masses in the numeric model are completely rigid and do not take into account the response of the ATD; therefore, comparisons between measured data and model predictions will be

offset by the ATD attenuation. To eliminate this gap, all accelerations and forces generated by the model are reported at 70% of full value. The calculated DRI is based on attenuated acceleration input in order to compare the value to the DRI curve calculated from the ATD pelvis accelerometer. The positions of the masses; however, are reported at 100% of calculated values as they pertain to total motion of the seat and occupant and are not subject to measurement offset.

Results for the 30 in. (0.762m) drop model validation run are listed in Table 13. Figures 29 and 30 show comparisons of the x- and z-axis pelvic accelerations predicted by the model with the 30 in. (0.762m) drop test data for varied damping constants of the cushion. The “medium” damping case represents the damping values finally selected for use. The predicted peak values for pelvic acceleration are within 9% and 14% of the measured data z-axis and x-axis values, respectively. Closer agreement of peak values may be achieved at the expense of wider or narrower pulse widths. Further testing will allow for more accurate tuning of the model. The predicted accelerations for both axes lead their corresponding measured data. The time delay is assumed to be representative of the time gap between the acceleration wave impinging on the pelvis and the sensor measuring it. The rigid body model has an ideal response, with all points moving at the same time. Figure 31 and Figure 32 show the comparison of the spine load and DRI predictions with measured test data. Peak spine load is in good agreement with the measured data (-1.9%). This is exceptionally good considering the highly simplified model of the spine that was used in the model. The DRI peak level also agrees well (+4%). The time traces of both model predictions compared reasonably well with their corresponding measured data.

**Table 13** 0.762m (30 in) Drop Model Validation Results

Output	Pelvic Acceleration X - Axis (m/s <sup>2</sup> )	Pelvic Acceleration Z - Axis (m/s <sup>2</sup> )	Spine Load (N)	DRI
Measured	74.0	242.8	-6191.9	15.1
Predicted	83.9	264.6	-6041.7	14.4
Percent Error	13.4	9.0	2.4	4.6

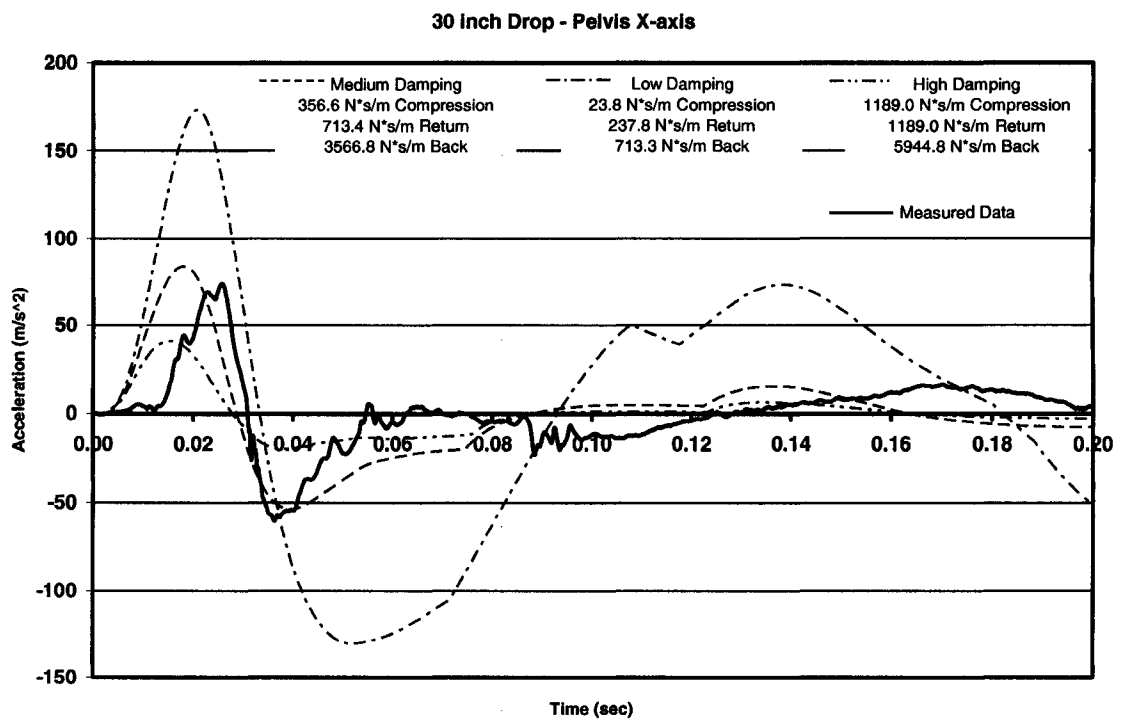


**Figure 29** Model Comparison of x-axis Pelvis Acceleration, 30 in. drop

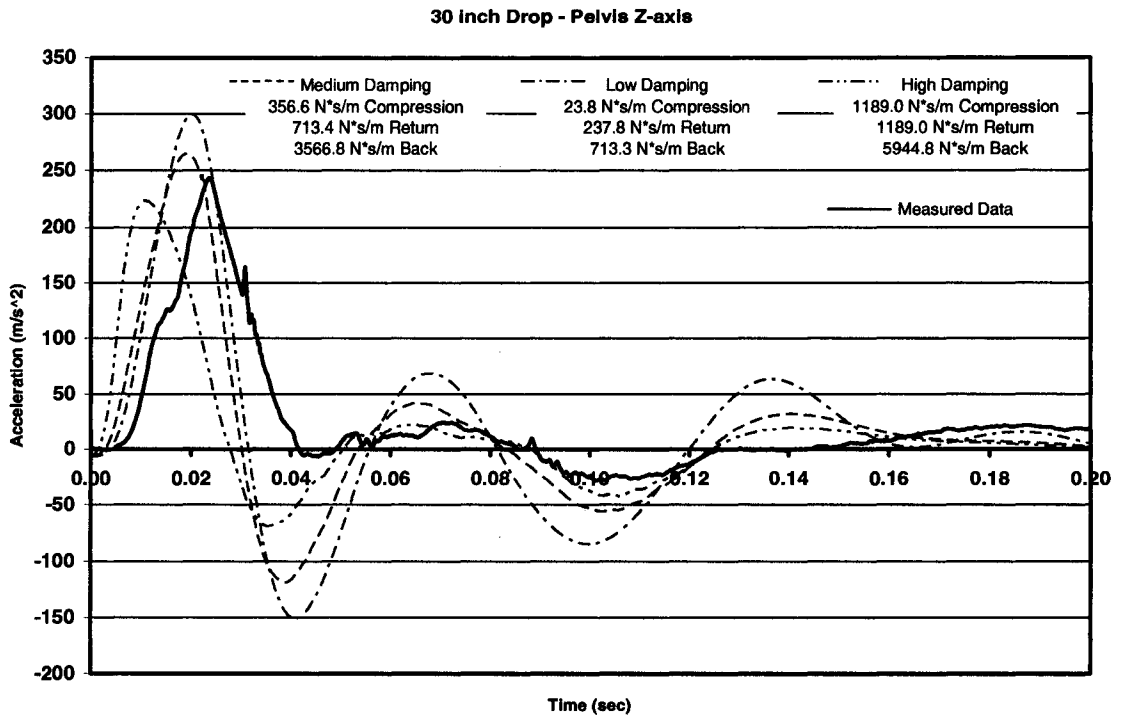


**Figure 30** Model Comparison of z-axis Pelvis Acceleration, 30 in. drop

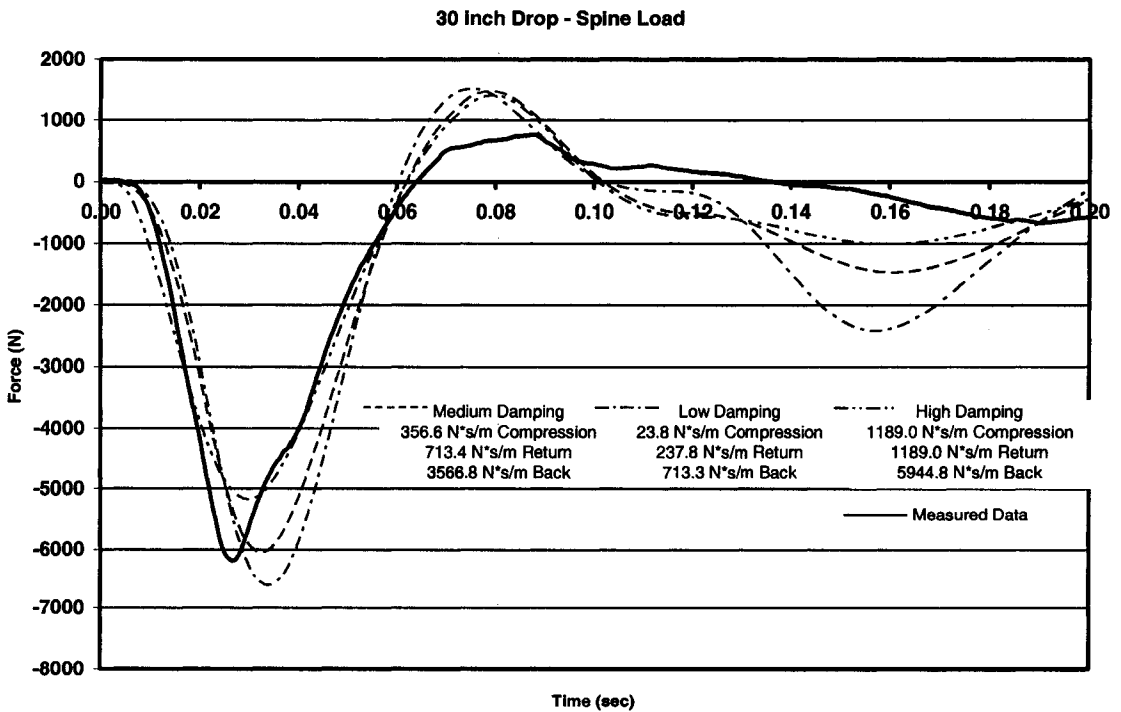


**Figure 31** Model Comparison of Spine Load, 30 in. drop

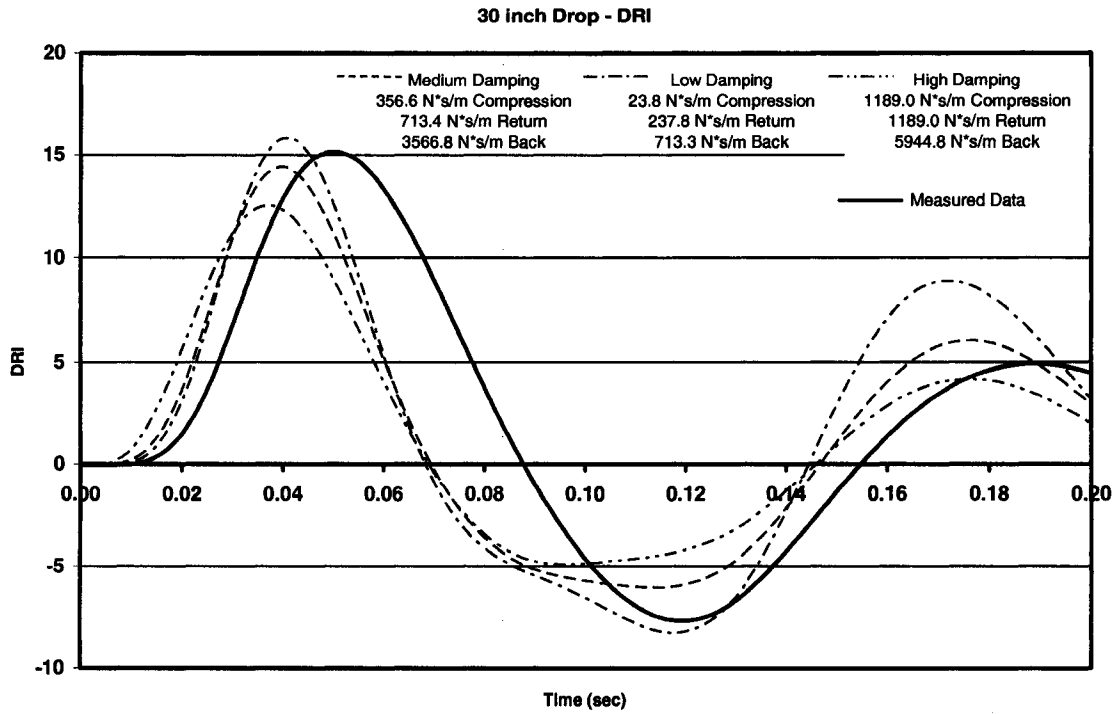


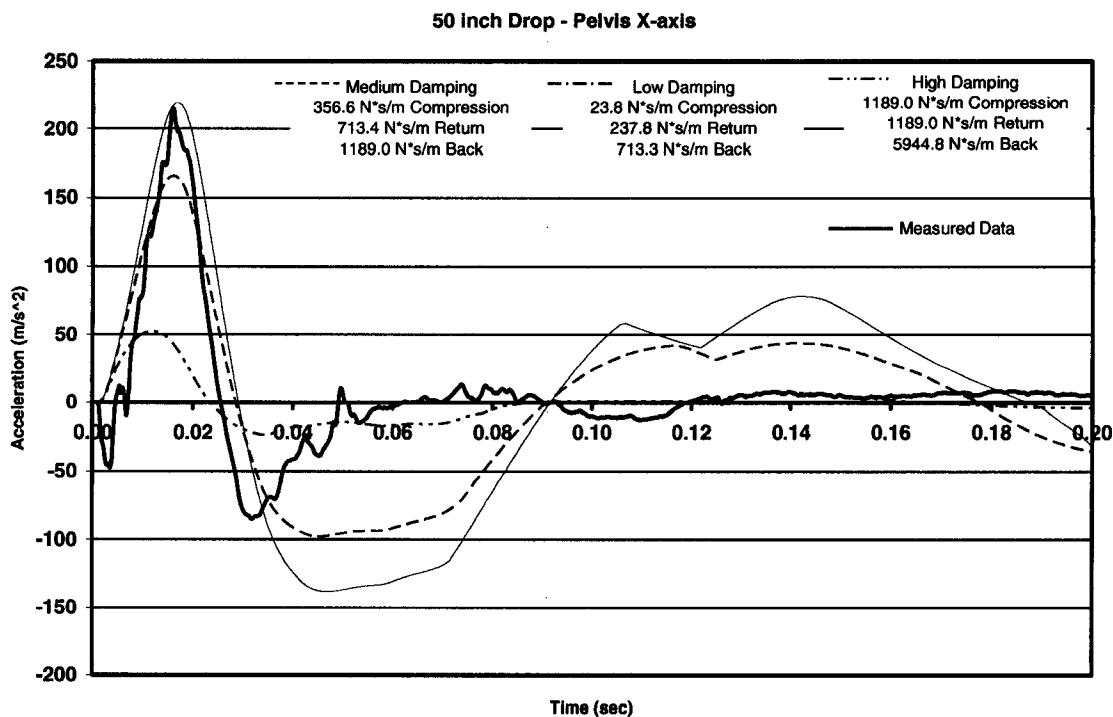
**Figure 32** Model Comparison of DRI, 30 in. drop

The next set of plots (Figures 33-36) represents the same series of comparisons for the 50 in. (1.27 m) drop. The test results are summarized in Table 14.

**Table 14** 1.27m (50 in) Drop Model Validation Results

Output	Pelvic Acceleration X - Axis (m/s <sup>2</sup> )	Pelvic Acceleration Z - Axis (m/s <sup>2</sup> )	Spine Load (N)	DRI
Measured	215.5	324.9	-6946.1	16.0
Predicted	166.0	318.8	-6984.4	16.9
Percent Error	23.0	1.9	0.6	5.6

The percent difference for the peak x-axis accelerations was -23%, which is due to the simplification of the model concerning frictional contact between the legs and the seat bottom (see discussion below). The acceleration peak can be forced to be equal to the measured peak, but the seat belt gives a corresponding return acceleration not seen in the measured data. It is believed that the ATD “submarines” the seat belt a small amount during the test, which accounts for the relatively small measured negative x-acceleration. The peak z-axis acceleration prediction is within 2%. The peak spine load and DRI levels are 1% and 6% greater than the measured data.



33 Model Comparison of x-axis Pelvis Acceleration, 50 in. drop

Figure

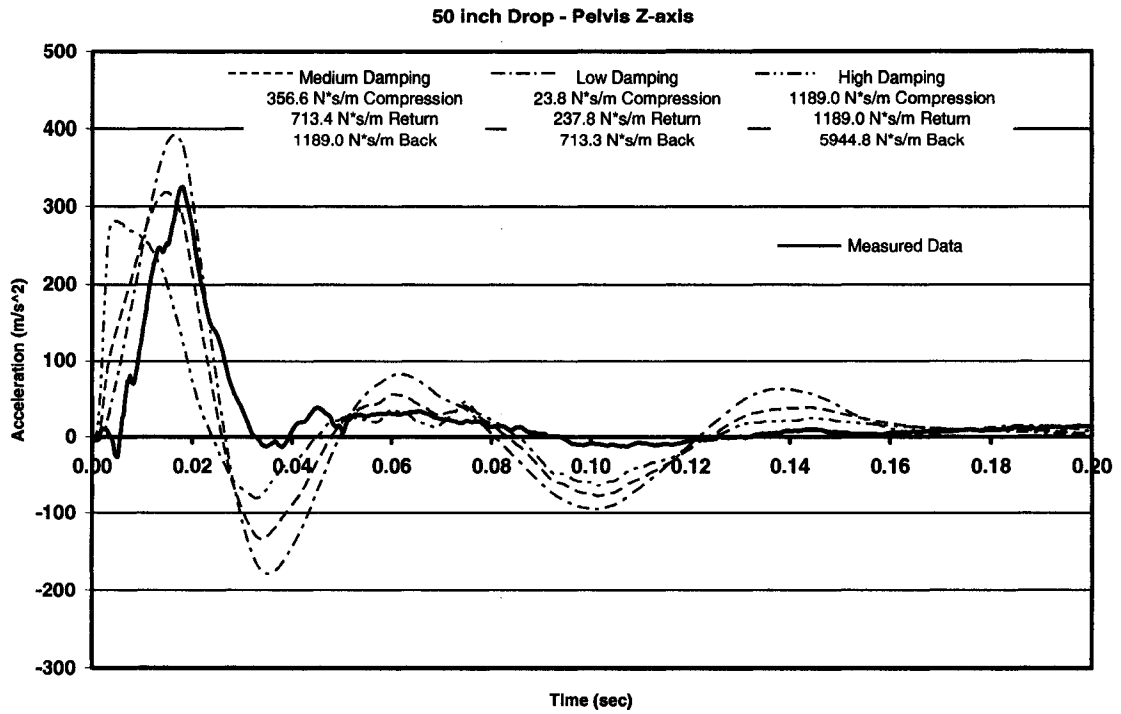


**Figure 34** Model Comparison of z-axis Pelvis Acceleration, 50 in. drop

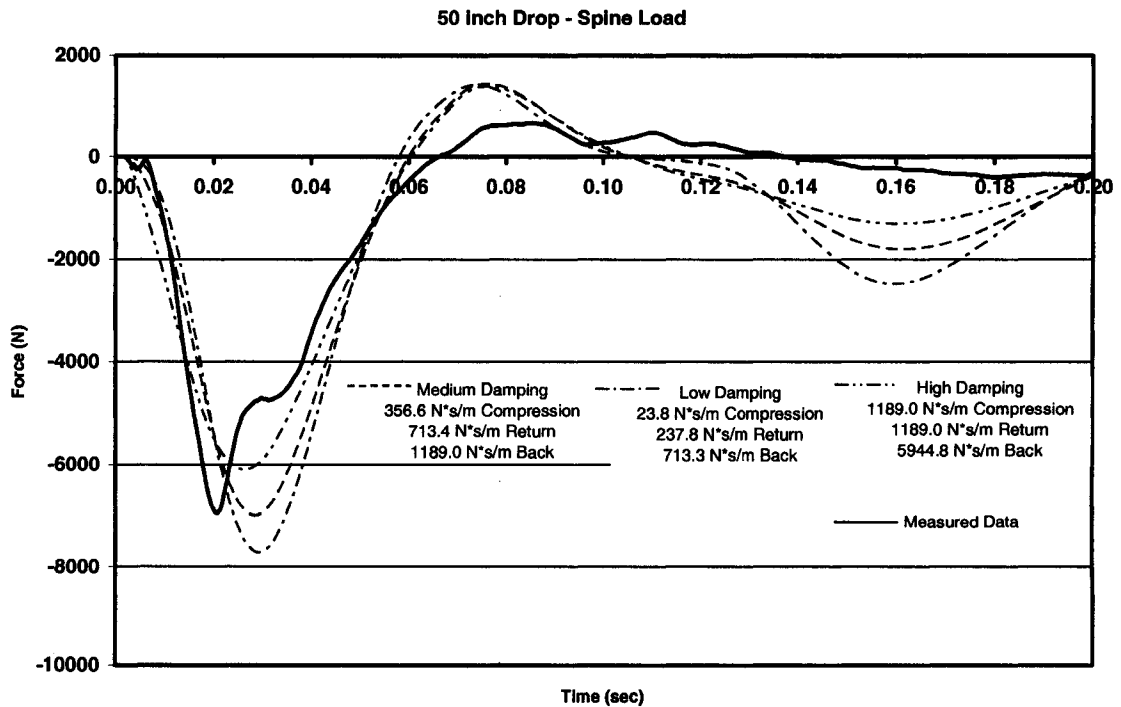


**Figure 35** Model Comparison of Spine Load, 50 in. drop

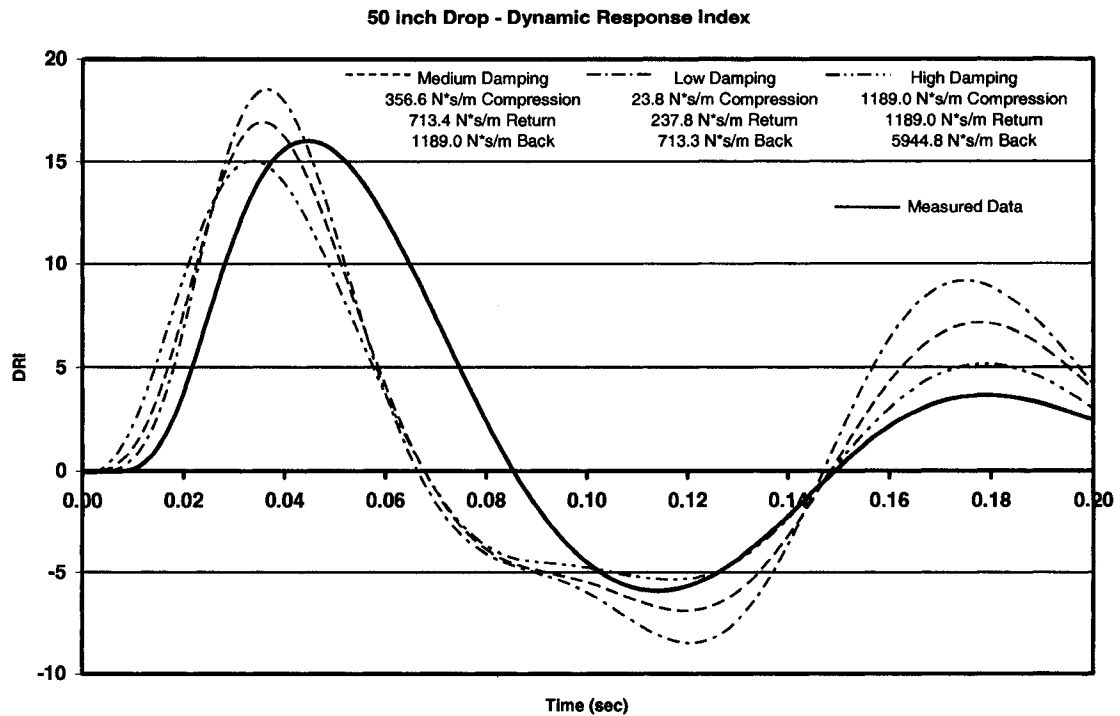


**Figure 36 Model Comparison of DRI, 50 in. drop**

### 5.1.1 Damping Constants

Damping forces inside the cushion and frictional forces on the cushion surfaces are not easily measured. Therefore, some assumptions were made about their nature. It was decided to treat both types of damping as linear and to add their effects together in parallel in the form of a higher damping constant. The seat cushion back and the human occupant were assumed to be in contact at all times, unlike the seat cushion bottom where the occupant was allowed to break contact with the seat (see Chapter 3, Seat Cushion Model). In the preceding plots, the damping constants used with the seat cushion back differed between the two drop heights. This was necessary to account for assumed differences in friction coefficient between the legs and the seat cushion bottom in the x-

axis for the two cases. The sliding friction coefficient is related to the normal force of the body pressing down on the cushion bottom. The normal force will be reduced for higher drops because the occupant rebounds from the seat cushion more quickly. Although the cushion bottom and back sections are internally connected, changes in the bottom damping coefficient had limited effect on the x-axis acceleration. Similarly, changes in the cushion back damping coefficient had little influence on the z-axis accelerations. The damping values were chosen to best match the acceleration profiles and to give realistic positions for the associated masses. The damping ratios and constants selected for the seat cushion bottom and back sections are reported in Tables 15 and 16.

**Table 15** Seat Cushion Bottom Damping Constants

<b>Mode</b>	<b>Damping Ratio <math>\zeta</math></b>	<b>Damping Coefficient (N*s/m)</b>
Compression > 0.5 m/s	0.15	356.6
Recovery	0.30	713.4
Compression < 0.5 m/s	0.30	713.4

**Table 16** Seat Cushion Back Damping Constants

<b>Drop Height</b>	<b>Damping Ratio <math>\zeta</math></b>	<b>Damping Coefficient (N*s/m)</b>
50	0.5	1189.0
40	1.0	713.4
30	2.0	3566.8

## CHAPTER 6

### MODEL RESULTS

The numeric model was used to simulate the shock reduction capabilities of different energy absorbing devices. Test cases included the 0.762m (30in), 1.02m (40in), and 1.27m (50in) drop height input acceleration curves (Figure 22) with the associated velocity curves (Figure 23), displacement curves (Figure 24) and initial conditions (Table 10). Comparison runs were made for the air bladder cushion only, the air bladder with rope spring force limiters, and the air bladder with a crushable honeycomb force limiter.

#### 6.1 Forces and Accelerations

The force deflection performance of these devices was discussed in Chapters 3 and 4. The rope spring had a total available deflection of 2.7 in. (0.068 m). The honeycomb panel had a crushable depth of 3 in. (0.0762 m) and a 2000 lbf (8896 N) load limit. The outputs of the model were the pelvic acceleration in the x and z directions, spine load, and DRI. Tables 17-19 give the peak values of these outputs that are used to determine injury potential for each drop height input. Plots of these outputs are available in Appendix 1 and Appendix 3. Typical plots for the 50 inch drop are presented in Figures 37 through 40. The 50 inch drop was the most severe case of interest to the Army. The

figures clearly show the advantage of using the rope springs and crushable honeycomb force limiter in conjunction with the air bladder seat cushion.

**Table 17** 30 inch Drop Model Predictions

<b>Output</b>	<b>Pelvic Acceleration x - Axis (m/s<sup>2</sup>)</b>	<b>Pelvic Acceleration z - Axis (m/s<sup>2</sup>)</b>	<b>Spine Load (N)</b>	<b>DRI</b>
Cushion Only	83.9	264.6	-6041.74	14.4
Cushion + Spring	46.2	149.6	-4210.58	10.1
Cushion + Honeycomb	64.0	205.9	-5026.15	12.0

**Table 18** 40 inch Drop Model Predictions

<b>Output</b>	<b>Pelvic Acceleration x - Axis (m/s<sup>2</sup>)</b>	<b>Pelvic Acceleration z - Axis (m/s<sup>2</sup>)</b>	<b>Spine Load (N)</b>	<b>DRI</b>
Cushion Only	115.9	291.9	-6432.8	15.4
Cushion + Spring	63.5	161.1	-4509.7	10.9
Cushion + Honeycomb	81.0	205.8	-5155.0	12.4

**Table 19** 50 inch Drop Model Predictions

<b>Output</b>	<b>Pelvic Acceleration x - Axis (m/s<sup>2</sup>)</b>	<b>Pelvic Acceleration z - Axis (m/s<sup>2</sup>)</b>	<b>Spine Load (N)</b>	<b>DRI</b>
Cushion Only	166.0	318.8	-6984.4	16.9
Cushion + Spring	96.9	179.2	-5367.6	13.1
Cushion + Honeycomb	102.0	190.7	-5344.4	13.1
Recommended Limit	N/A	225.5	6672	17.8

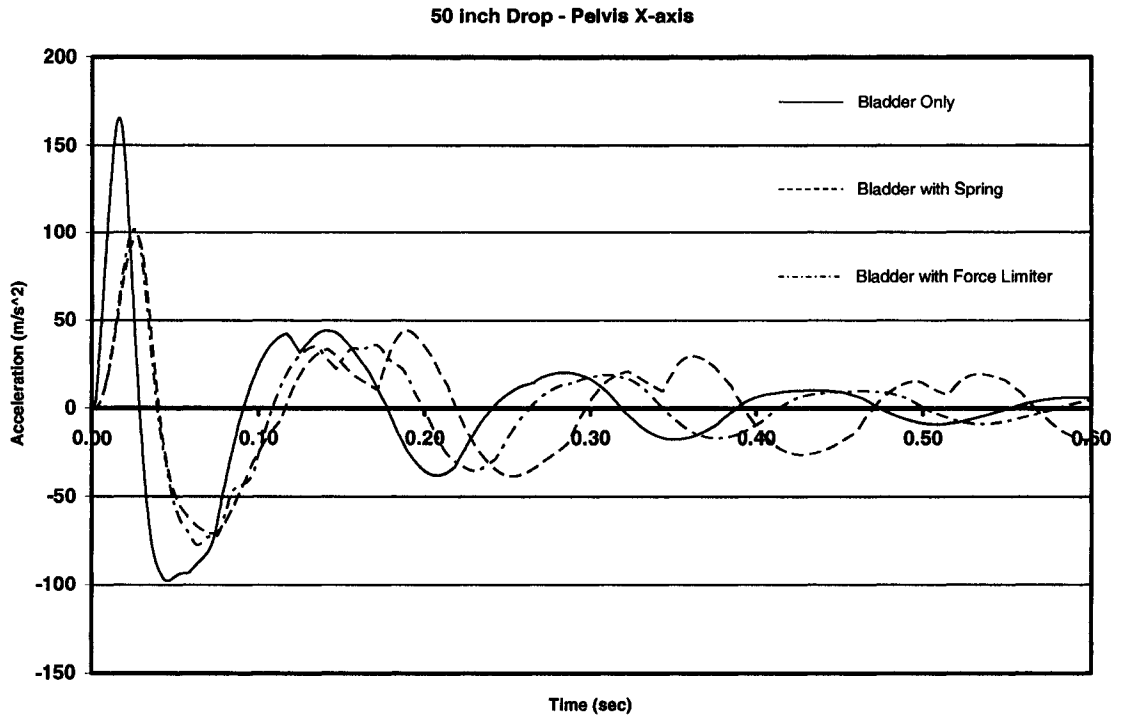


**Figure 37** 50 inch drop force limiter comparison, Pelvis x-axis acceleration

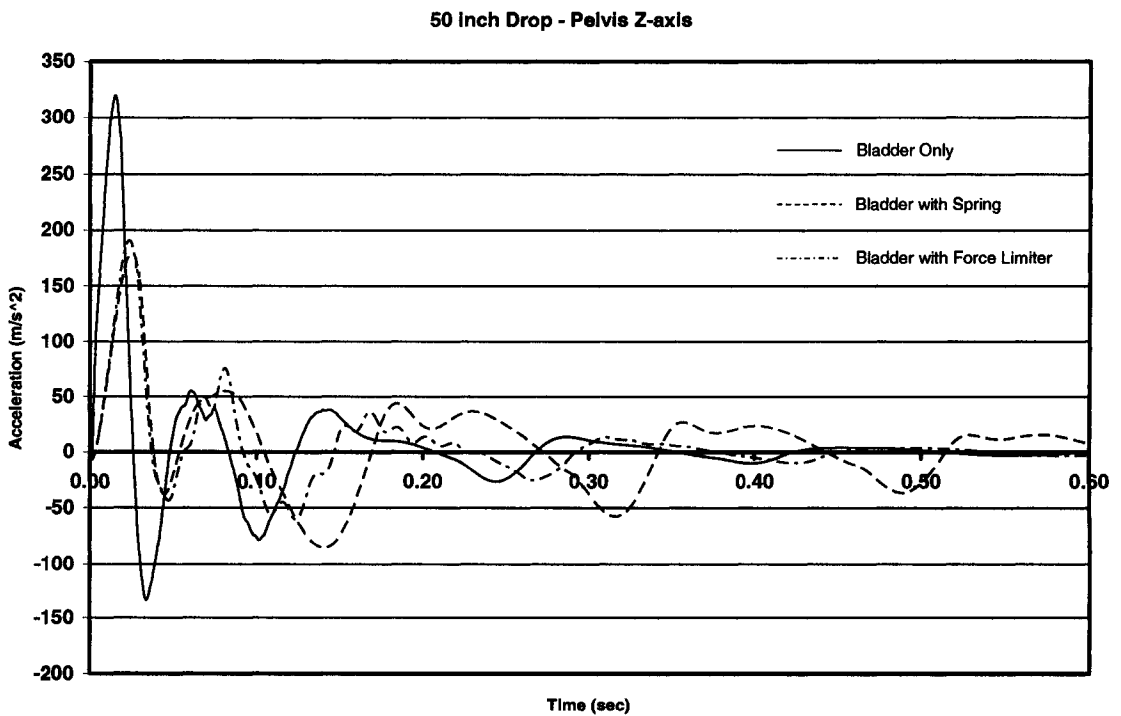


**Figure 38** 50 inch drop force limiter comparison, Pelvis z-axis acceleration

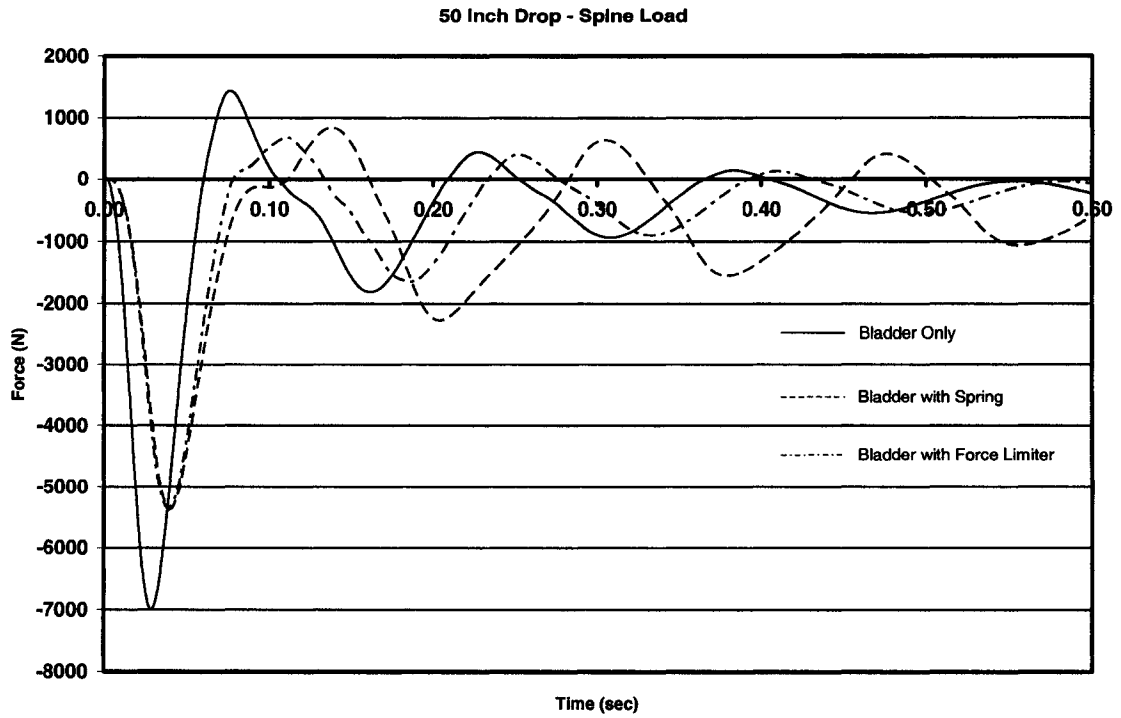


**Figure 39** 50 inch drop force limiter comparison, Spine Load

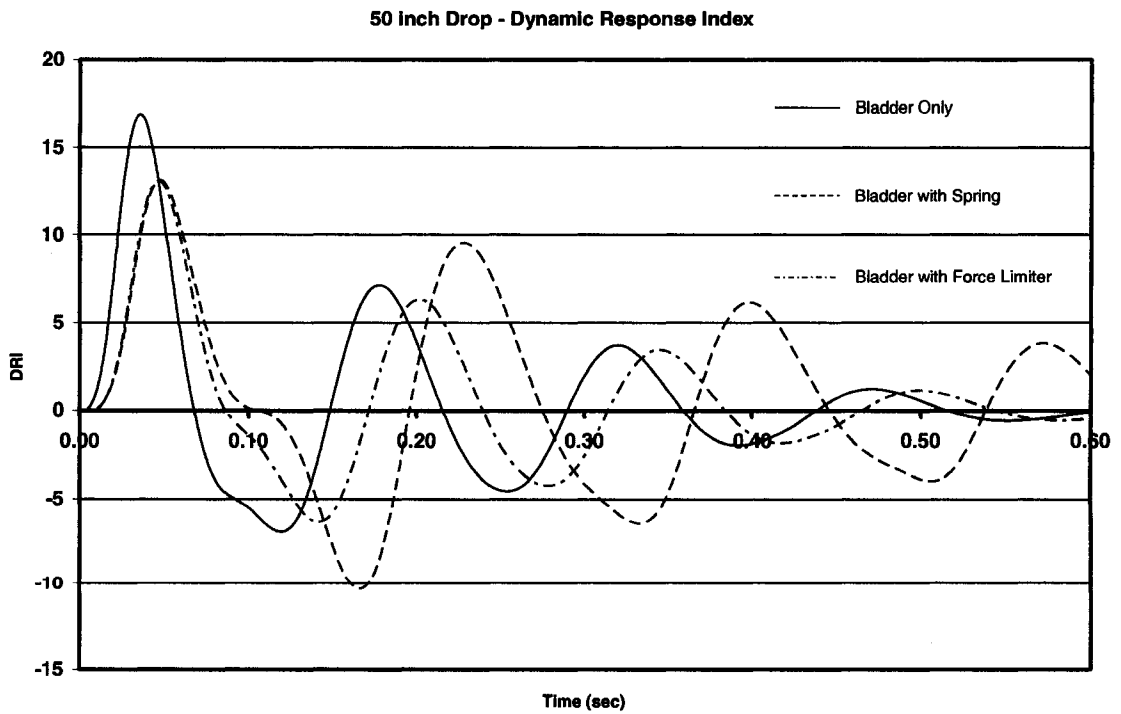


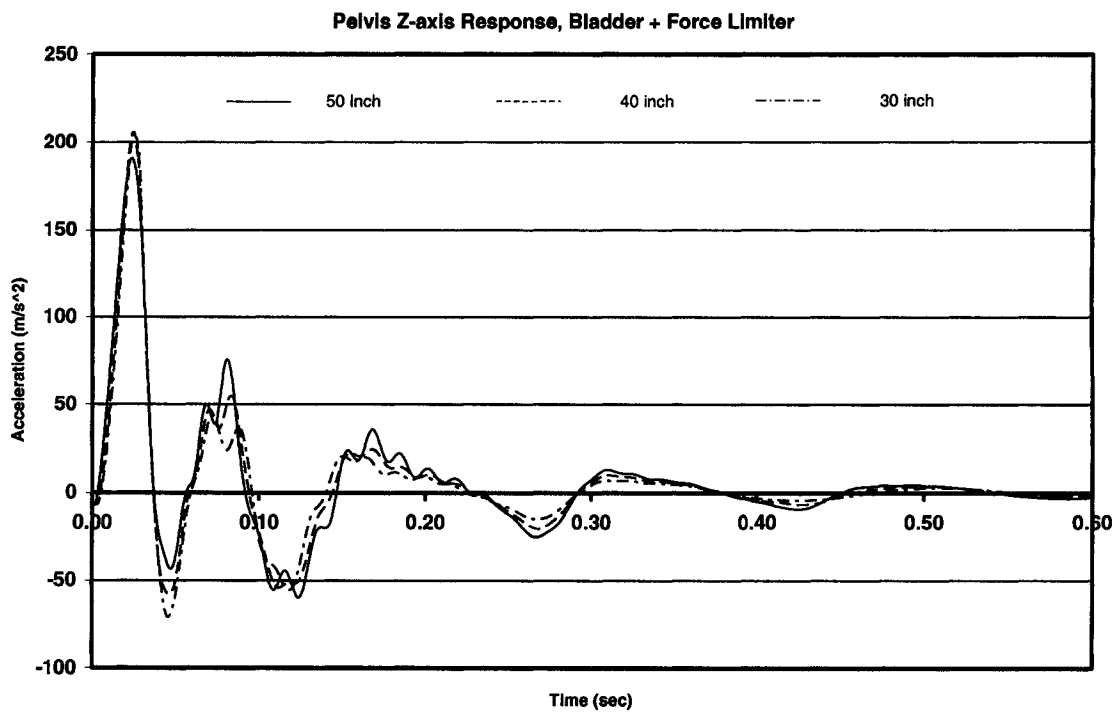
**Figure 40** 50 inch drop force limiter comparison, DRI

The DRI value for the cushion only case for the 50-in. (1.27 m) drop height was 16.9, which is below the NATO limit (17.7). However, the peak z-axis pelvic acceleration is above the Army recommended limit of  $225 \text{ m/s}^2$ . While this acceleration is not high enough to cause soft tissue injury (see chest injury criteria), it highlights an important feature of DRI. The calculation method for determining DRI was designed to blend the effects of peak level and time duration into one “acceleration exposure” number. Because of this, the calculation will assign a low weight to very high accelerations with short durations. The pelvic acceleration time history should be checked to ensure that the level is within human tolerance rather than relying solely on DRI alone.

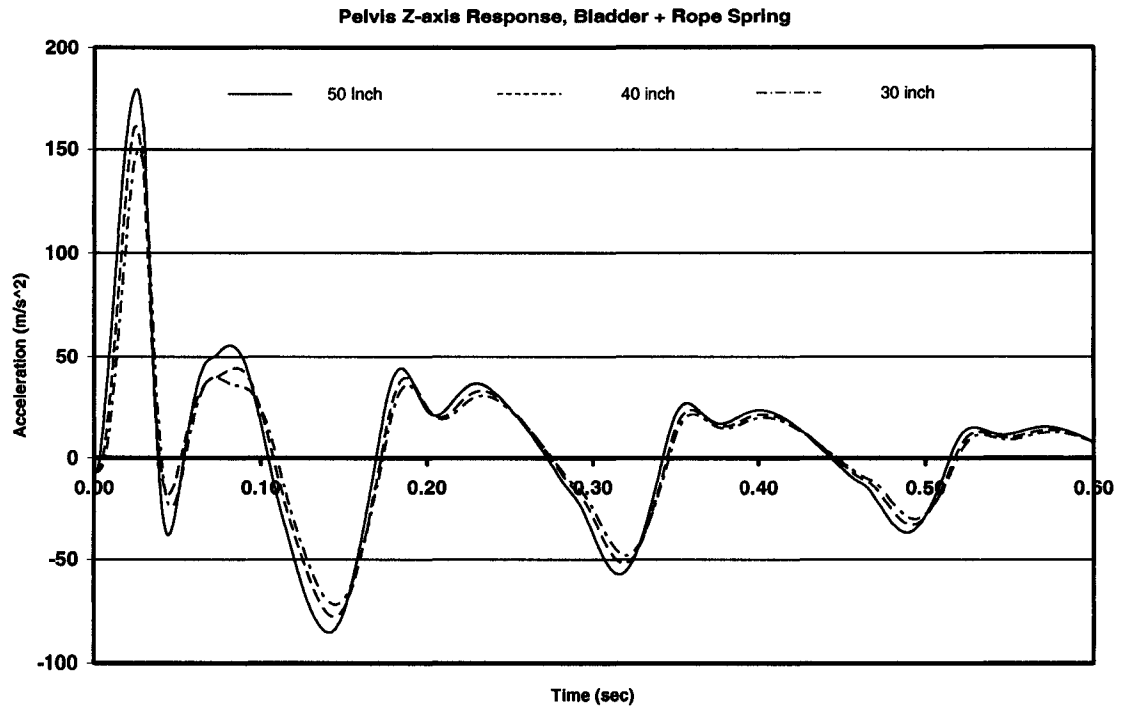
With the use of the cable rope springs and the crushable honeycomb force limiter, the acceleration, spine load, and DRI values were substantially reduced. Figure 37-39 show that there is little difference in terms of accelerations (and consequentially spine forces) between the cable rope spring and the crushable honeycomb force limiter. This is the expected result if either element does not bottom out. A certain acceleration profile is required to match the velocity of the seat occupant with that of the cabin floor. This velocity is the same for each run, so the plots are very close. The air bladder seat cushion alone bottoms out so that the internal foam is crushed and the stiffness is greatly increased. The effect is higher peak accelerations than when either the cable rope spring or the crushable honeycomb force limiter is used.

Figure 41 is a plot of z-axis pelvic accelerations for different drop heights when the crushable honeycomb force limiter is used. It shows that if the input signal is large enough to activate the force limiter, the acceleration profile remains more or less consistent, regardless of input level. If the honeycomb material is activated and

functioning as a linear force limiter, the force on the occupant should be equal to the load limit of the panel. The mass of the occupant does not change; therefore, the acceleration profile should be the same. The same plot for the bladder and the rope spring is shown in Figure 42. The rope spring forces are dependant on deflection and the resulting accelerations will change with the input level.



**Figure 41** Pelvis Acceleration, z-axis, Bladder + Honeycomb Force Limiter



**Figure 42 Pelvis Acceleration, z-axis, Bladder + Spring**

## 6.2 Displacements

The main difference between the cable rope spring and the crushable honeycomb force limiter can be seen in plots of the absolute position of the pelvis. The positions of the pelvis in the z direction are presented in Figures 43-45 for the 50-in. (1.27 m) drop height. Figure 46-47 show the corresponding compression distances for the air bladder seat cushion, cable rope spring, and crushable honeycomb force limiter. Appendix 2 contains a complete set of plots for all three drop heights. The curves labeled “Bladder Only” refer to cases where the air cushion is used on top of the seat pan, which is rigidly connected to the vehicle floor. The curves labeled “Bladder with Spring” represent an air cushion placed on the seat pan and a coil spring installed beneath the seat pan. The

curves labeled “Bladder with Force Limiter” apply to an air cushion on the seat pan and a crushable honeycomb panel installed below the seat pan. The cable rope spring stores energy and spreads out the acceleration profile in time so that the peak level is lowered. This achieves the goal in terms of injury prevention; however, even though the spring has some damping associated with it, the bulk of the stored energy is returned to the occupant during recovery. In the case of the 50 inch (1.27 m) drop, the maximum spring back was approximately 1 in (0.02 m) (See Figure 44 between 0.10 and 0.20 s.). This spring back effect, although tolerable in terms of acceleration, may result in the crewmember impacting the roof of the vehicle. The seat cushion air bladder alone has relatively little spring back, confirmed by the pelvis z-axis position plot and video test recordings. The crushable honeycomb force limiter is designed to have negligible spring back.

The rotation of the pelvis that is shown in Figure 45 is less than 5 degrees for all cases, except the air cushion alone where it is approximated 5.3 degrees. This is an important condition to be met in order to use the DRI scale recommended by NATO. The overall rotation of the pelvis can be adjusted in the model by selecting a stiffer pelvis spring ( $K_{\text{pelvis}}$  in Figure 11); however this will also affect the x- and z-axis acceleration values.

50 inch drop - Pelvis Position X-axis

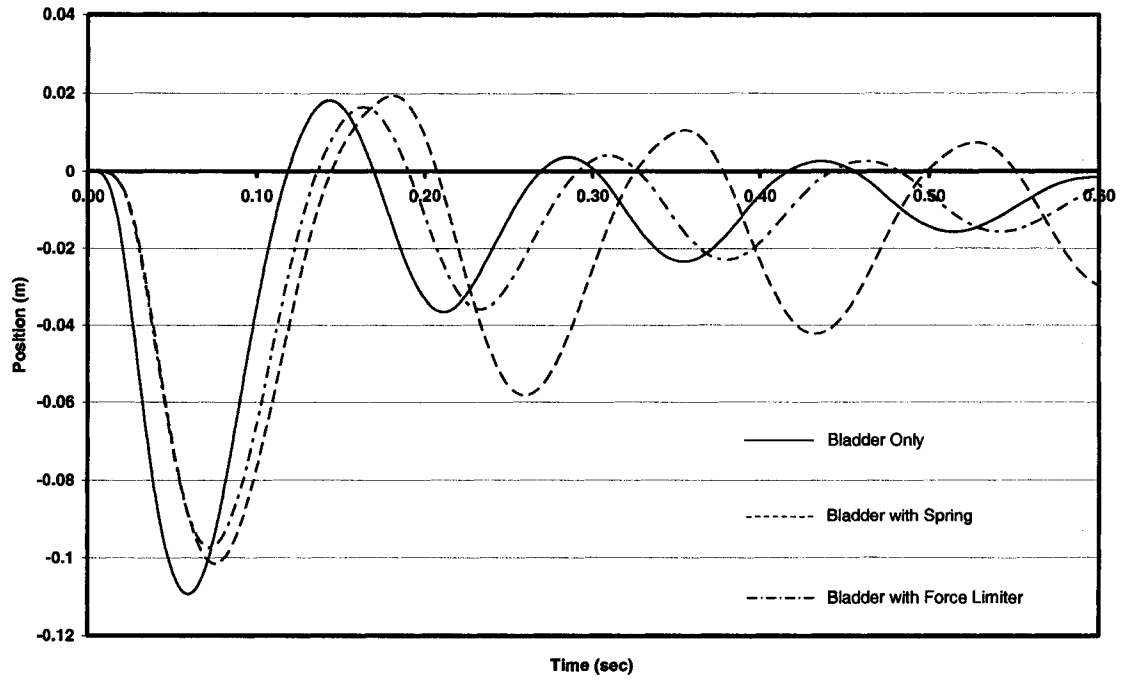


Figure 43 50 inch drop, Pelvis Position x-Axis

50 inch drop - Pelvis Position Z-axis

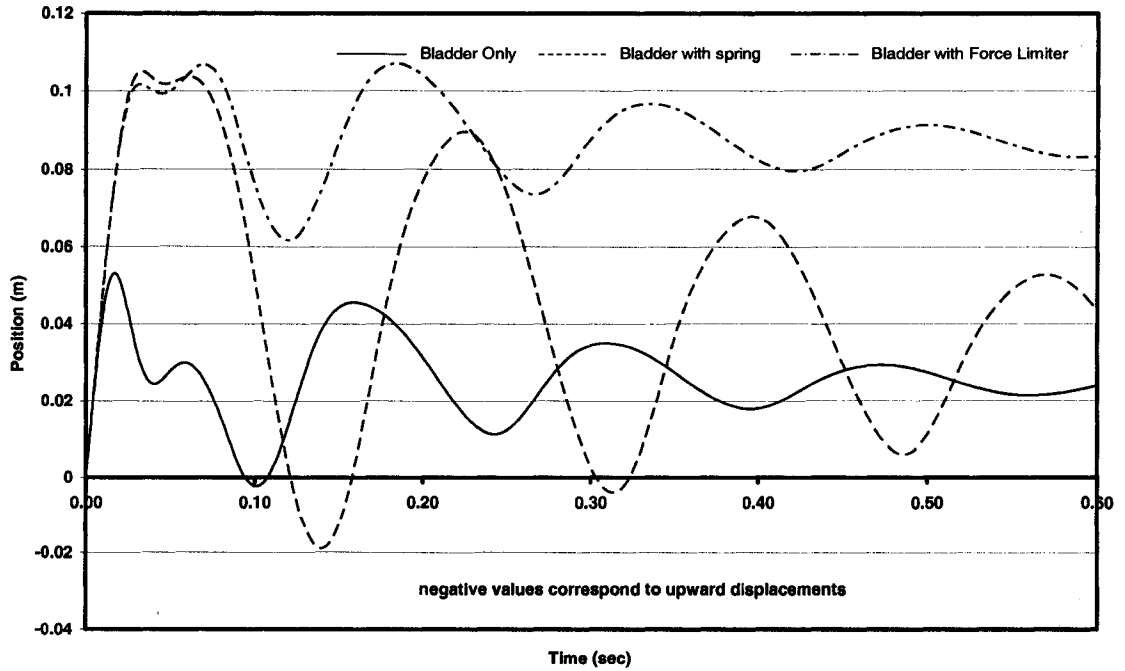
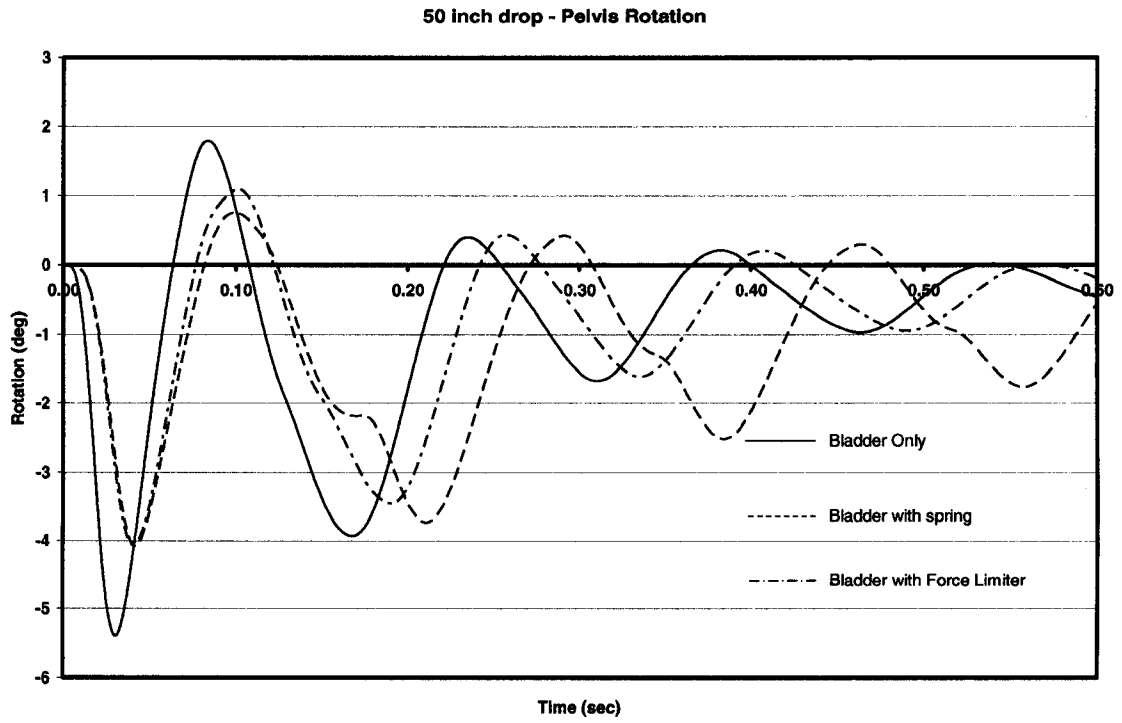
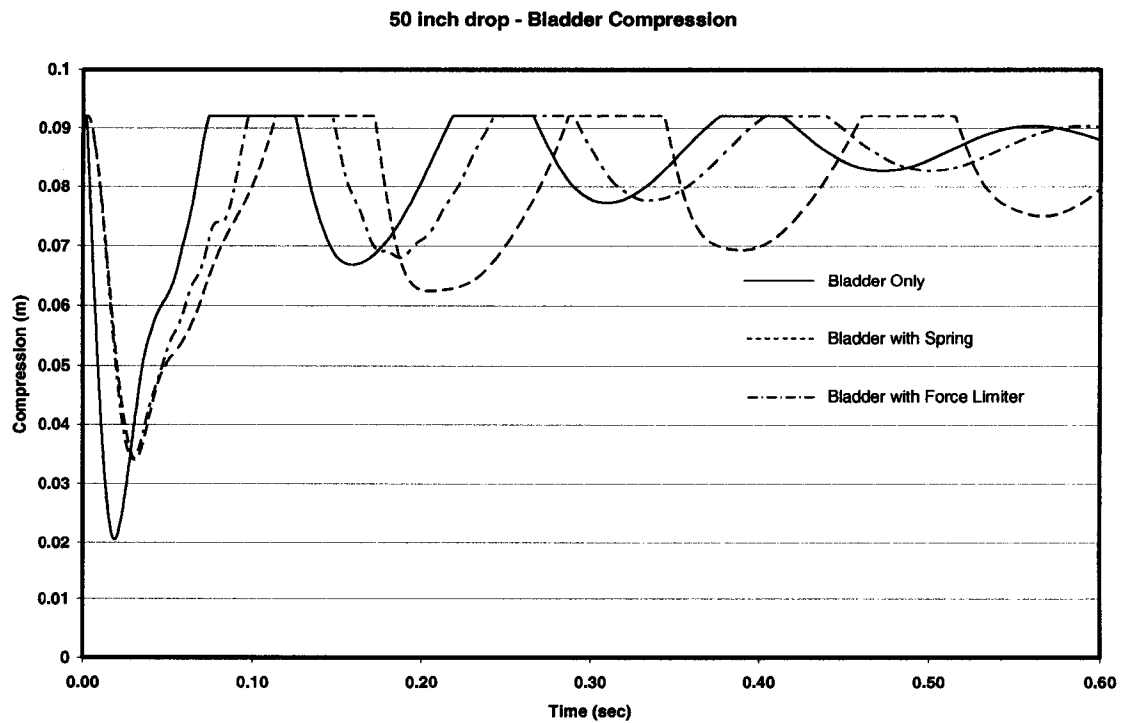


Figure 44 50 inch drop, Pelvis Position z-Axis



**Figure 45** 50 inch drop, Pelvis Position  $\theta$ -Axis



**Figure 46** 50 inch drop, Bladder Compression

50 inch drop - Spring Compression

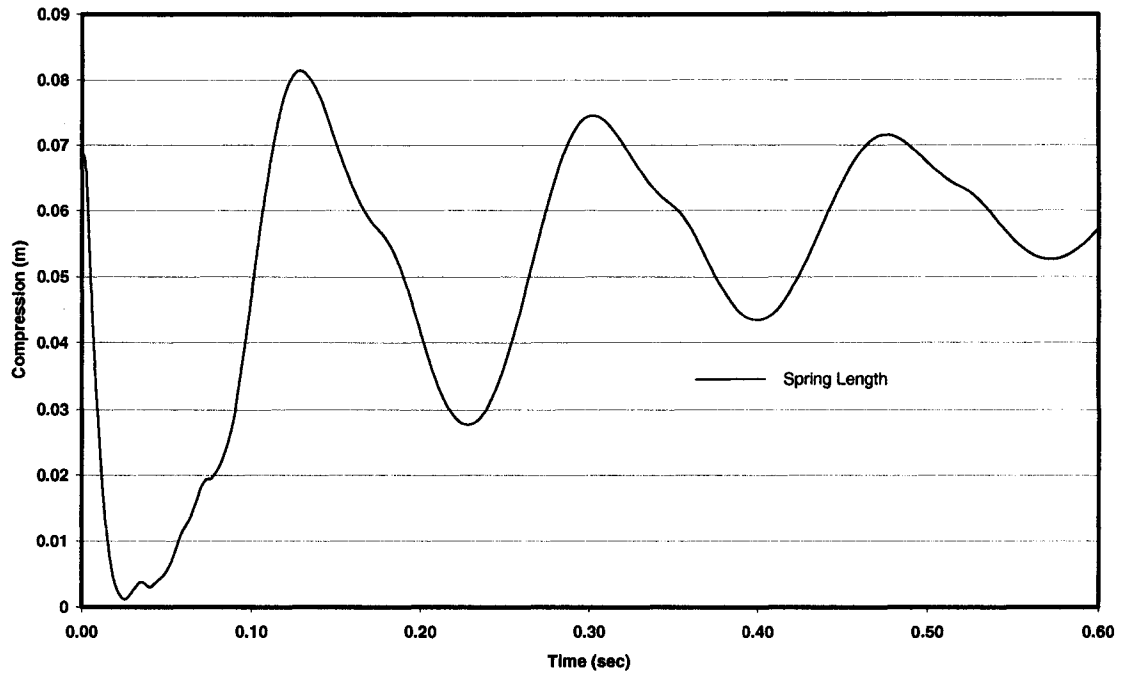


Figure 47 50 inch drop, Spring Compression

50 inch drop - Force Limiter Compression

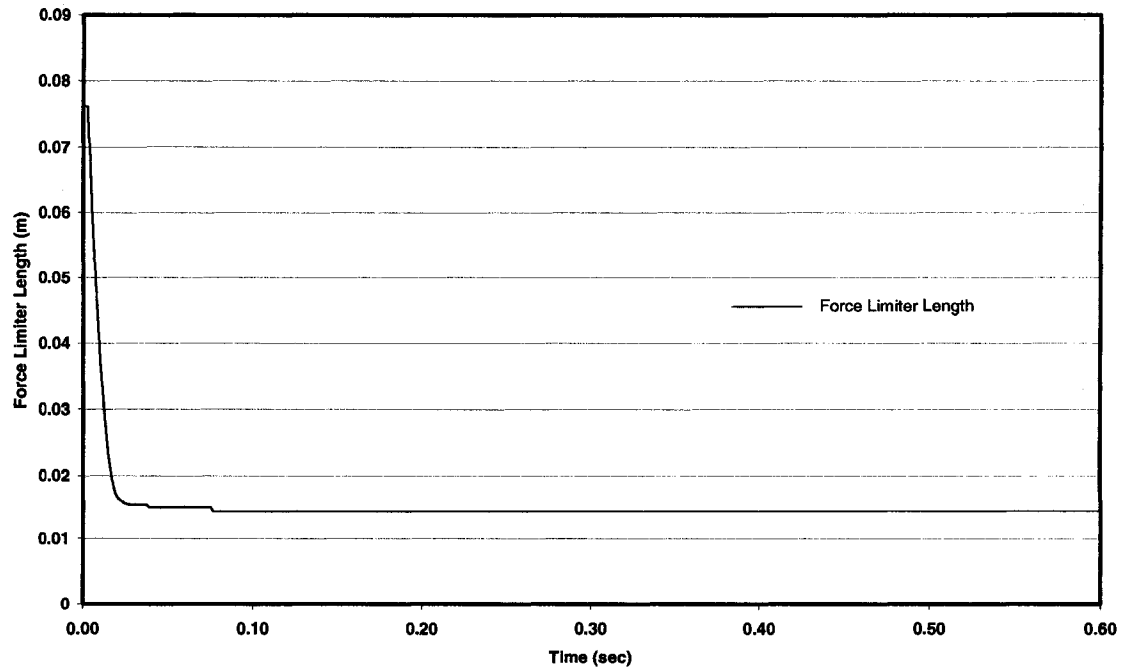


Figure 48 50 inch drop, Honeycomb Compression

The compression of the seat cushion air bladder is understandably greatest when used without either the cable rope spring or the crushable honeycomb force limiter. It does not appear to be completely compressed for the 50-in. (1.27 m) drop height in Figure 46. This is because of the way the air bladder compression is represented mathematically as a single-axis bulk property. Test data indicates that there is local compression under the legs and pelvis that exceeds the overall compression level predicted by the model, but the foam in the cushion cannot be completely compressed to zero thickness.

The plots of the compression distances for the cable rope spring (Figure 47) and the crushable honeycomb panel (Figure 48) show that neither element completely compresses, but that almost all of the available stroke length is used for the chosen physical properties of each element. This is ideal for the 50-in. (1.27 m) drop height test case. The properties of these elements (Chapter 3) have been selected to provide acceptable injury protection according to the established injury criteria when exposed to the 1.27m (50in) input. Higher input levels may result in injurious forces; however, according to the Army, the 395-g (3,875 m/s<sup>2</sup>) input already includes an overestimation of the expected mine blast exposure level.

### 6.3 Occupant Weight

The model has been run to ensure that the seat design will function for occupants that are lighter or heavier than the nominal mass used for testing. The lightweight occupant (59.7 kg) was assumed to be 80% of the nominal level (74.7 kg). The heavy occupant was 120% (89.6 kg) of the nominal level. The model outputs for the two cases are shown in Tables 20 and 21 and are plotted in Appendix 4. For the lightweight occupant, the

accelerations and DRI levels are higher and the spine force is lower. The z-axis pelvic acceleration exceeds the maximum limit recommended by the Army even when the honeycomb isolator is used. The cable rope spring results in better performance for this occupant. For the heavy occupant, the spine force increases and the accelerations and DRI decrease. The spine load is within tolerance for both the cable rope spring and the crushable honeycomb force limiter. For the heavy occupant, the honeycomb gives better all around performance.

**Table 20** 50 inch Drop Model Predictions, 80% Occupant Weight

<b>Output</b>	<b>Pelvic Acceleration x - Axis (m/s<sup>2</sup>)</b>	<b>Pelvic Acceleration z - Axis (m/s<sup>2</sup>)</b>	<b>Spine Load (N)</b>	<b>DRI</b>
Cushion Only	180.4	337.3	-6322.7	17.0
Cushion + Spring	102.3	187.7	-4532.9	13.0
Cushion + Honeycomb	127.2	235.9	-5074.5	14.0
Recommended Limit	N/A	225.5	6672	17.8

**Table 21** 50 inch Drop Model Predictions, 120% Occupant Weight

<b>Output</b>	<b>Pelvic Acceleration x - Axis (m/s<sup>2</sup>)</b>	<b>Pelvic Acceleration z - Axis (m/s<sup>2</sup>)</b>	<b>Spine Load (N)</b>	<b>DRI</b>
Cushion Only	155.0	304.2	-7567.8	16.9
Cushion + Spring	112.9	218.0	-5952.2	13.1
Cushion + Honeycomb	84.5	159.3	-5584.8	12.2
Recommended Limit	N/A	225.5	6672	17.8

## CHAPTER 7

### SUMMARY OF RESULTS, CONCLUSIONS AND RECOMMENDATIONS

The research into the development of seat shock isolation system has resulted in two major products, a numerical model and a recommended seat shock isolation design.

#### 7.1 Numerical Model Validation

1. A two-dimensional, five-degree-of-freedom, mass-spring-damper model of the upper legs, thighs, pelvis/lower-torso and upper torso coupled to seat shock isolation system has been developed and validated. The model included the parametric characteristics for a seat cushion air bladder, cable rope springs, and a crushable honeycomb panel load limiter.
2. Features of the model include:
  - a. The model may be tailored to accommodate various seat system component responses and may also be adjusted for different occupant weights and geometries.
  - b. The architecture of the model allows for individual runs to be made on the order of a few seconds, making it an ideal design tool for the assessment of seat system components.
  - c. The inputs to the model are the initial velocities and positions of each mass representing the seat system and occupant. The model can also accept any

acceleration profile of the vehicle floor, provided it is evenly spaced and of sufficiently small time step.

- d. The outputs of the model are the positions, velocities, and accelerations of the system masses, the forces of the connecting elements, such as the seat cushion force, the load limiter force, and spinal force, and the Dynamic Response Index based on pelvic z-axis acceleration.
3. With regard to a 118 g ( $1,158 \text{ m/s}^2$ ) peak 10 ms shock input to the seat system with only the seat cushion air bladder, the deviation between the measured and predicted x-axis pelvis acceleration was 13.4 percent. The deviation for the z-axis acceleration was 9 percent. The deviation for the spinal load was 2.4 percent. The deviation for the DRI was 4.6 percent.
4. With regard to a 395 g ( $3,875 \text{ m/s}^2$ ) peak 5 ms shock input to the seat system with only the seat cushion air bladder, the deviation between the measured and predicted x-axis pelvis acceleration was 23 percent. The deviation for the z-axis acceleration was 1.9 percent. The deviation for the spinal load was 0.6 percent. The deviation for the DRI was 5.6 percent.

## 7.2 Numerical Model Results

1. With regard to a 118 g ( $1,158 \text{ m/s}^2$ ) peak 10 ms shock input to the seat system with only the seat cushion air bladder, the z-axis pelvis acceleration was  $264.6 \text{ m/s}^2$ , which slightly exceeded the acceleration of  $225.6 \text{ m/s}^2$  allowed by the U.S. Army. The spine load was 6,041.7 N, which was less than the 6,672.3 N allowed by the U.S. Army.

The DRI was 14.4, which was less than the DRI of 18 allowed by the U.S. Army and the DRI of 17.7 allowed by NATO.

2. With regard to a 395 g (3,875 m/s<sup>2</sup>) peak 5 ms shock input to the seat system with only the seat cushion air bladder, the z-axis pelvis acceleration was 318.4 m/s<sup>2</sup>, which exceeded the acceleration of 225.6 m/s<sup>2</sup> allowed by the U.S. Army. The spine load was 6,984.4 N, which slightly exceeded the 6,672.3 N allowed by the U.S. Army. The DRI was 16.9, which was less than the DRI of 18 allowed by the U.S. Army and the DRI of 17.7 allowed by NATO.
3. With regard to a 395 g (3,875 m/s<sup>2</sup>) peak 5 ms shock input to the seat system with the seat cushion air bladder and the cable rope springs, the z-axis pelvis acceleration was 179.2 m/s<sup>2</sup>, which is less than the acceleration of 225.6 m/s<sup>2</sup> allowed by the U.S. Army. The spine load was 5,367.6 N, which was less than the 6,672.3 N allowed by the U.S. Army. The DRI was 13.1, which was less than the DRI of 18 allowed by the U.S. Army and the DRI of 17.7 allowed by NATO.
4. With regard to a 395 g (3,875 m/s<sup>2</sup>) peak 5 ms shock input to the seat system with the seat cushion air bladder and the crushable honeycomb panel load limiter, the z-axis pelvis acceleration was 190.7 m/s<sup>2</sup>, which is less than the acceleration of 225.6 m/s<sup>2</sup> allowed by the U.S. Army. The spine load was 5,344.4 N, which was less than the 6,672.3 N allowed by the U.S. Army. The DRI was 13.1, which was less than the DRI of 18 allowed by the U.S. Army and the DRI of 17.7 allowed by NATO.

### 7.3 General Conclusions

1. With regard to the z-axis pelvis acceleration, spine load and DRI, the agreement between the drop tower test results and the corresponding model predictions was good. The comparison with regard to the x-axis pelvis acceleration was marginal. However, the x-axis pelvis acceleration is not used in injury assessment. The application of the dummy response used in the x-axis may be greater than the actual response of the ATD, but no external information was available to quantify the dummy attenuation. The z-axis attenuation factor was used for the x-axis response.
2. A seat shock isolation system with only the seat cushion air bladders when exposed to a 395 g (3,875 m/s<sup>2</sup>) peak 5 ms shock input to the seat system will meet the U.S. Army injury criterion requirement of a maximum DRI of 18 and the NATO injury criterion requirement of a maximum DRI of 17.7. It will not meet the U.S. Army z-axis and spine load injury criteria.
3. A seat shock isolation system with the seat cushion air bladders and with either the cable rope springs or the crushable honeycomb panel load limiter when exposed to a 395 g (3,875 m/s<sup>2</sup>) peak 5 ms shock input to the seat system will meet the injury criteria of the U.S. Army criteria of a maximum z-axis pelvis acceleration of 225.6 m/s<sup>2</sup>, a maximum spinal load of 6,672.3 N and a maximum DRI of 18.
4. A seat shock isolation system with the seat cushion air bladders and with either the cable rope springs or the crushable honeycomb panel load limiter when exposed to a 395 g (3,875 m/s<sup>2</sup>) peak 5 ms shock input to the seat system will meet the NATO injury criterion requirement of a maximum DRI of 17.7.

5. The two-dimensional, five-degree-of-freedom, mass-spring-damper model of the upper legs, thighs, pelvis/lower-torso and upper torso coupled to seat shock isolation system can be used to conduct parametric studies with regard to variation in the system parameters that characterize the seat cushion air bladder and the resilient elements or load limiters that support the seat shock isolation system.
6. The two-dimensional, five-degree-of-freedom, mass-spring-damper model of the upper legs, thighs, pelvis/lower-torso and upper torso coupled to seat shock isolation system can be used to validate and calibrate finite element models of proposed seat shock isolation systems.
7. The assumed values for the seat cushion damping in the z-axis and the cushion back damping and frictional damping in the x-axis had a significant effect on the acceleration response of the model.

#### 7.4 Recommended Seat Design

Two seat shock isolation system concepts have been designed using the numerical model and readily available commercial components. Both designs use air-pneumatic seat cushion technology. For force limiting, one design uses coil rope spring isolators and the other uses an 8896N (2000lb<sub>f</sub>) honeycomb panel force limiter that is sized to fit in current U.S. military vehicle envelopes. Table 22 gives the numerical model predictions for the performance indicators when the seat design with a standard weight occupant is exposed to a 395g peak input with a duration of 5ms, which is typical of mine blast exposure levels.

**Table 22** Model Predictions for Recommended Seat Designs

System	Peak z-axis pelvic acceleration (m/s <sup>2</sup> )	Spine load (N)	DRI
Cushion + Rope Spring	179.2	5368	13.1
Cushion + Honeycomb	191	5344	13.1

These levels are acceptable according to Army and NATO recommendations for the survivability of the seated crewmember exposed to a mine blast. A prototype of the seat system is being assembled at UNLV, and preliminary testing of system components is being performed. A schematic of the prototype seat system fitted with coil rope spring isolators is shown in Figure 49. The same seat with honeycomb panel force limiters is shown in Figure 50.

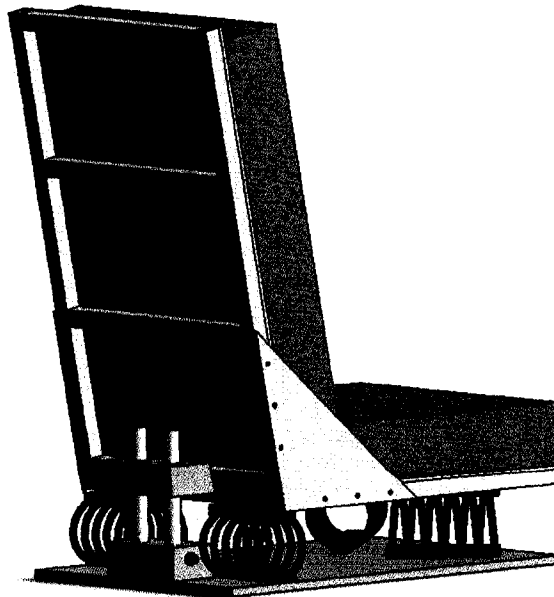


**Figure 49** Prototype Seat Design with Coil Rope Springs

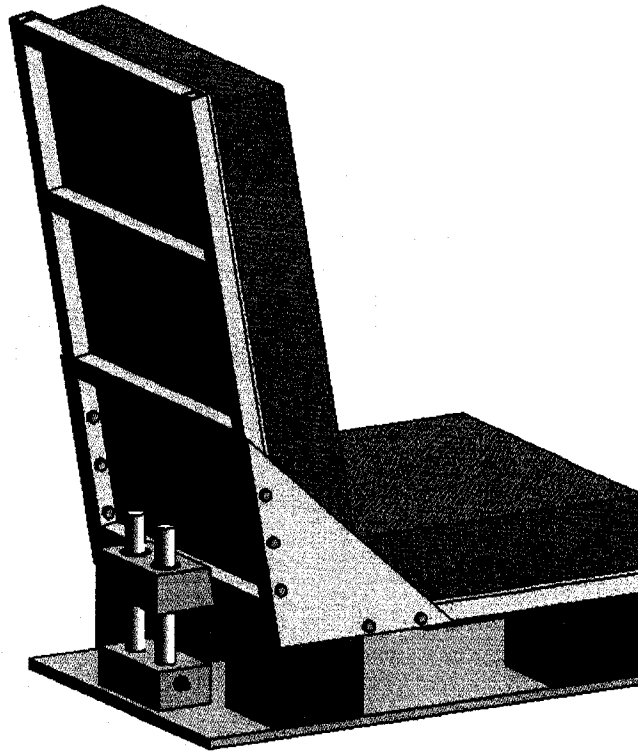


**Figure 50** Prototype Seat Design with Honeycomb Panel Force Limiters

### 7.5 Ongoing Research

Verification of the model predictions for the performance of the prototype seat system will consist of drop tower testing done at the Army Research Lab. The Thor III ATD will be used for these tests and will provide excellent data to fine tune the model. Based on the ARL drop tower testing results, the prototype seat may be approved for actual mine blast exposure testing in a new military vehicle core structure.

The UNLV research team has constructed a drop tower test platform for preliminary evaluation of seat concepts. The data from these tests can also be used for model refinement. A single degree of freedom ATD that has been constructed for UNLV use will be used as the occupant.

Further development of the air seat cushion is also in progress. A variety of foams are being investigated, as well as other methods to control the damping of the cushion. Puncture resistant coverings are also being considered. Once the shock behavior of the new cushions is ascertained, predictive equations can be determined and inserted into the model to calculate the response of the whole seat system.

## 7.6 Recommendations

The numeric model has been designed to mimic the ARL drop tower and Thor III dummy response. Modifications will need to be made to accommodate a different ATD, such as the one currently employed by UNLV. The design of this ATD is much simpler than the Thor III, so the numerical model may only need a single axis to capture all the physics of the ATD response. Tri-axial measurement of the ATD will indicate if a significant cross talk signal is present for the UNLV ATD.

The ARL drop tests were conducted with a zero-degree, full upright back angle of the ATD and the model has been designed accordingly. Most commercial seat designs have a seat back angle of around 10 degrees. The model will need to be modified to include this by altering the statically undeflected position of the hip spring and the initial conditions of the pelvis rotation. It may also be necessary to account for the angular difference between the coordinate frames of the ATD sensors and the absolute coordinate frame of the model if the back angle is increased.

The damping of the air cushion has been difficult to quantify. The internal structure of the air bladder has several variables that can be altered which will affect the damping force. Several test cases will need to be run to determine the relationship of these factors

to the damping response. Modeling the flow of the air inside the cushion may be possible once the damping forces are better understood.

Currently, frictional forces in the x-axis are not handled separately from the cushion back damping. If the test data shows poor agreement in the x-axis, the frictional effects should be decoupled from the cushion damping effects. In order to quantify the sliding friction, estimation of the contact force between the cushion and the occupant and of the contact friction factor will be necessary. This may be complicated by the presence of clothes on the ATD.

Lastly, robust design techniques, in terms of experimental design, will be highly useful in designing the seat system to perform well in a military environment. The basic tenant of robust design is to reduce variability in the performance of the seat system when it is exposed to external noise factors. The weight of the occupant and the strength of the blast are examples of typical noise factors. After the variability in performance has been minimized, the average performance of the seat can be steered to meet operational goals. In order to produce a working prototype seat system in a short time period, the design of the seat system was based on components that were readily available. There were few properties about the components that could be adjusted to significantly affect the system performance, so robust design could not successfully be applied. When the new seat cushion and the force limiting components are available, robust design of experiments will aid in creating an optimal seat system.

## BIBLIOGRAPHY

- [1] Lafrance, L.P., "Mine Blast Protection System for Military Support Vehicles", American Society of Mechanical Engineers PVP, Vol. 361, c1998, pg 305-309
- [2] Coltman, J.W., C. Van Ingen, N.B. Johnson, and R.E. Zimmermann, December 1989. "Aircraft Crash Survival Design Guide Volume II-Aircraft Design Crash Impact Conditions and Human Tolerance.
- [3] Durocher, Robert, Jowz Valley Mine Strike Preliminary Technical Report, Defense research and Development Center, Canada – Valcartier c2003
- [4] Aircraft Crash Survival Design Guide Final Report Volume IV, Aircraft Seats, Restraints, Litters, and Cockpit/cabin Delethalization, USAAVSCOM TR 89-D-22D, Simula Inc., c1989
- [5] Moore H., Testerman R., "Effects of Structural and Occupant Provision Improvements to the Static and Dynamic Response of the V-22 Osprey Energy Attenuating Troop Seating System", Proceedings of 61<sup>st</sup> Annual Forum of the American Helicopter Society, 2005.
- [6] Eichelberger C., "Development of an Energy-absorbing Passenger Seat for a Transport Aircraft", NASA conference publication, 1985, p39-58.
- [7] Labun, Lance C., Rapaport, Martin, "A Third Generation Energy Absorber for Crash Attenuating Helicopter Seating", 50<sup>th</sup> Annual Forum, American Helicopter Society, May 11-13, 1994, p 521-535.
- [8] Richards, Martin K., Podob, Rodger, "Development of an Advanced Energy Absorber", Proceedings of 35<sup>th</sup> Annual Symposium, SAFE Association, Sept 8-10, 1997, p 321-327.
- [9] Volvo press release, "Volvo "Ride-Down" Concept: The Future of Safety", 9 February 2005
- [10] Perry C., Nguyen T., Pint S., "Evaluation of Proposed Seat Cushions to Vertical Impact", Proceedings of Annual Symposium, SAFE Association, 2000, p 50-55.
- [11] Naasz, E., "The Importance of Seat Cushion Design in Energy Absorbing Seat Systems", Proceedings of Annual Symposium, SAFE Association, 2001, p 84-94.

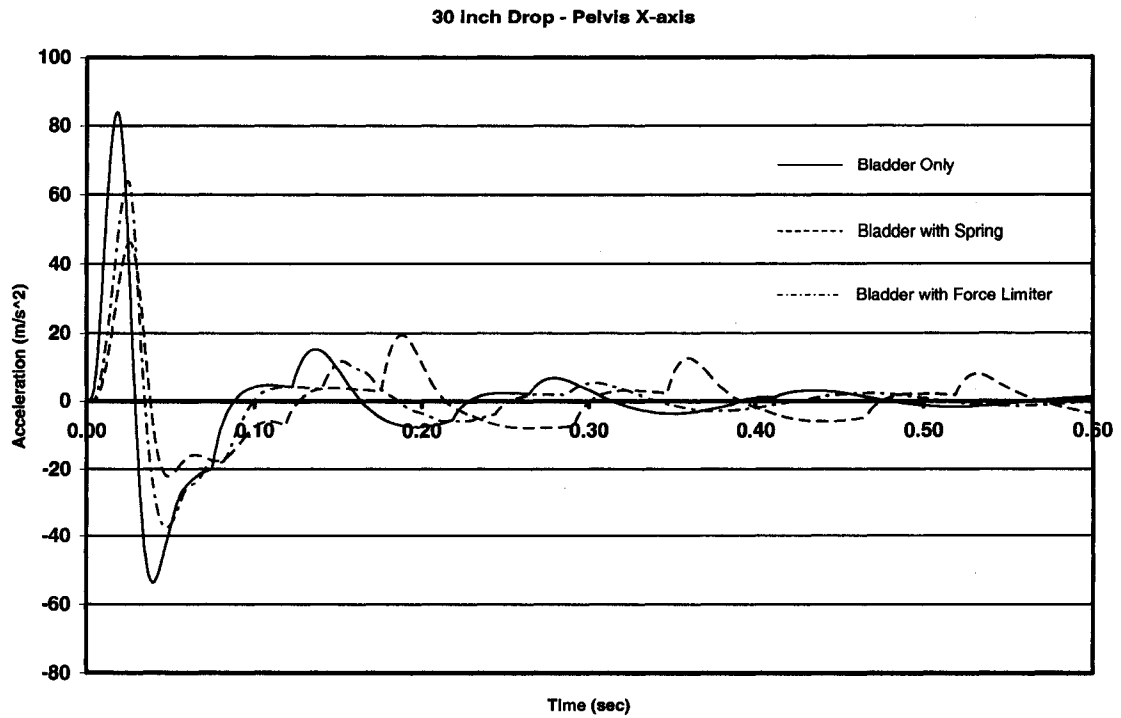
- [12] Choi, Y.T., Wereley, N.M., "Mitigation of Biodynamic Response to Vibratory and Blast -Induced Shock Loads Using Magnetorheological Seat Suspensions", Proceedings of SPIE. Vol. 5056, c2003. pg 277-291
- [13] Hirsch, A.H., January 1964. "Man's Response to Shock Motions." Report 1797. David Taylor Model Basin, Structural Mechanics Laboratory, Washington D.C.
- [14] Axelsson, H. and Odd S., January 2003. "Mine Clearance Vehicles, Crew Safety Standard." The Swedish Defense Material Administration, Test Range Karlsborg 8.
- [15] Stech, E.L. and Payne, P.R., November 1969. "Dynamic Models of the Human Body." AMRLTR-66-157, Wright-Patterson AFB, Ohio.
- [16] Brinkley, J.W. and Shaffer, J.T., October 1970. "Dynamic Simulation Techniques for the Design of Escape Systems: Current applications and Future Air Force Requirements." AMRL Symposium on Biodynamic Models and Their Applications, Report No. AMRL-TR-71-29, Wright-Patterson AFB, Ohio.
- [17] Cheng, Z.Q., Pilkey, W.D., Balandin, D.V., Bolotnik, N.N., Crandall, J.R., and Shaw, C.G., 2001. "Optimal Control of Helicopter Seat Cushions for the Reduction of Spinal Injuries." International Journal of Crashworthiness. Volume 6.3.
- [18] Department of Army, "Occupant Crash Protection Handbook For Tactical Ground Vehicles (Light, Medium, and Heavy Duty).", November 2000.
- [19] Eiband, M.A., June 1959. "Human Tolerance to Rapidly Applied Accelerations: A Summary of the Literature." NASA Memo 5-19-59E.
- [20] Dillon, J.M., Strittmatter, K.V., Sergi, S.A., Wright, N.J., Sousk, S.F., Anderson, T.H., Nguyen, H.N., Fasulo, J., and Loving, Jr., H., July 1998. "Tactical Wheeled Vehicles and Crew Survivability in Landmine Explosions" Report to the U.S. Marine Corps Systems Command.
- [21] Holburn, A.H.S., 1945. "Mechanics of Brain Injuries." British Medical Bulletin, Vol. 3, Number 6.
- [22] Kornhauser, M., 1945. "Prediction and Evaluation of Sensitivity to Transient Acceleration." Journal of Applied Mechanics, Vol. 21.
- [23] Gadd, C.W., 1966. "Use of a Weighted-Impulse Criterion for Estimating Injury Hazard." Proceedings, Tenth Stapp Car Crash Conference, Society of Automotive Engineers, New York.
- [24] Alem, N.M., 2004. Personal Correspondence. Aircrew Protection Division, U.S. Army Aeromedical Research Laboratory, Fort Rucker, Alabama.

[25] North Atlantic Treaty Organization, HFM-090 Task Group 25, April 2007  
“Test Methodology for Protection of Vehicle Occupants against Anti-Vehicular  
Landmine Effects”

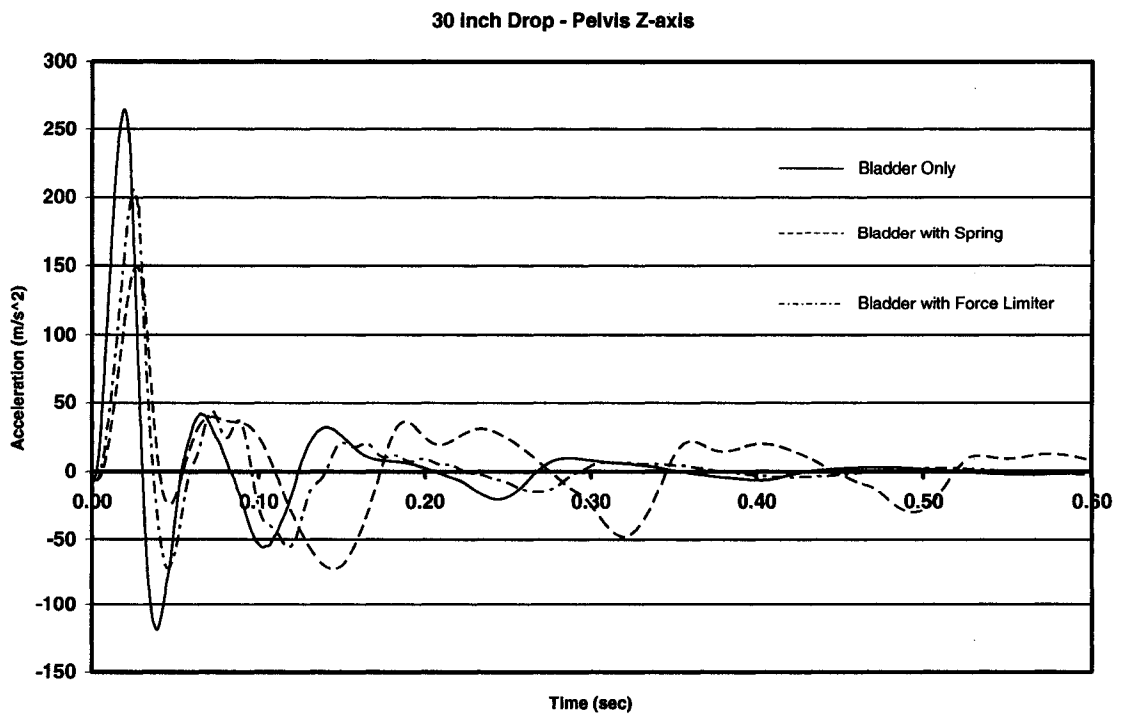
[26] Clauser, C.E., McConville, J.T, and Young J.W, August 1969. “Weight, Volume,  
and Center of Mass of Segments of the Human Body” Aerospace Medical Research  
Laboratory, Aerospace Medical Division, Air Force Systems Command, Wright-  
Patterson Air Force Base, Ohio.

**APPENDIX 1**

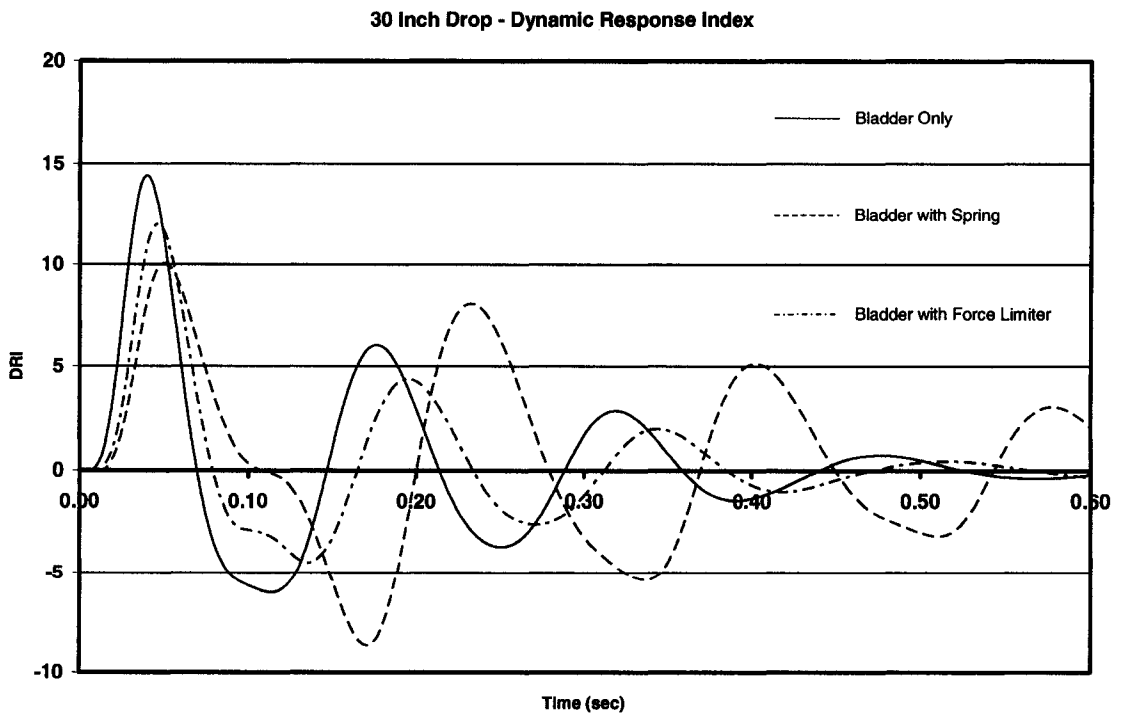
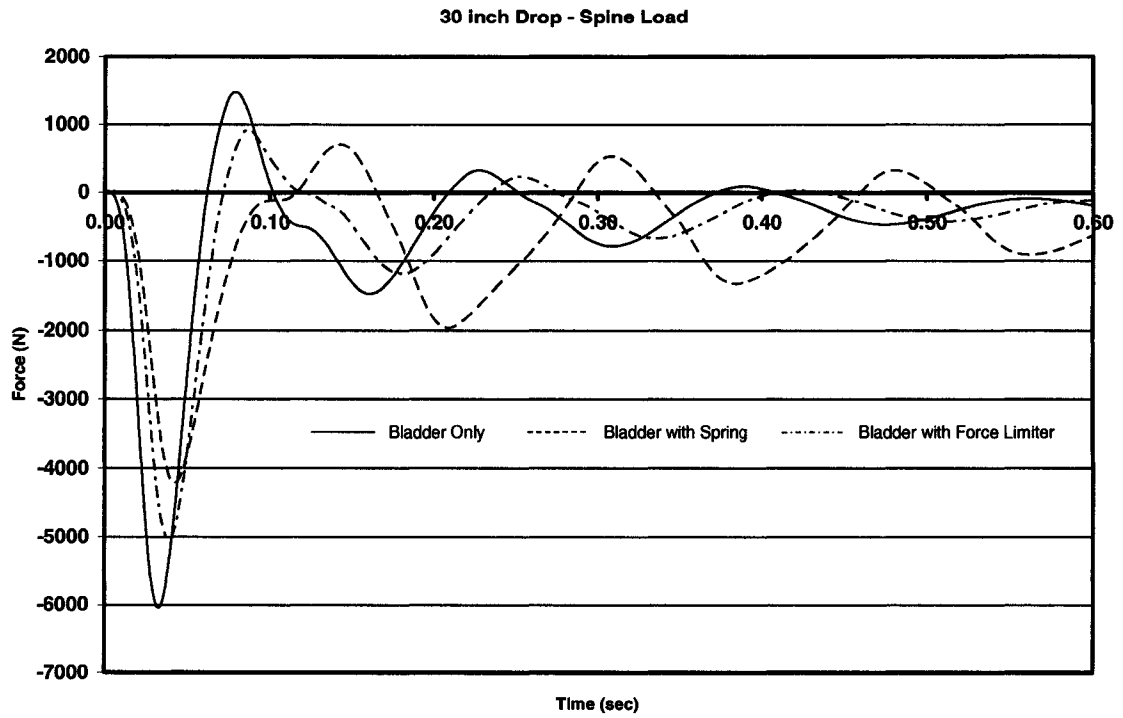
**FORCE LIMITER COMPARISON PLOTS**



**Figure A1-1 30 Inch Drop, X-axis Pelvic Acceleration**



**Figure A1-2 30 Inch Drop, Z-axis Pelvic Acceleration**



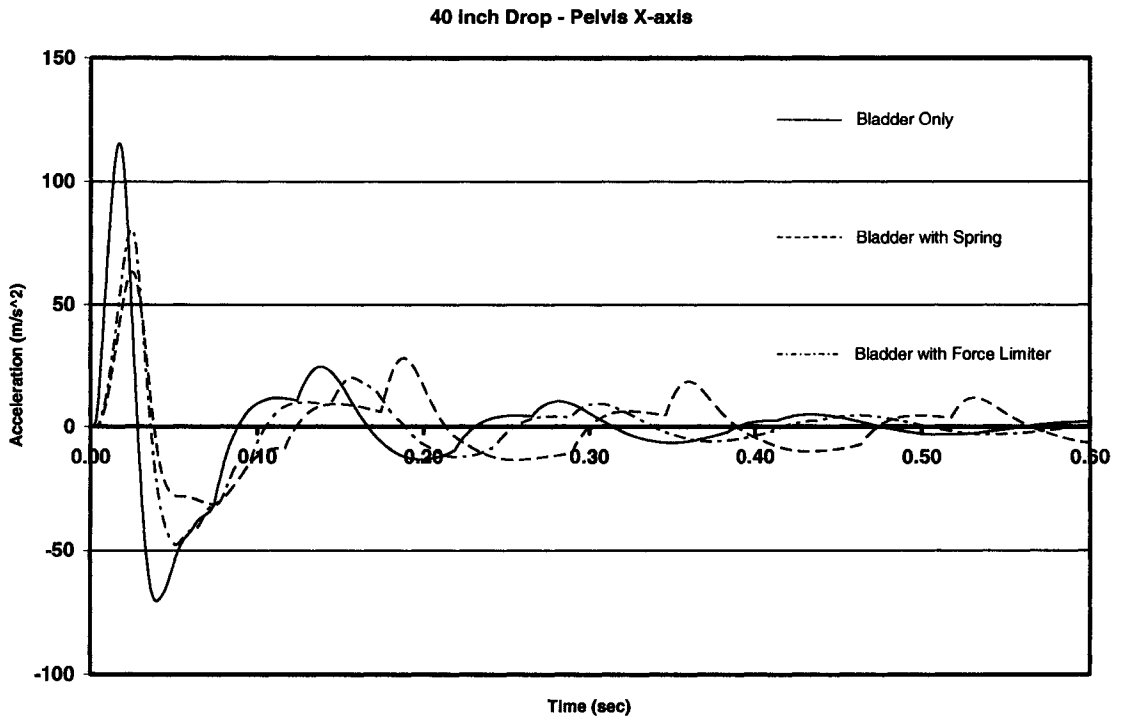


**Figure A1-5 40 Inch Drop, X-axis Pelvic Acceleration**

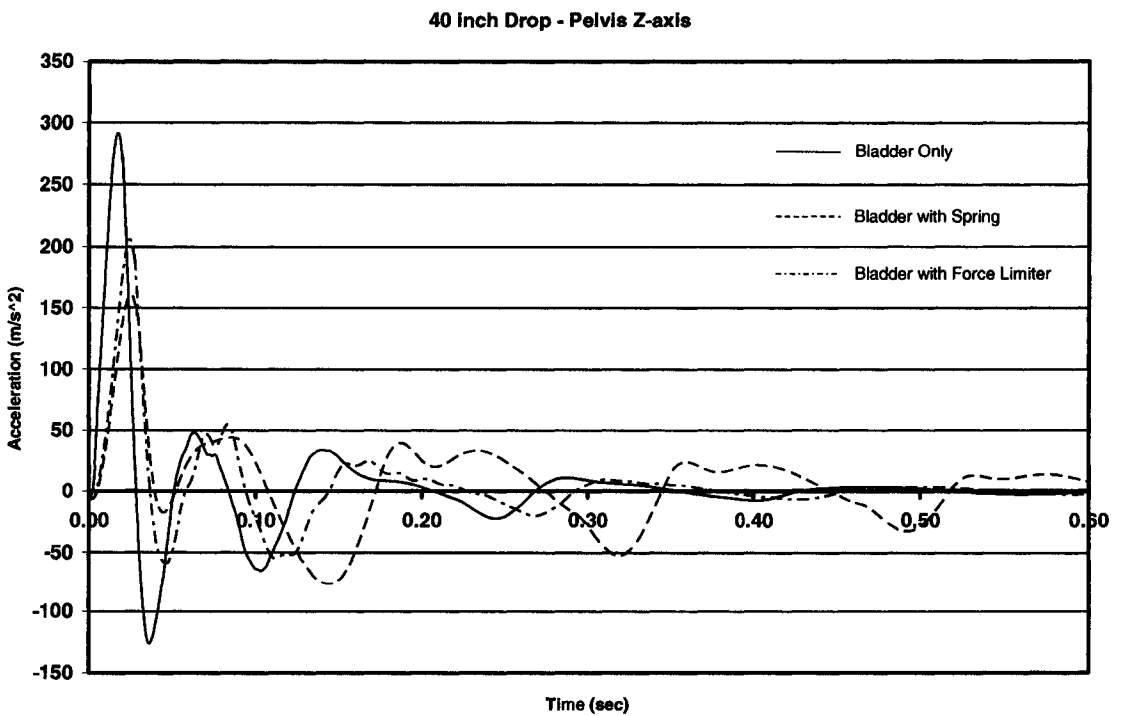


**Figure A1-6 40 Inch Drop, Z-axis Pelvic Acceleration**

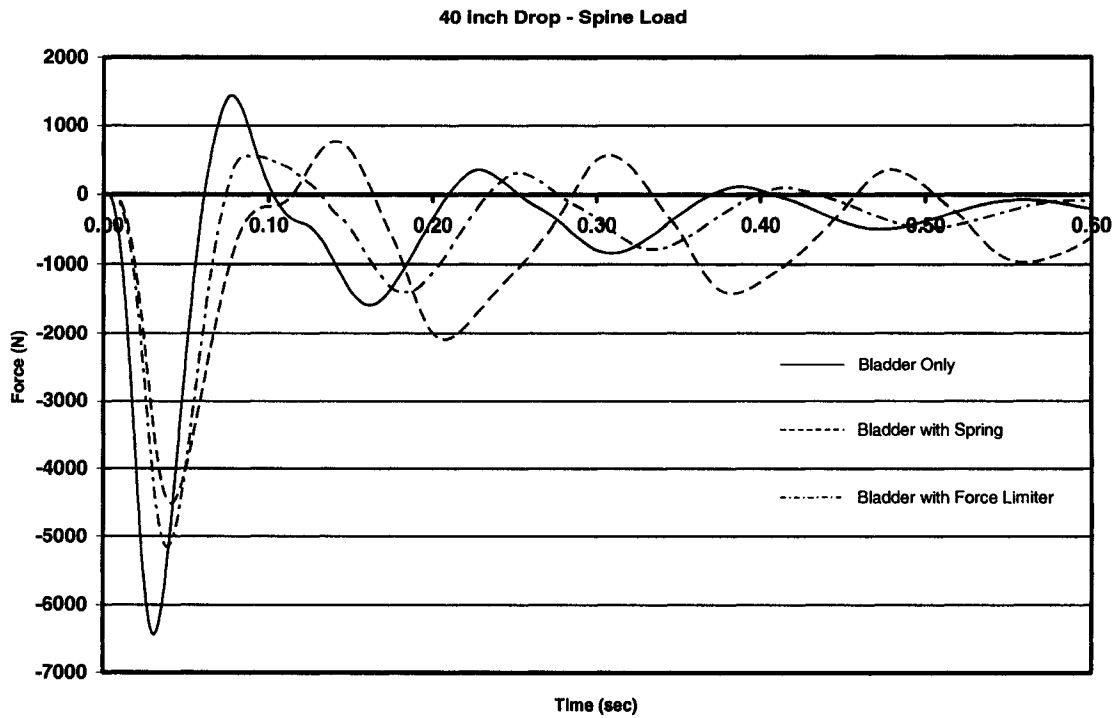


**Figure A1-7 40 Inch Drop, Spine Load**

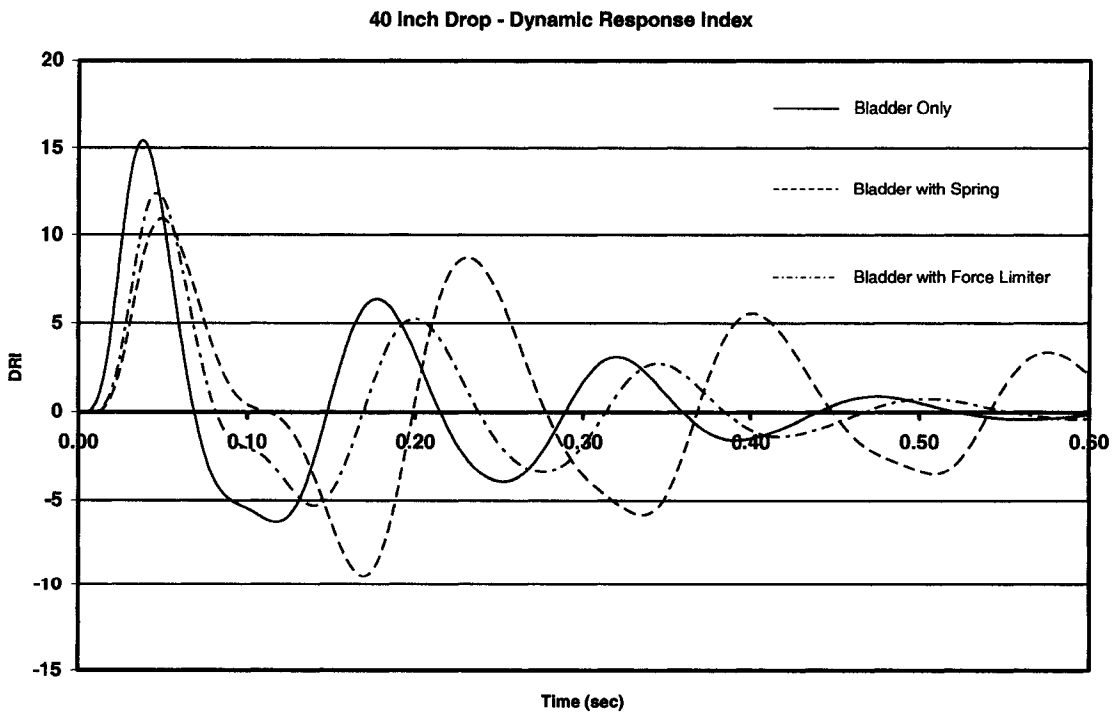


**Figure A1-8 40 Inch Drop, DRI**

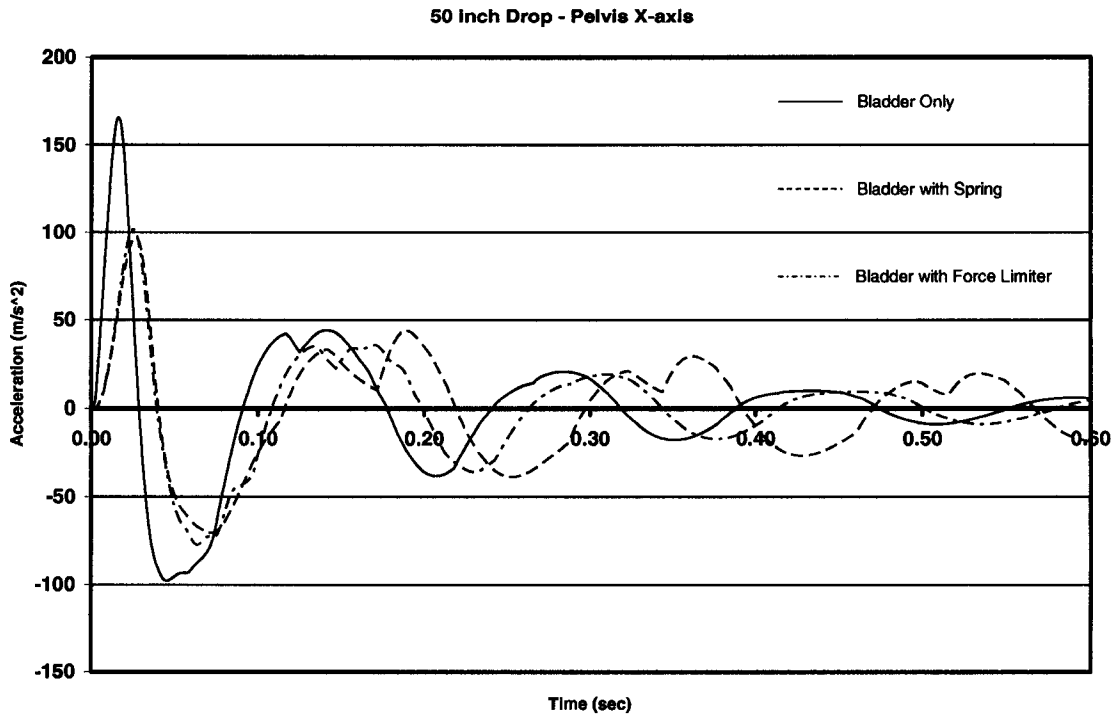


**Figure A1-9 50 Inch Drop, X-axis Pelvic Acceleration**

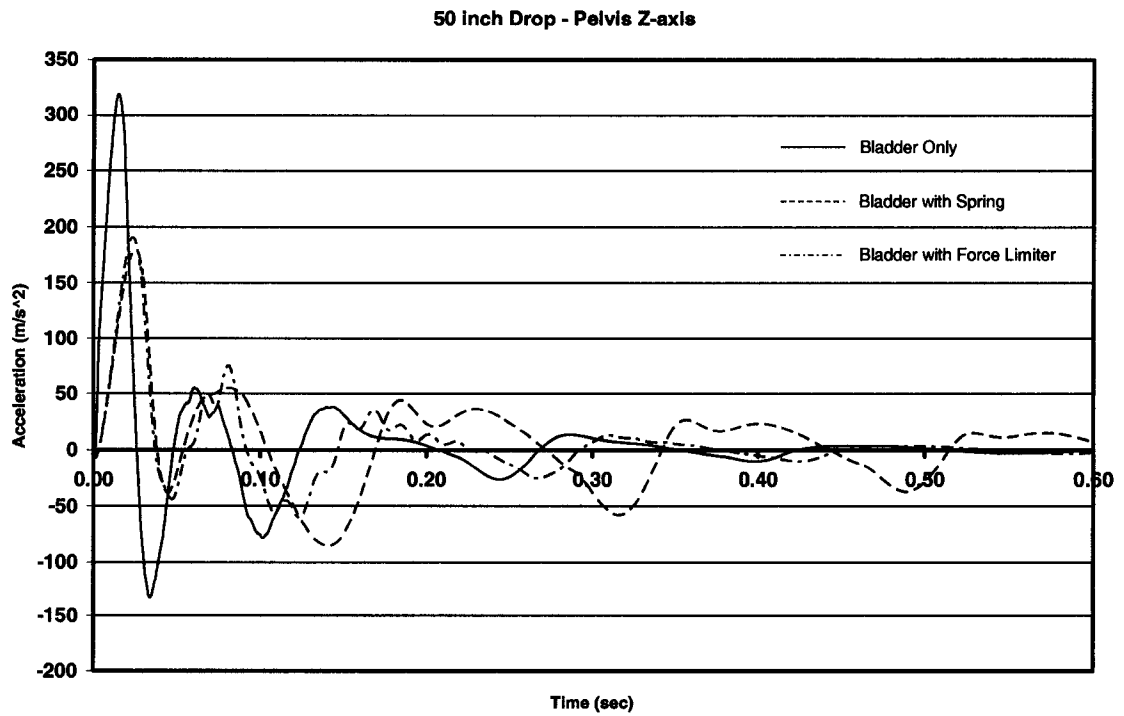


**Figure A1-10 50 Inch Drop, Z-axis Pelvic Acceleration**

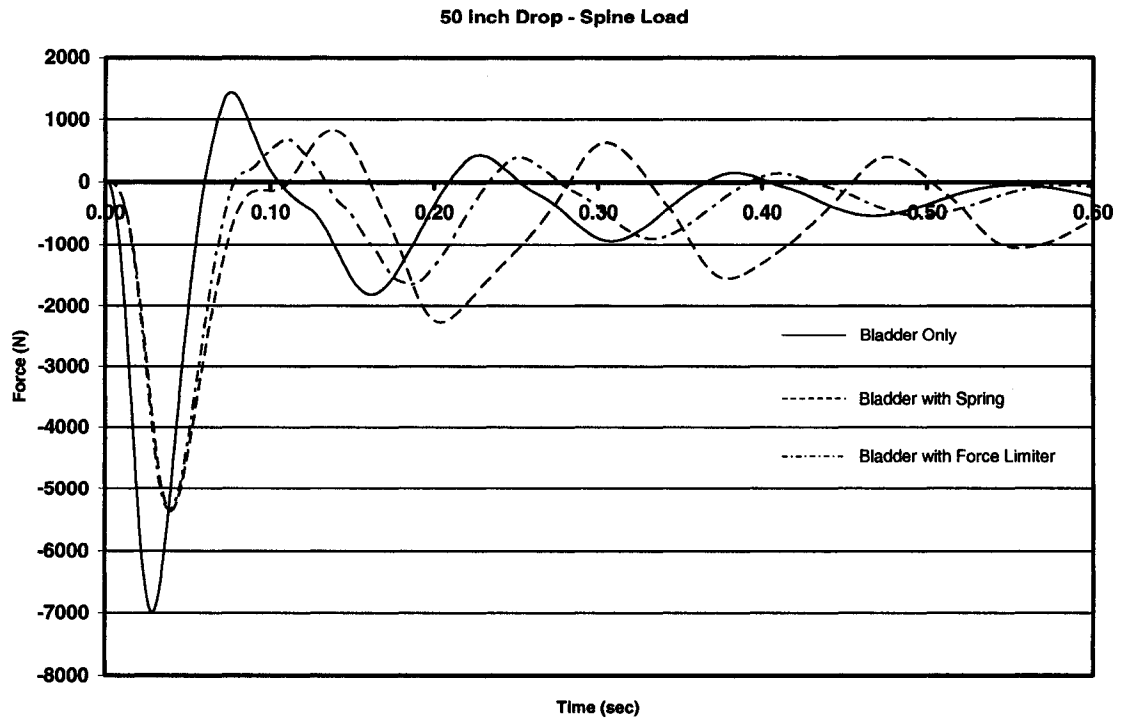


**Figure A1-11 50 Inch Drop, Spine Load**

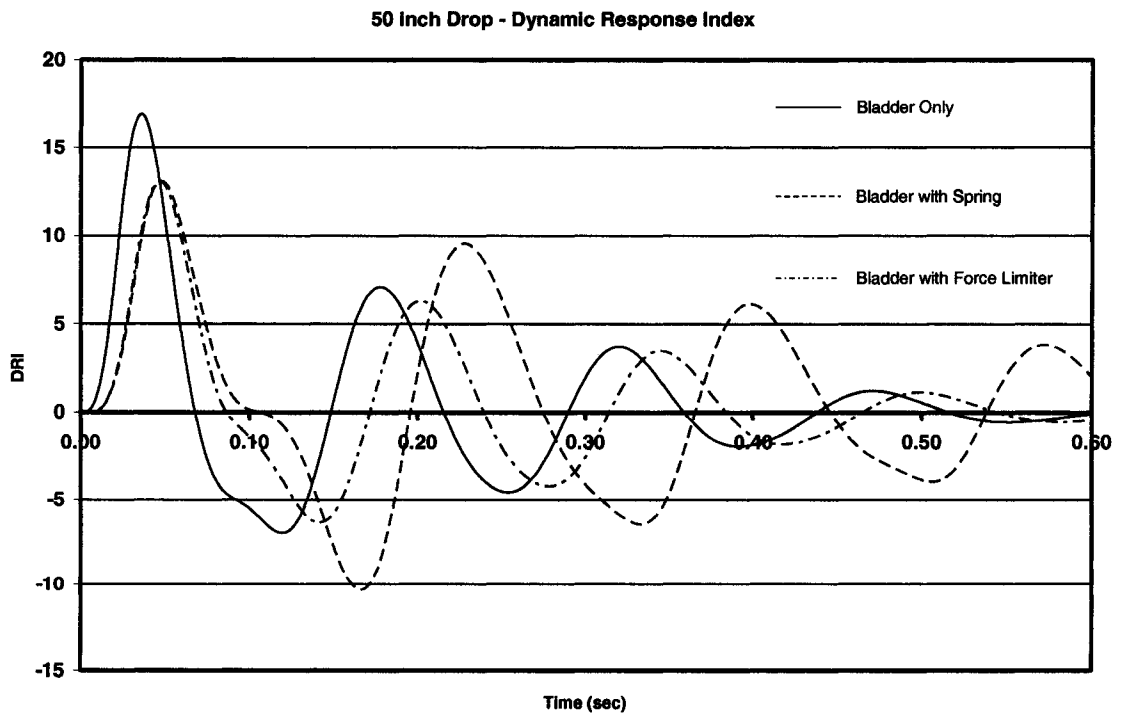


**Figure A1-12 50 Inch Drop, DRI**

## APPENDIX 2

### FORCE LIMITER POSITION PLOTS

30 inch drop - Pelvis Position X-axis

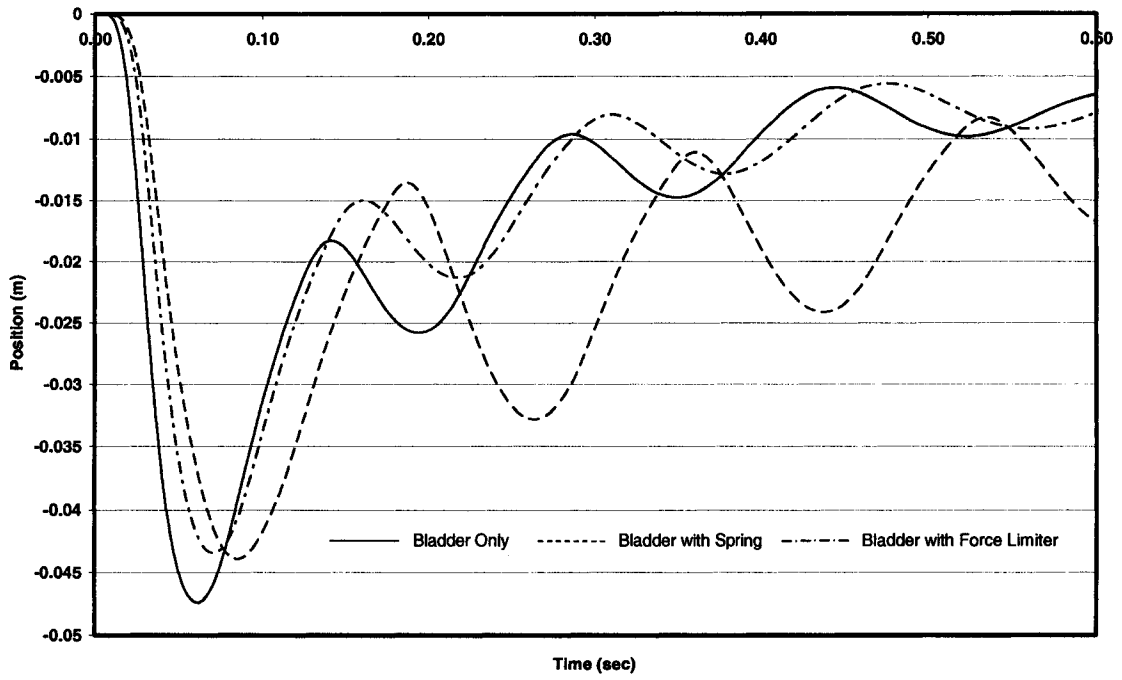


Figure A2-1 30 inch drop, Pelvis X-axis Position

30 inch drop - Pelvis Position Z-axis

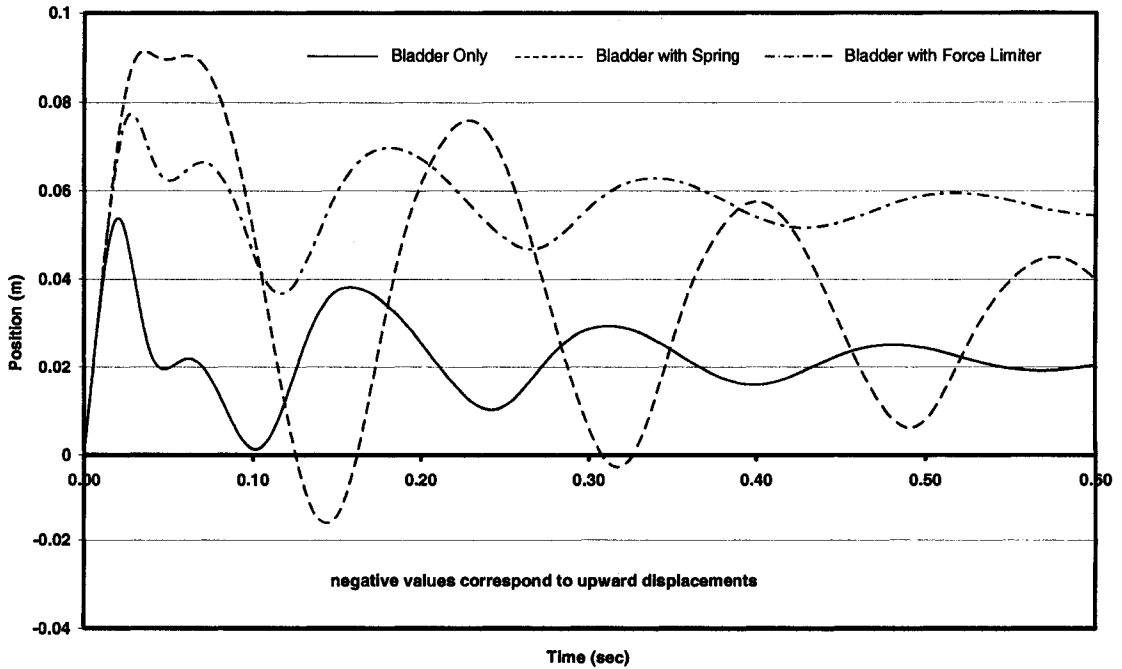
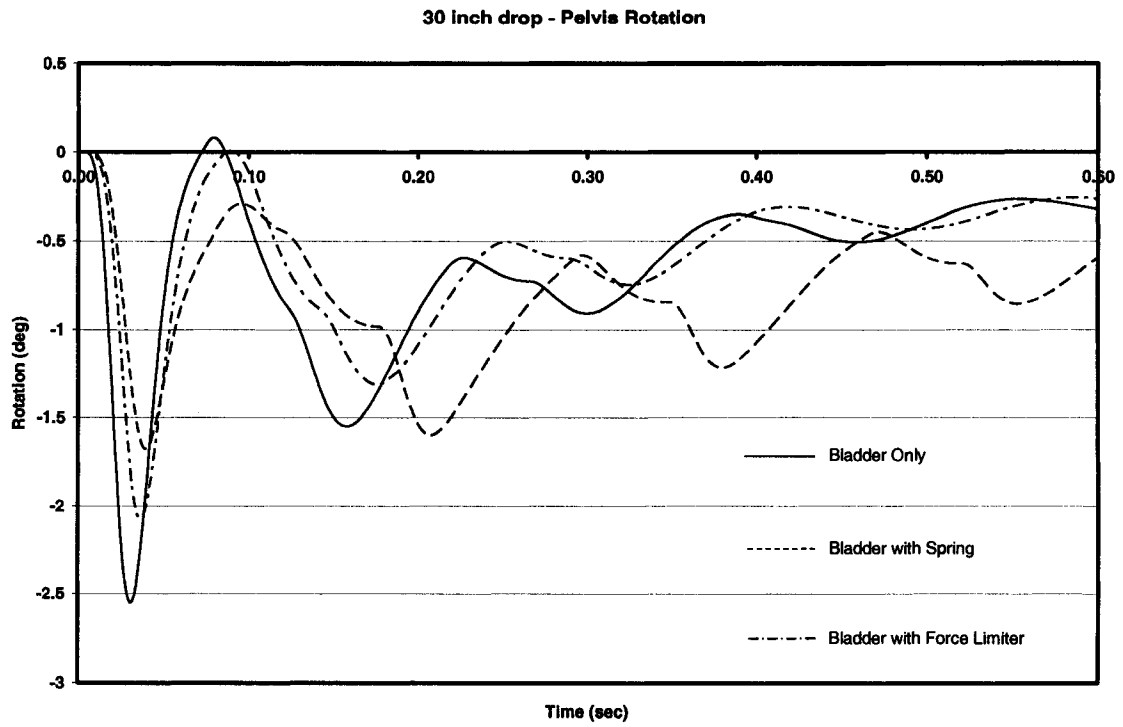
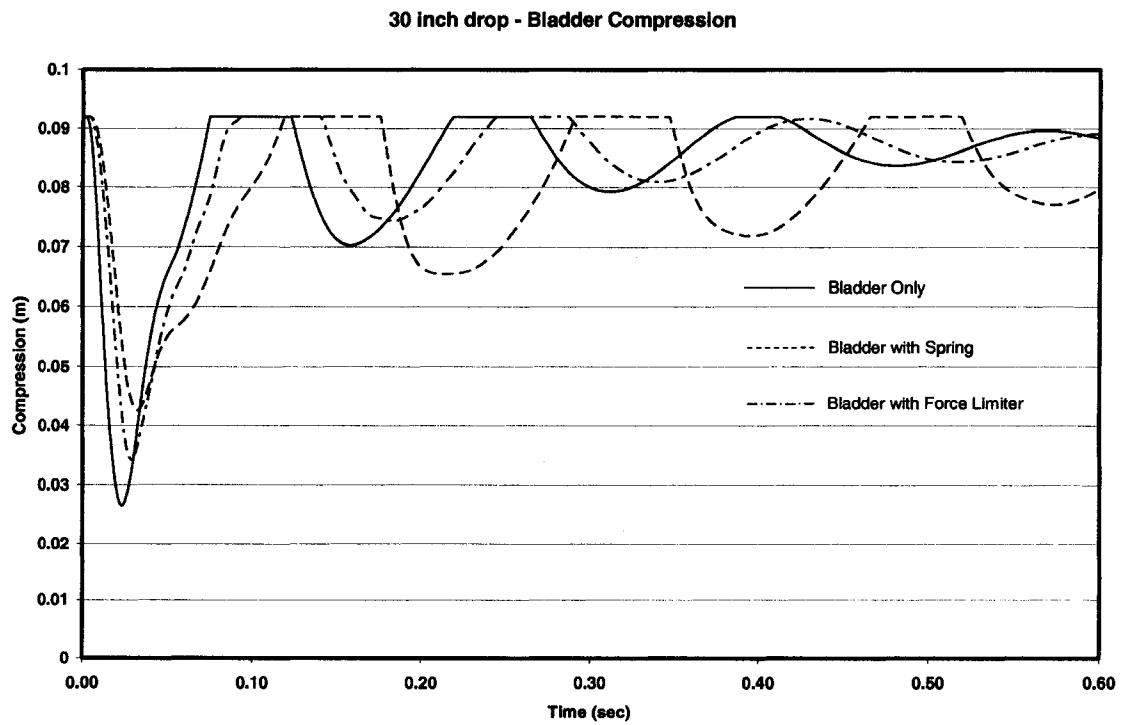


Figure A2-2 30 inch drop, Pelvis Z-axis Position



**Figure A2-3 30 inch drop, Pelvis  $\theta$ -axis Position**



**Figure A2-4 30 inch drop, Bladder Compression**

30 Inch drop - Spring Compression

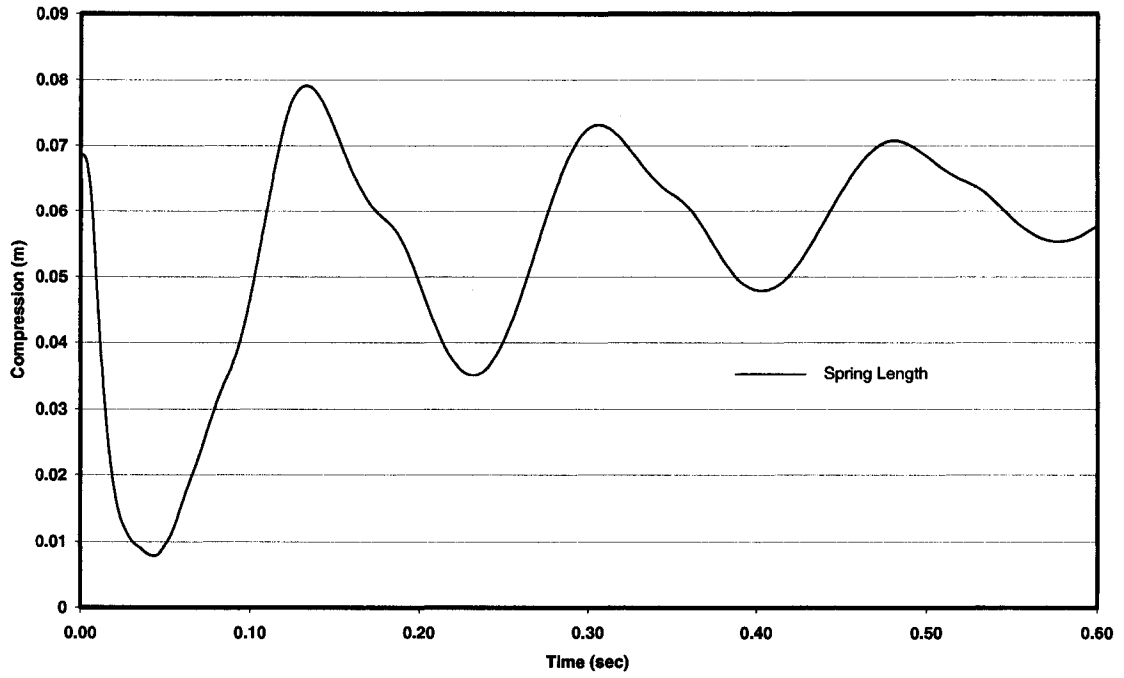


Figure A2-5 30 inch drop, Spring Compression

30 Inch drop - Force Limiter Compression

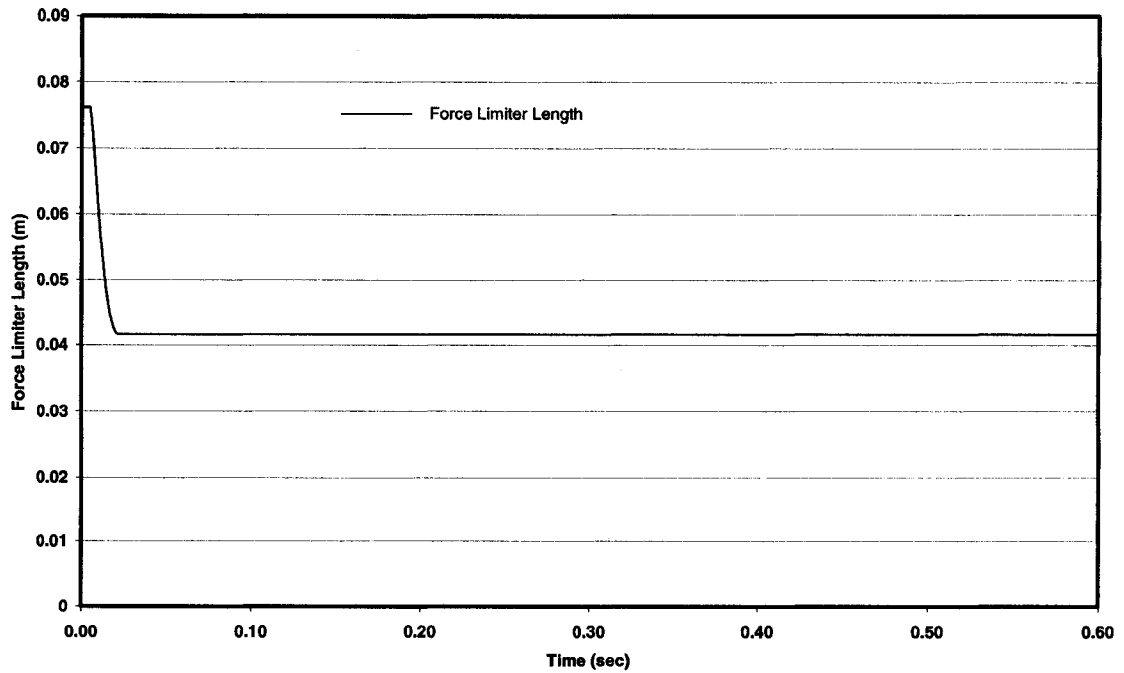
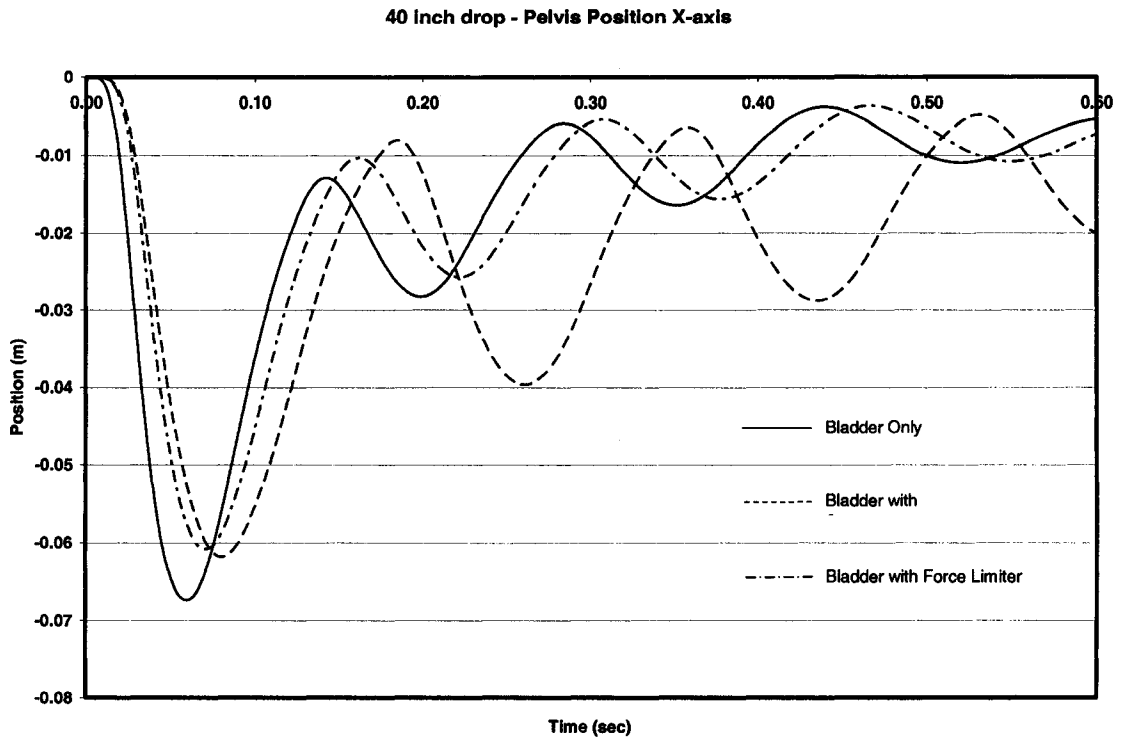
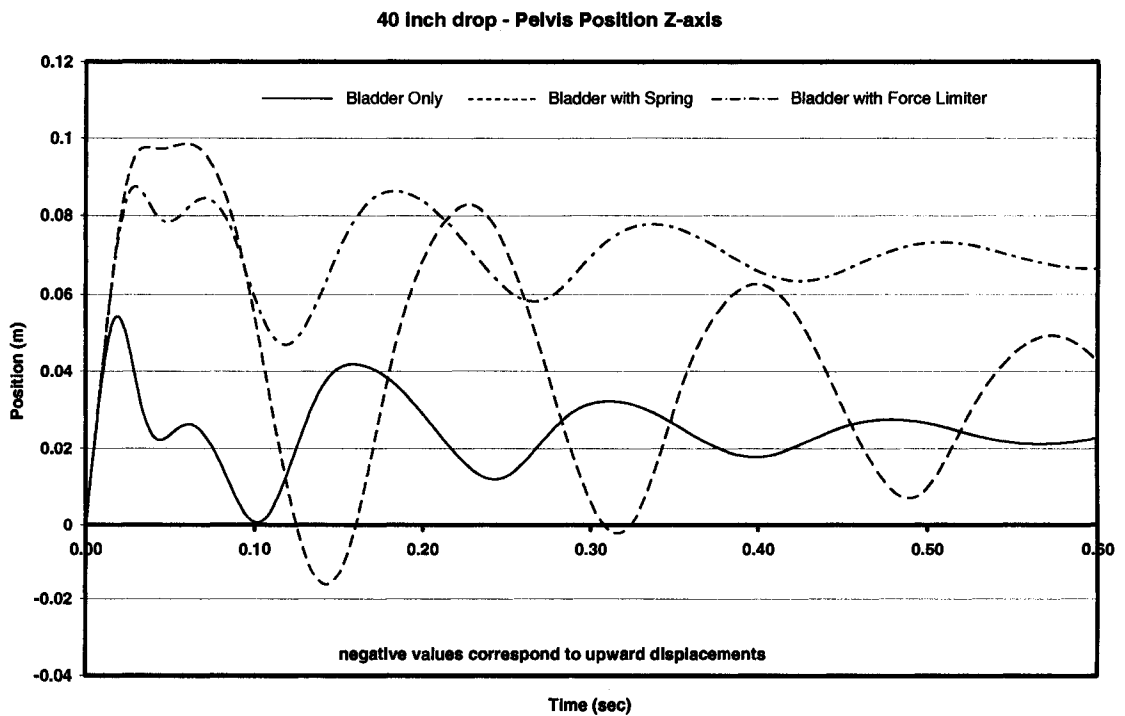


Figure A2-6 30 inch drop, Honeycomb Compression



**Figure A2-7 40 inch drop, Pelvis X-axis Position**



**Figure A2-8 40 inch drop, Pelvis Z-axis Position**

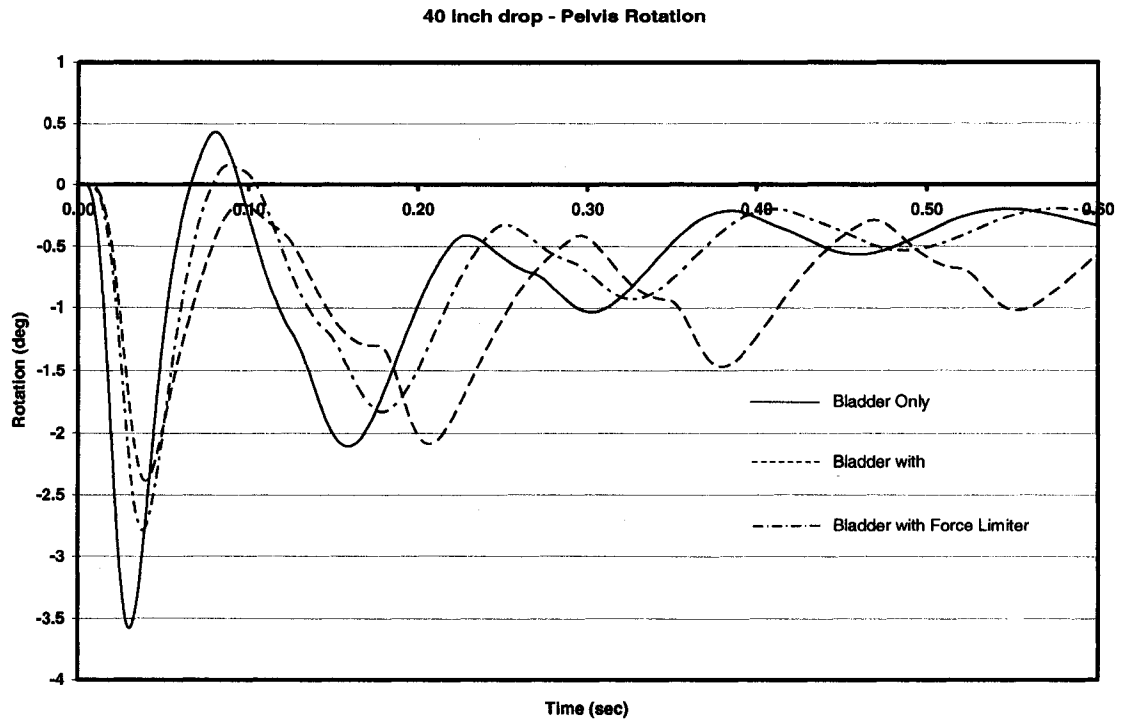


**Figure A2-9** 40 inch drop, Pelvis  $\theta$ -axis Position

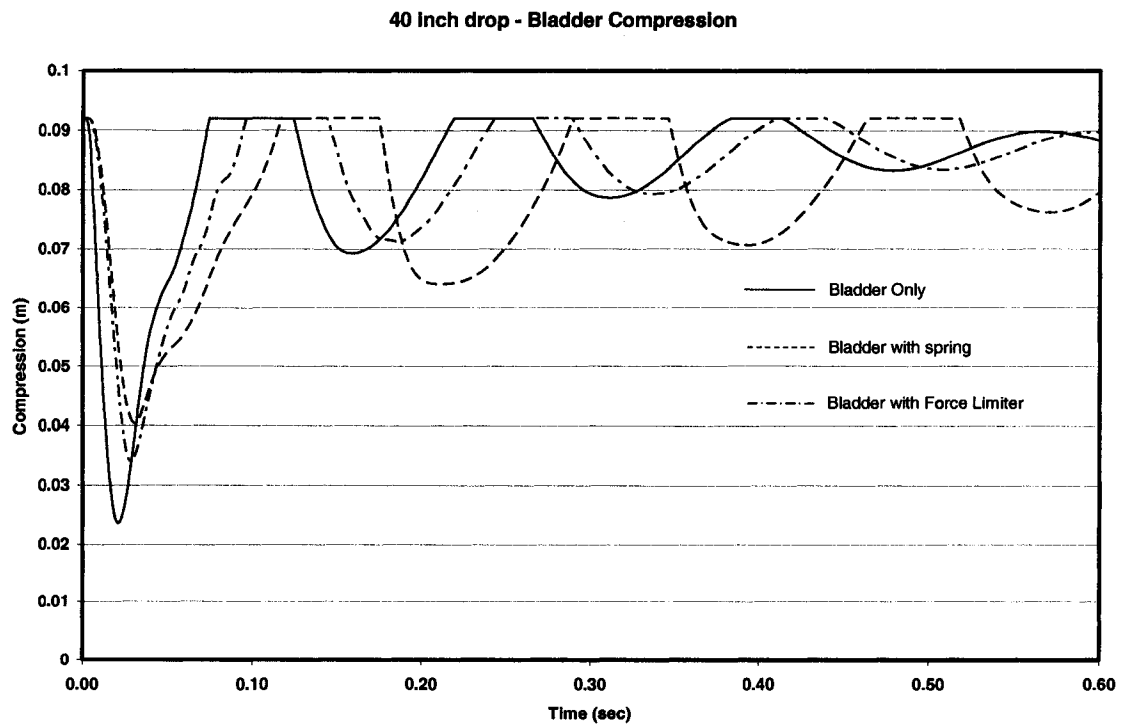


**Figure A2-10** 40 inch drop, Bladder Compression

40 Inch drop - Spring Compression

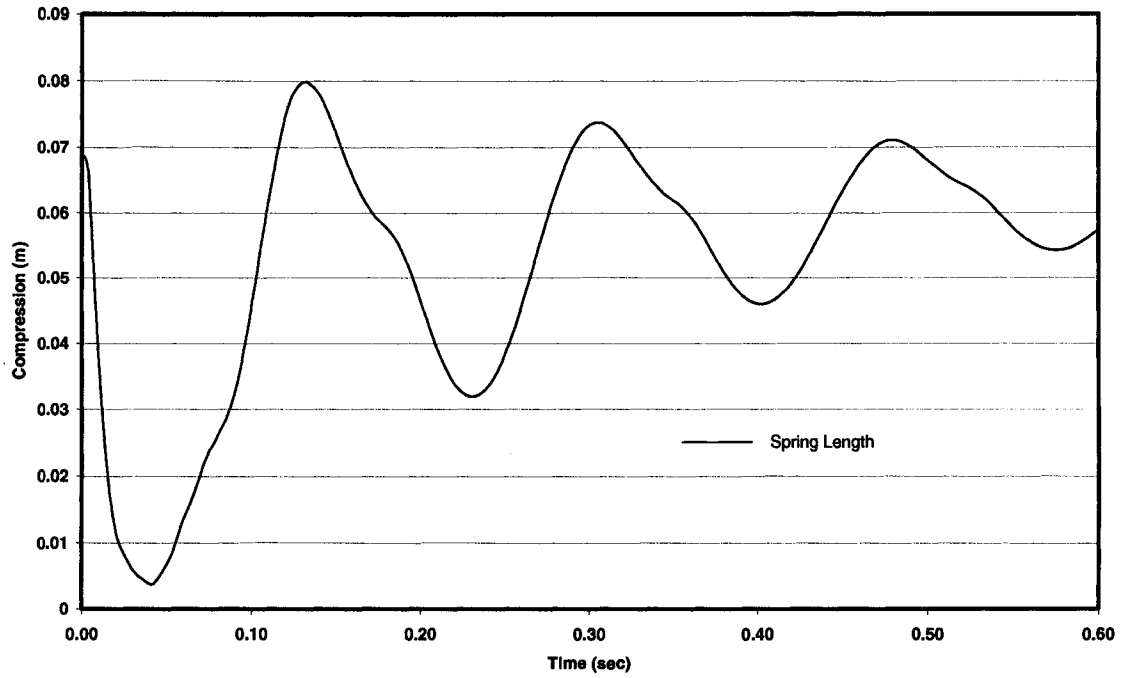


Figure A2-11 40 inch drop, Spring Compression

40 Inch drop - Force Limiter Compression

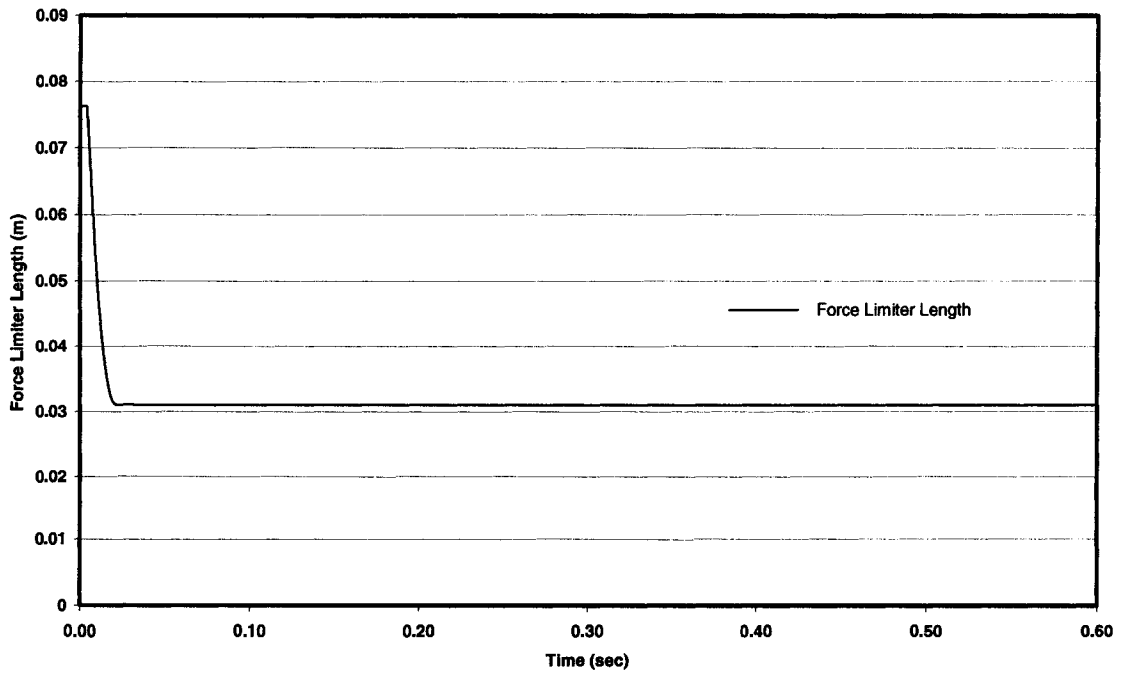


Figure A2-12 40 inch drop, Honeycomb Compression

50 inch drop - Pelvis Position X-axis

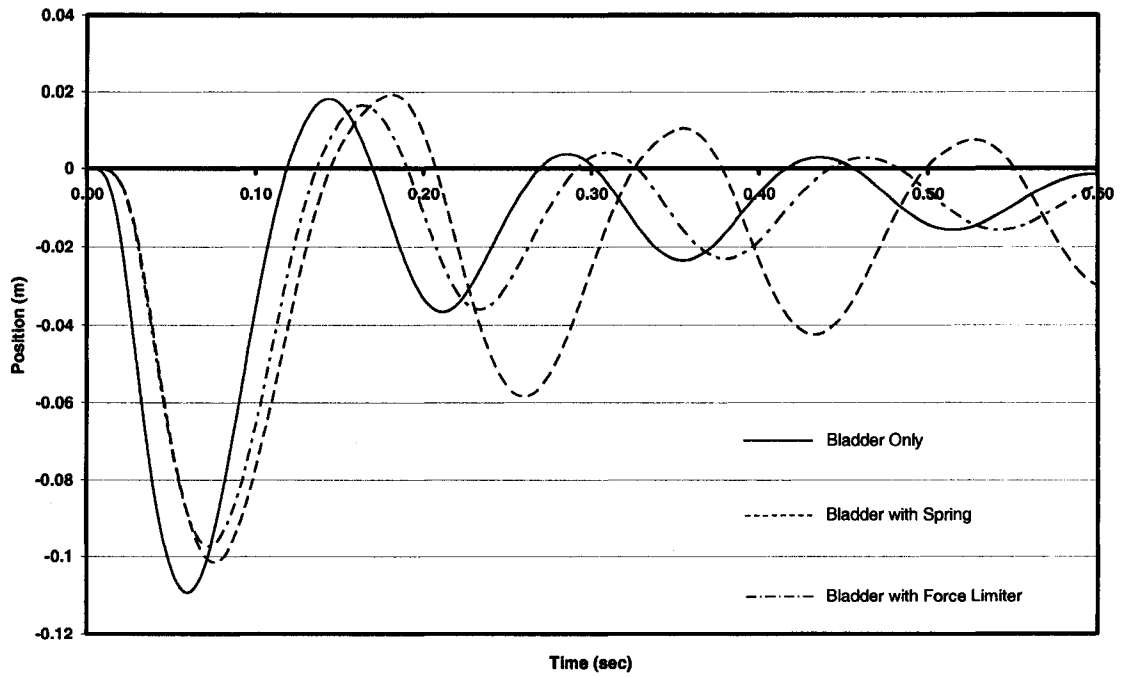


Figure A2-13 50 inch drop, Pelvis X-Axis Position

50 inch drop - Pelvis Position Z-axis

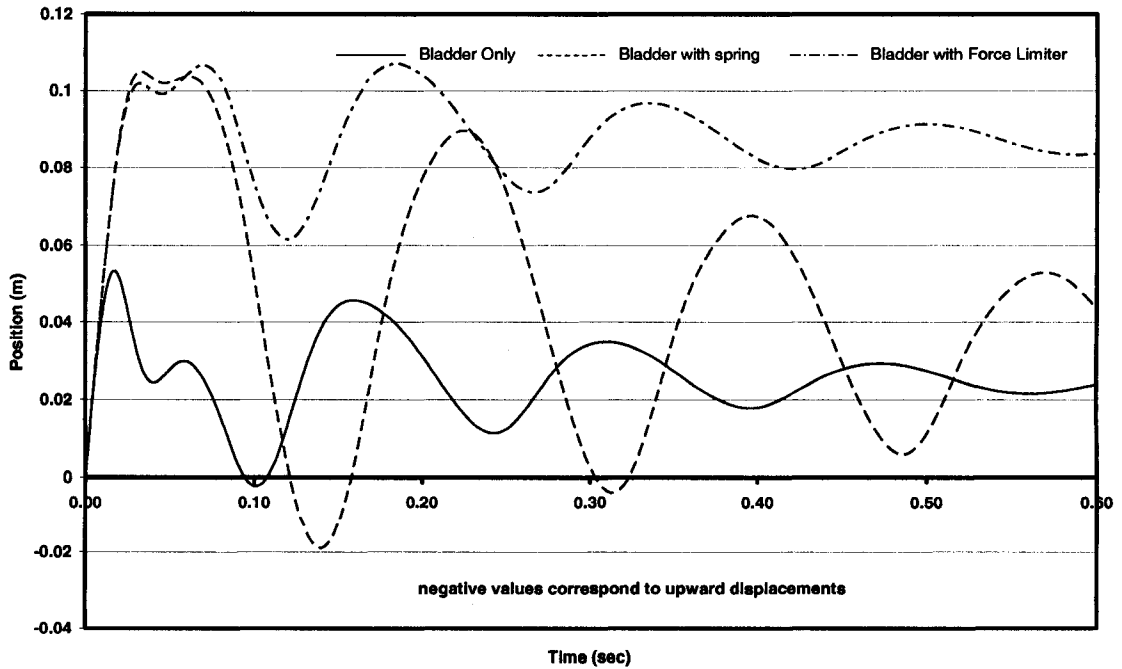
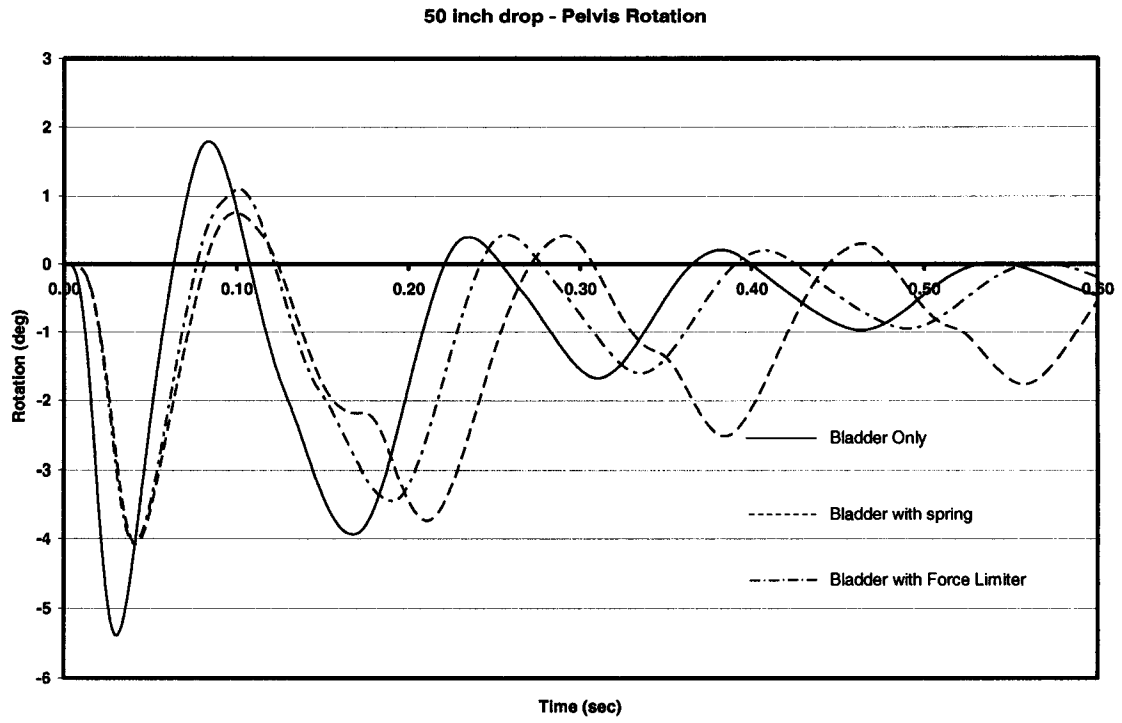
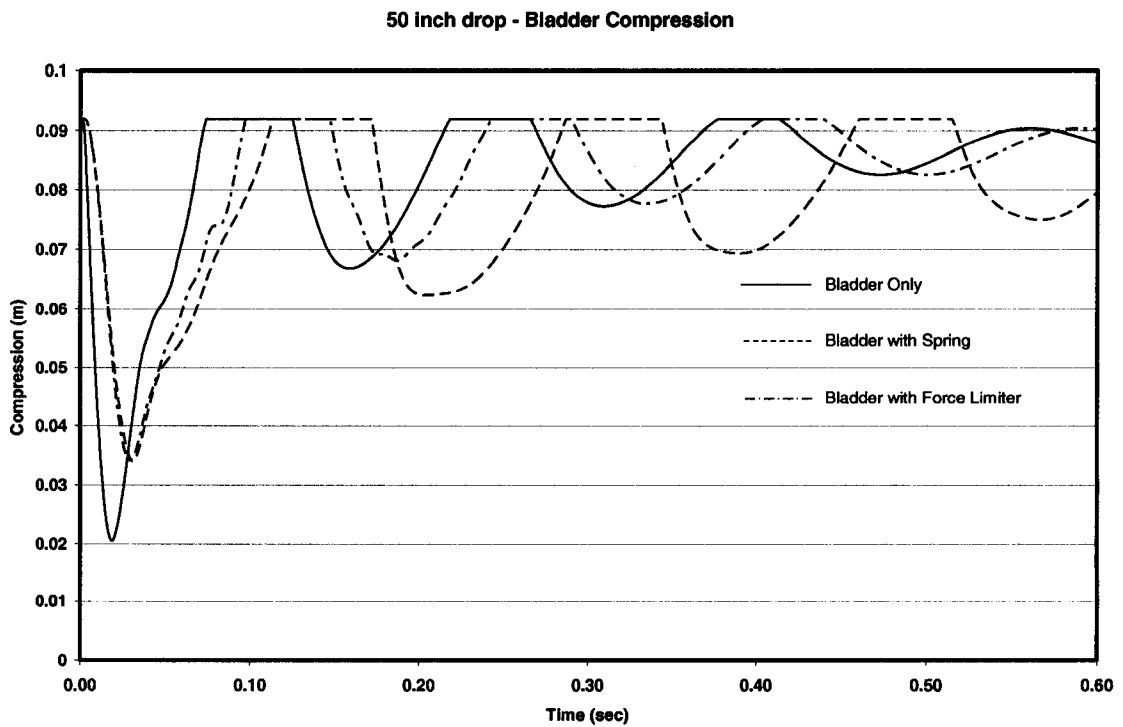


Figure A2-14 50 inch drop, Pelvis Z-Axis Position



**Figure A2-15 50 inch drop, Pelvis  $\theta$ -Axis Position**



**Figure A2-16 50 inch drop, Bladder Compression**

50 inch drop - Spring Compression

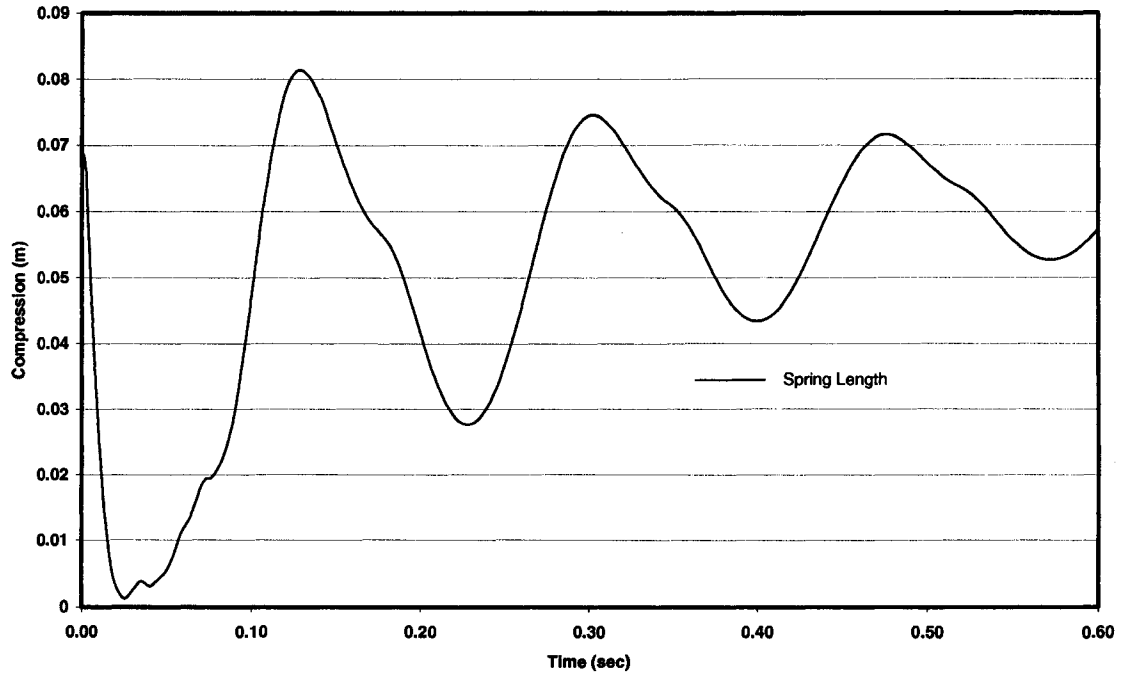


Figure A2-17 50 inch drop, Spring Compression

50 inch drop - Force Limiter Compression

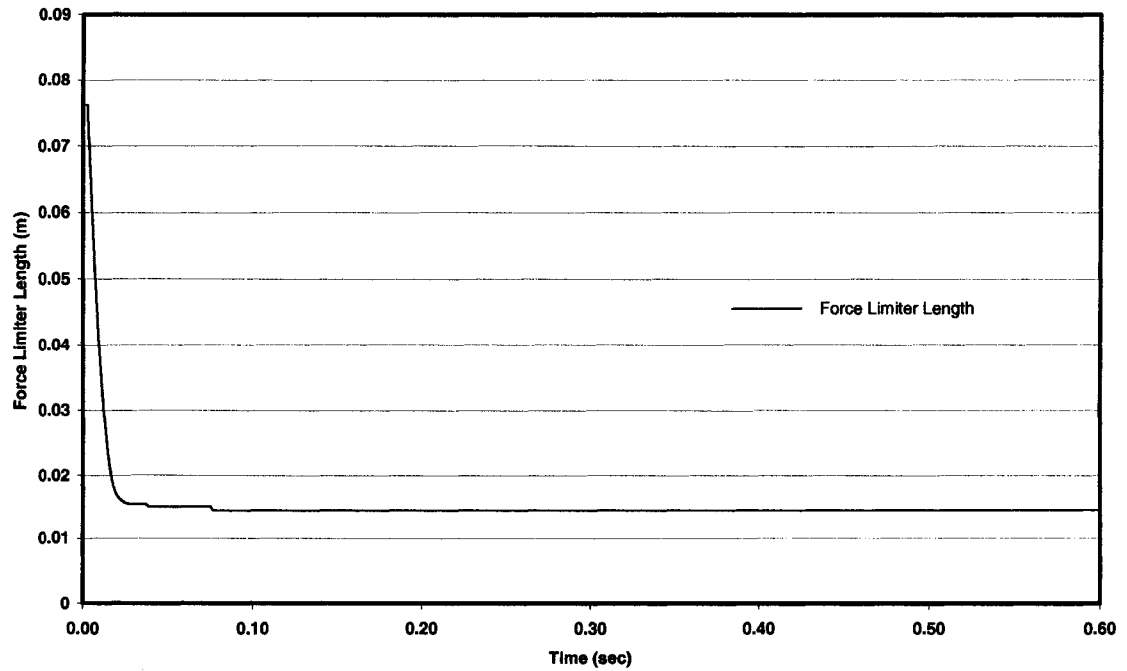
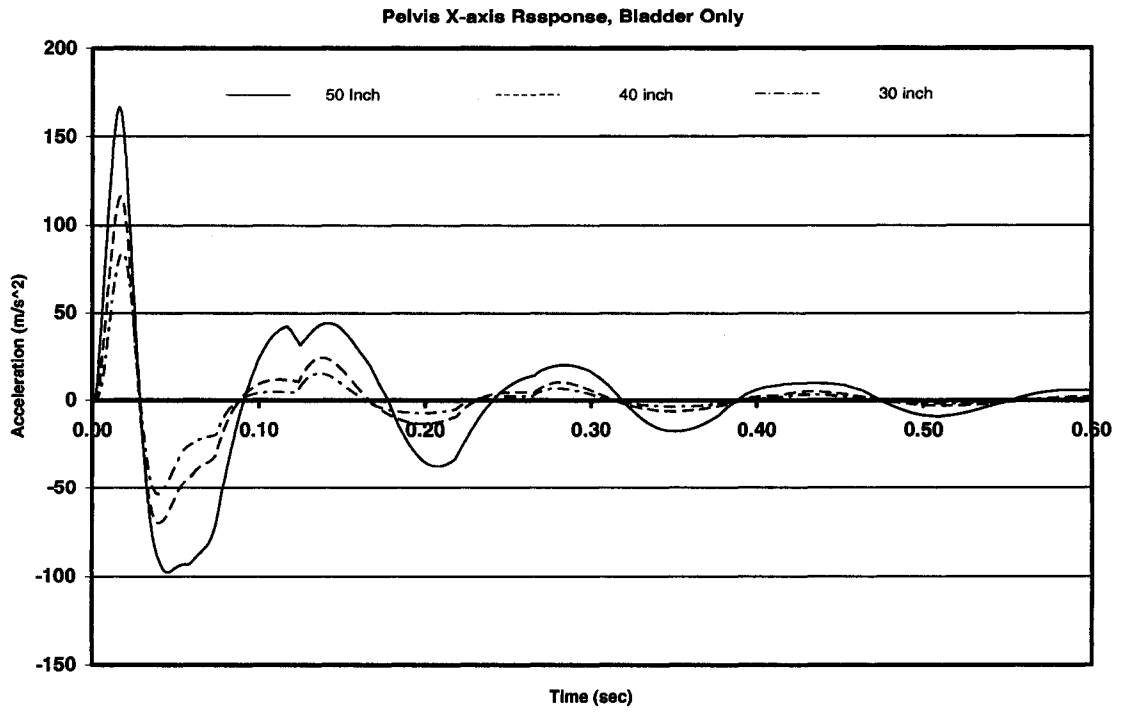


Figure A2-18 50 inch drop, Honeycomb Compression

## APPENDIX 3

### INPUT COMPARISON PLOTS



**Figure A3-1, Pelvis X-axis Acceleration , Bladder Only**

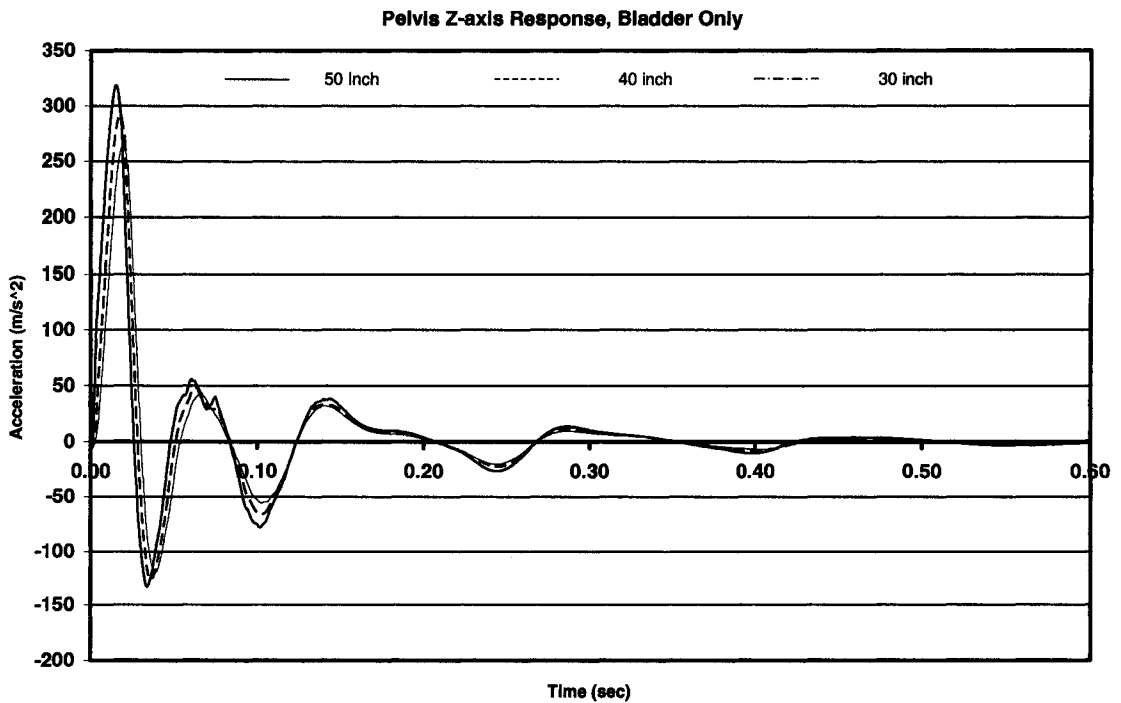


**Figure A3-2 Pelvis Z-axis Acceleration, Bladder Only**

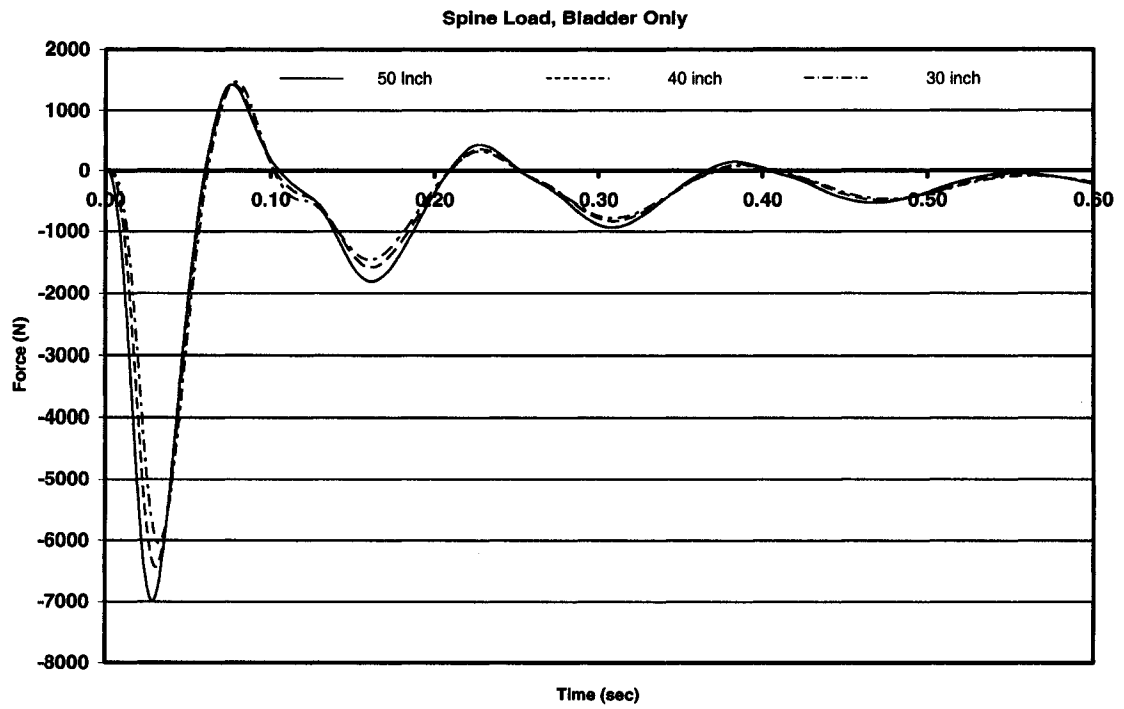


**Figure A3-3 Spine Load, Bladder Only**

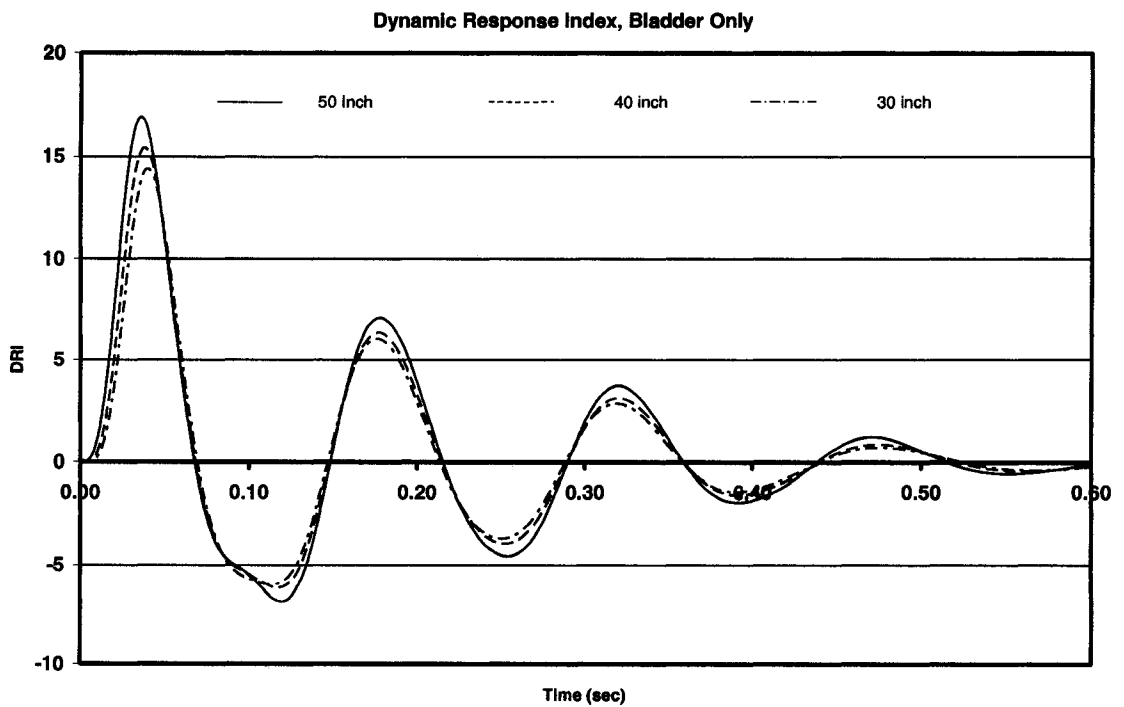


**Figure A3-4 Dynamic Response Index, Bladder Only**

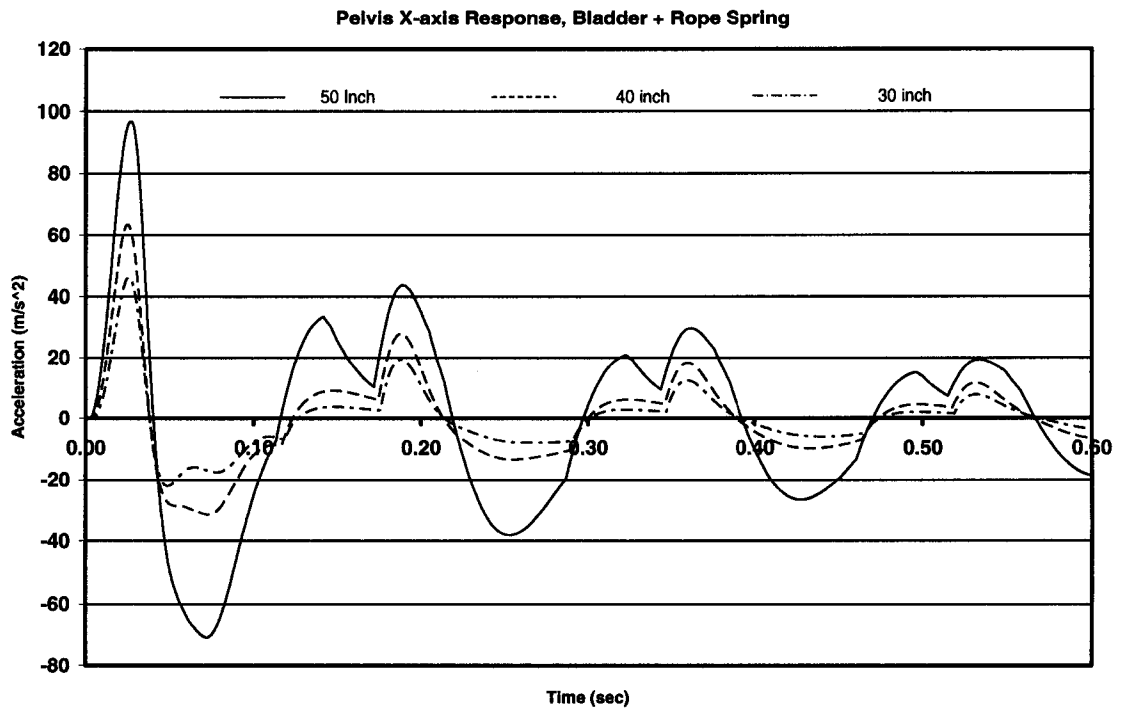


**Figure A3-5 Pelvis Acceleration, X-axis, Bladder + Rope Spring**

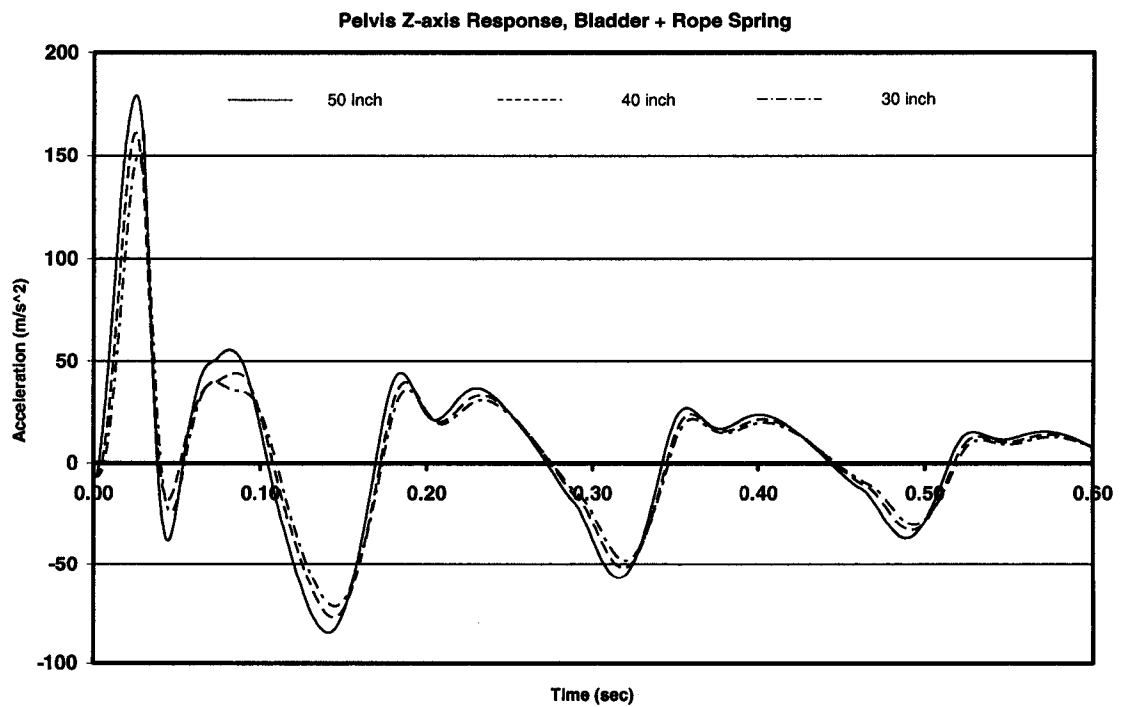


**Figure A3-6 Pelvis Acceleration, Z-axis, Bladder + Rope Spring**

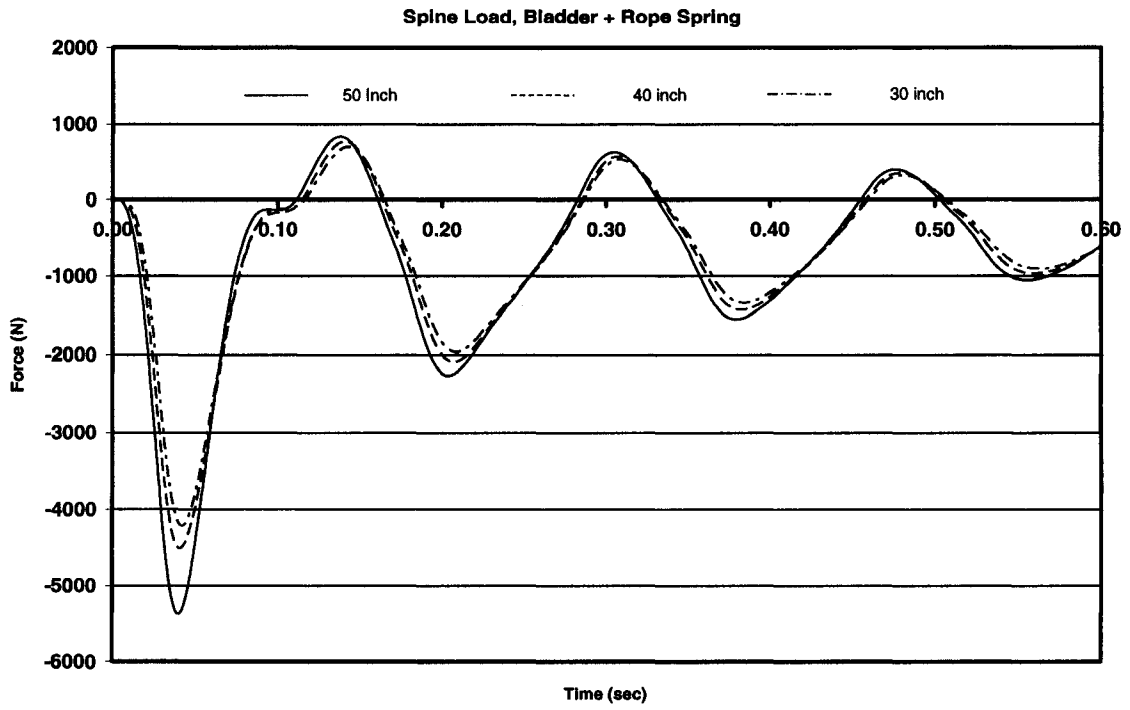


Figure A3-7 Spine Load, Bladder + Rope Spring

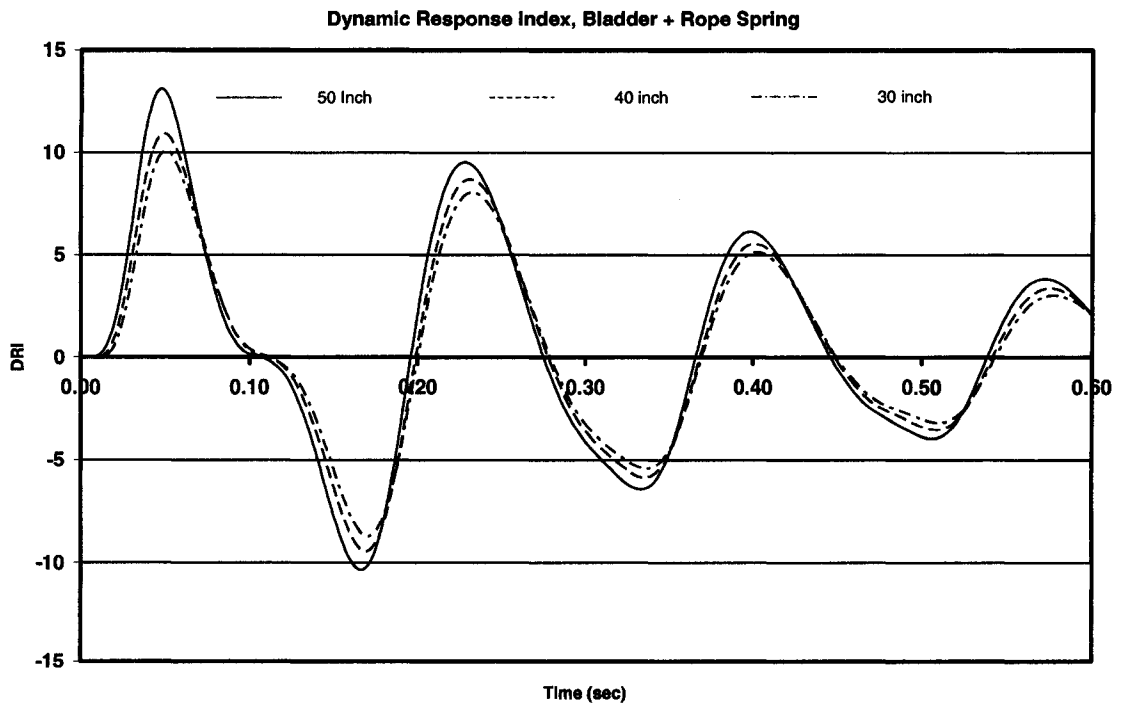
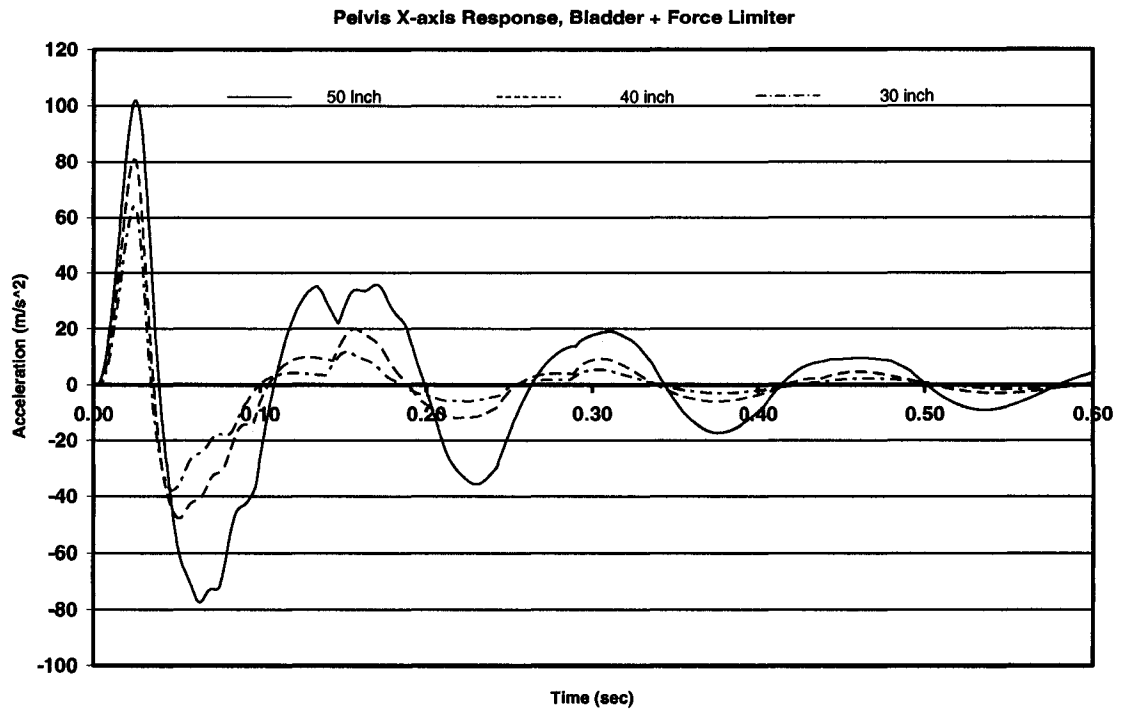
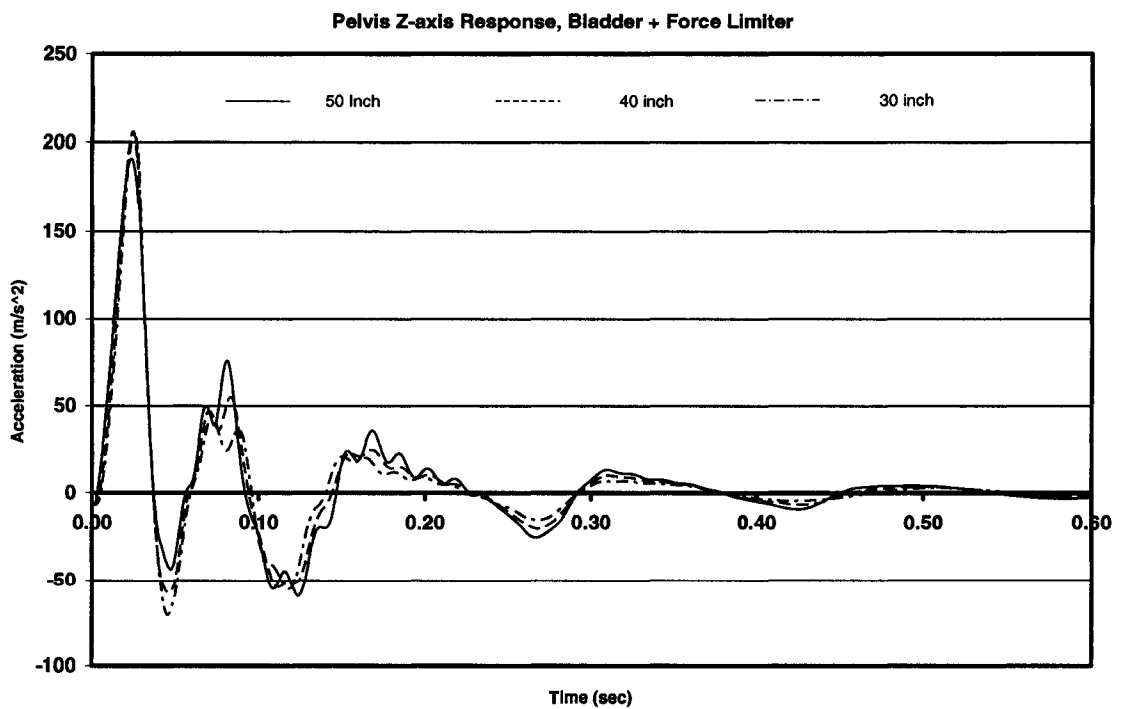


Figure A3-8 Dynamic Response, Bladder + Rope Spring



**Figure A3-9 Pelvis Acceleration, X-axis, Bladder + Honeycomb Isolator**



**Figure A3-10 Pelvis Acceleration, Z-axis, Bladder + Honeycomb Isolator**

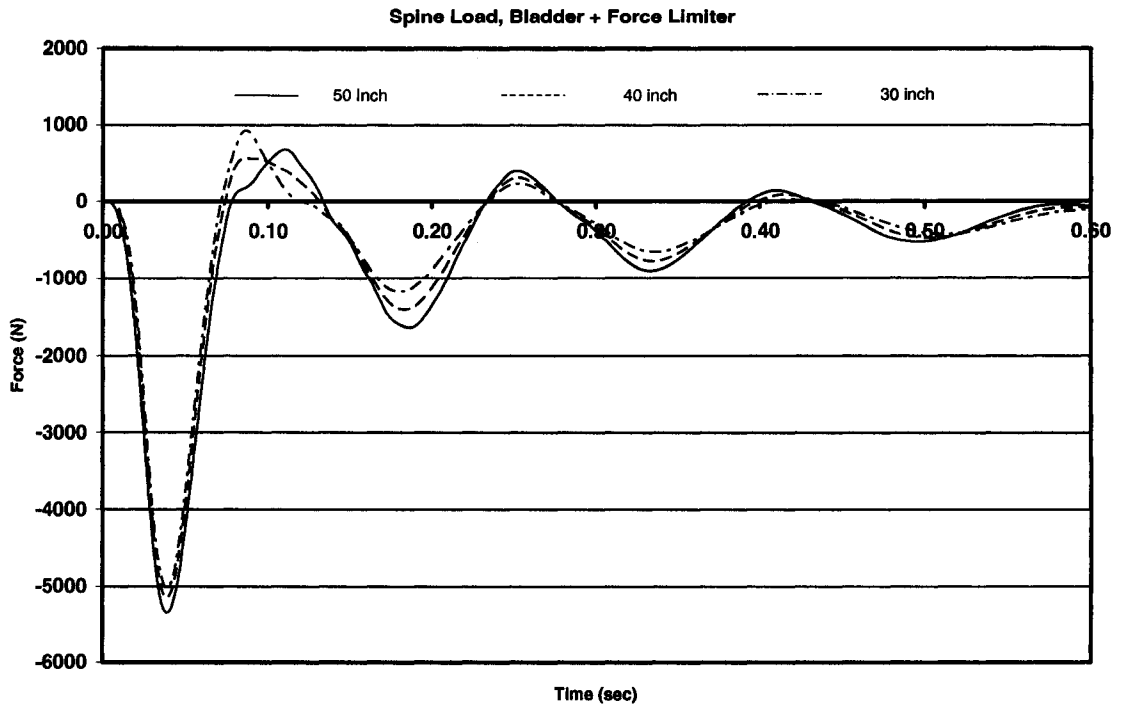


Figure A3-11 Spine Load, Bladder + Honeycomb Isolator

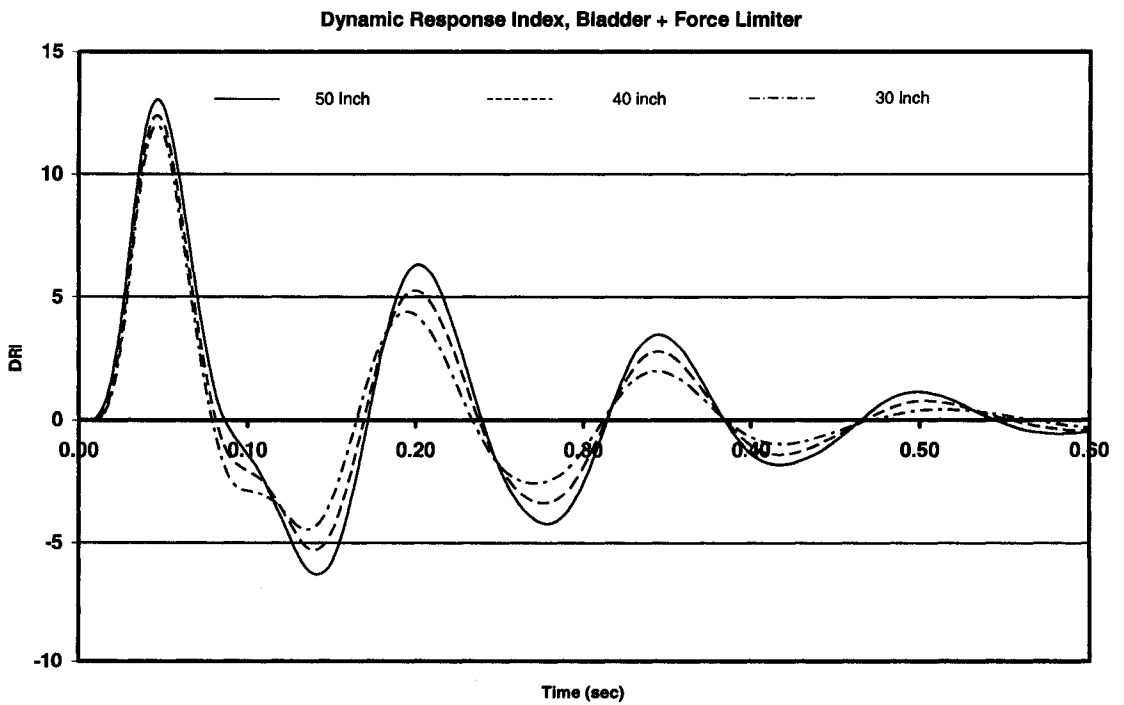
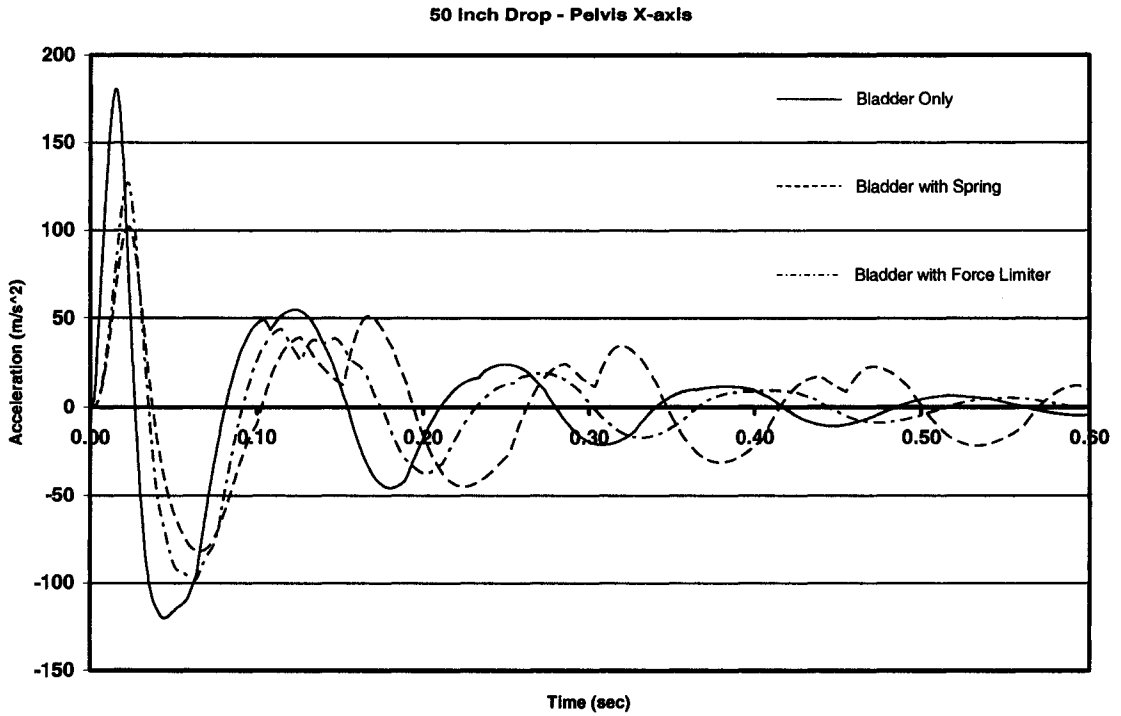


Figure A3-12 Dynamic Response Index, Bladder + Honeycomb Isolator

## APPENDIX 4

### OCCUPANT WEIGHT COMPARISON PLOTS



**Figure A4-1, Pelvis X-axis Acceleration , 80% Occupant Weight**

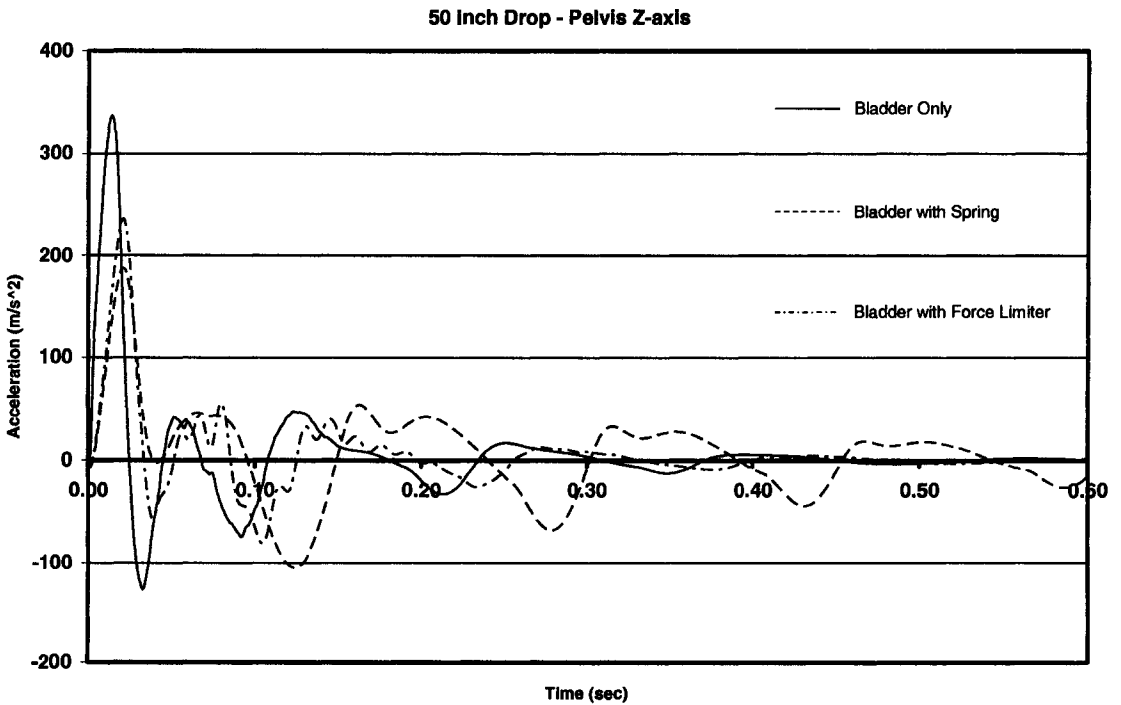


**Figure A4-2 Pelvis Z-axis Acceleration, 80% Occupant Weight**

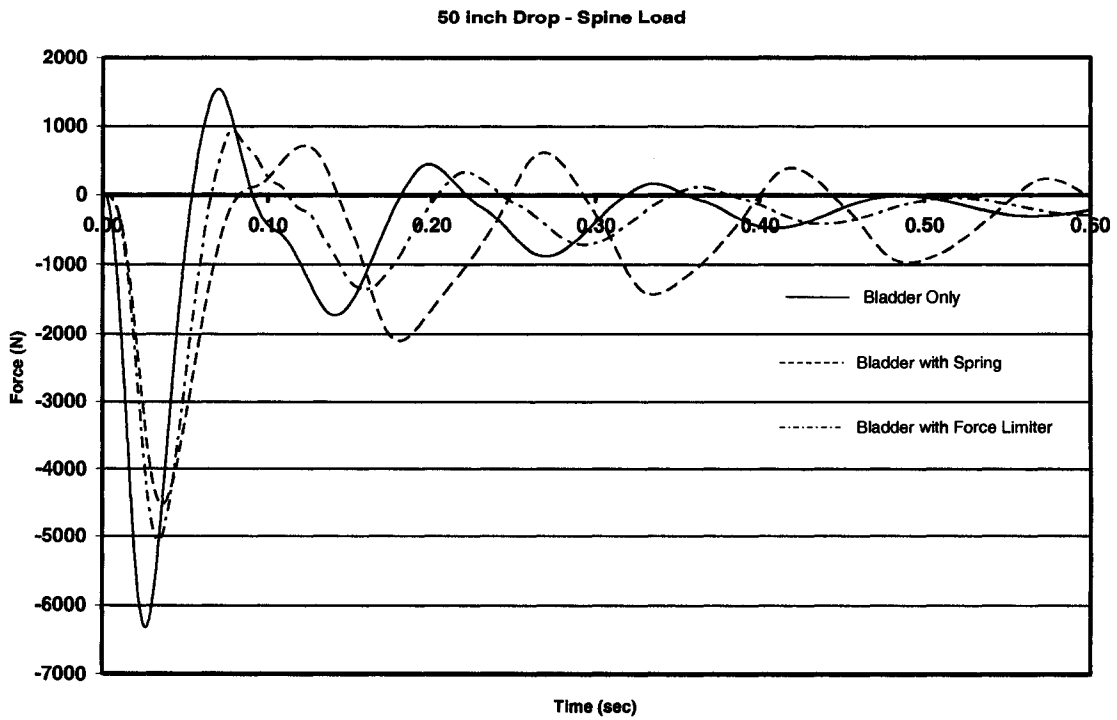


Figure A4-3 Spine Load, 80% Occupant Weight

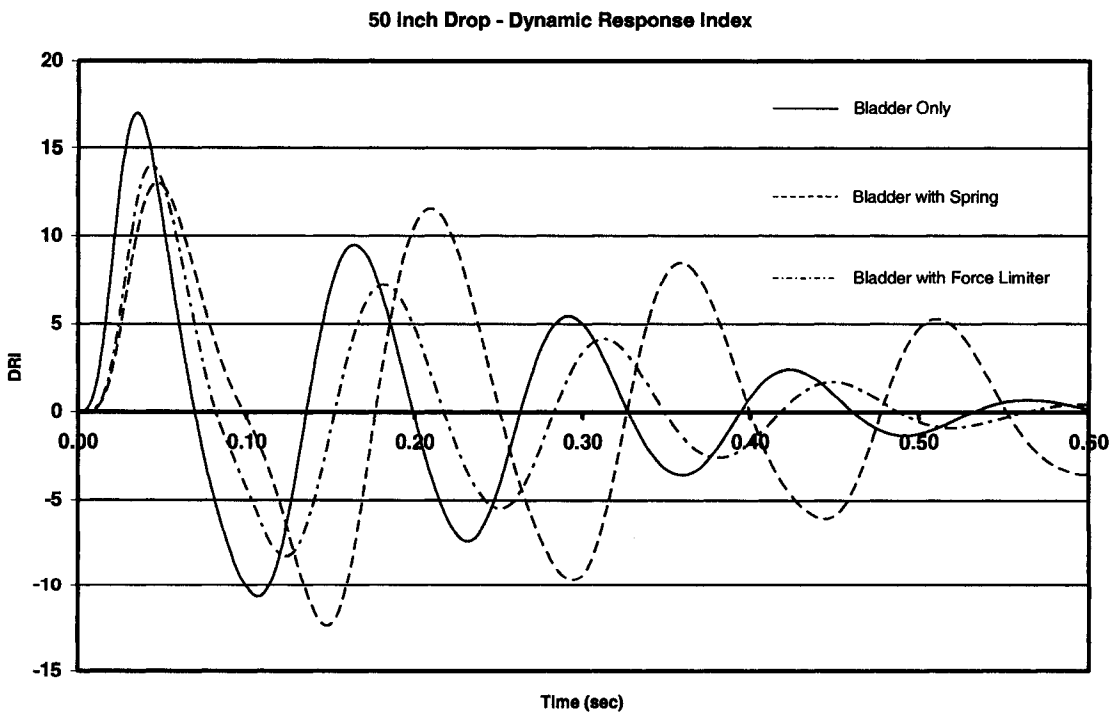
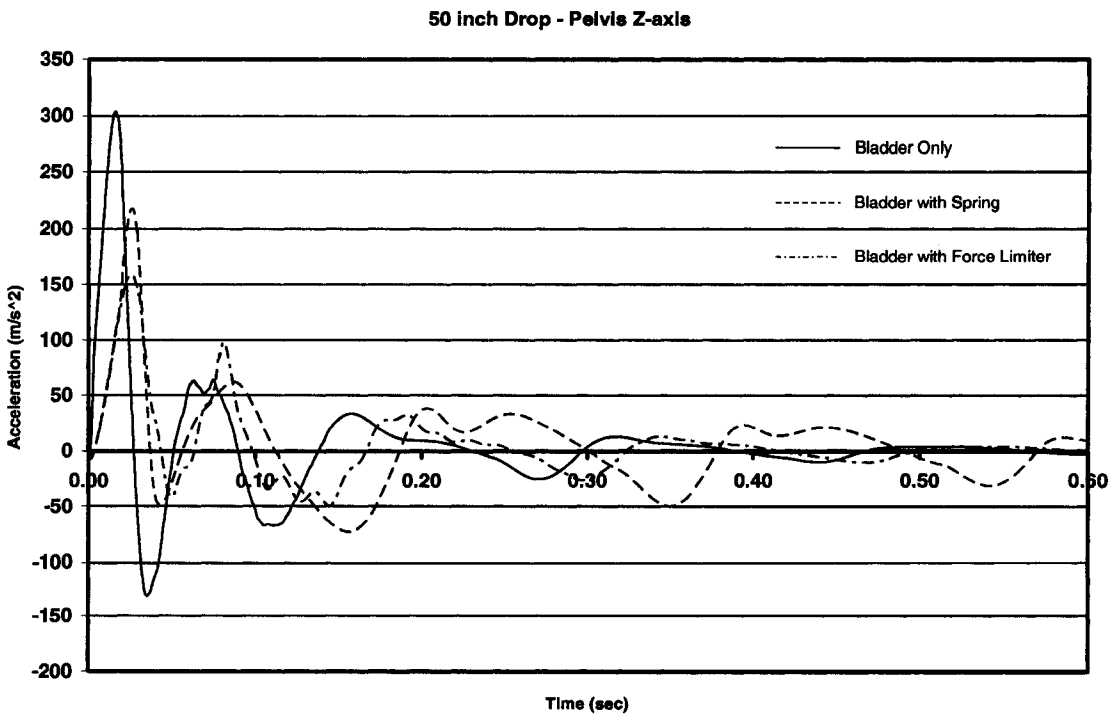
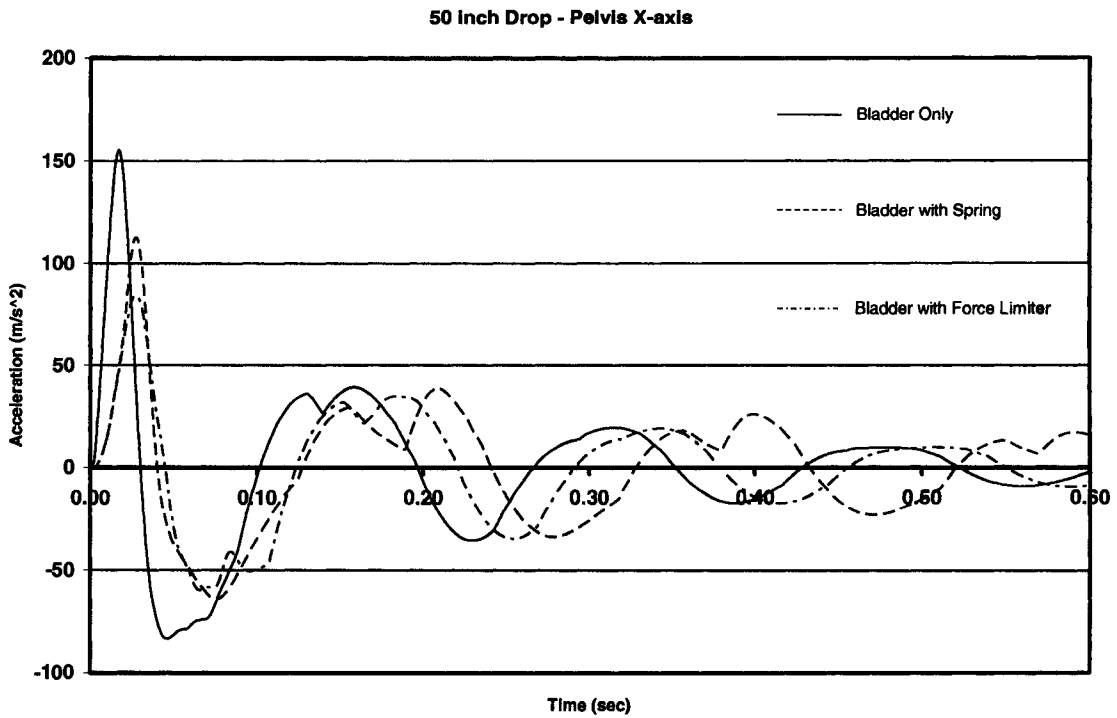
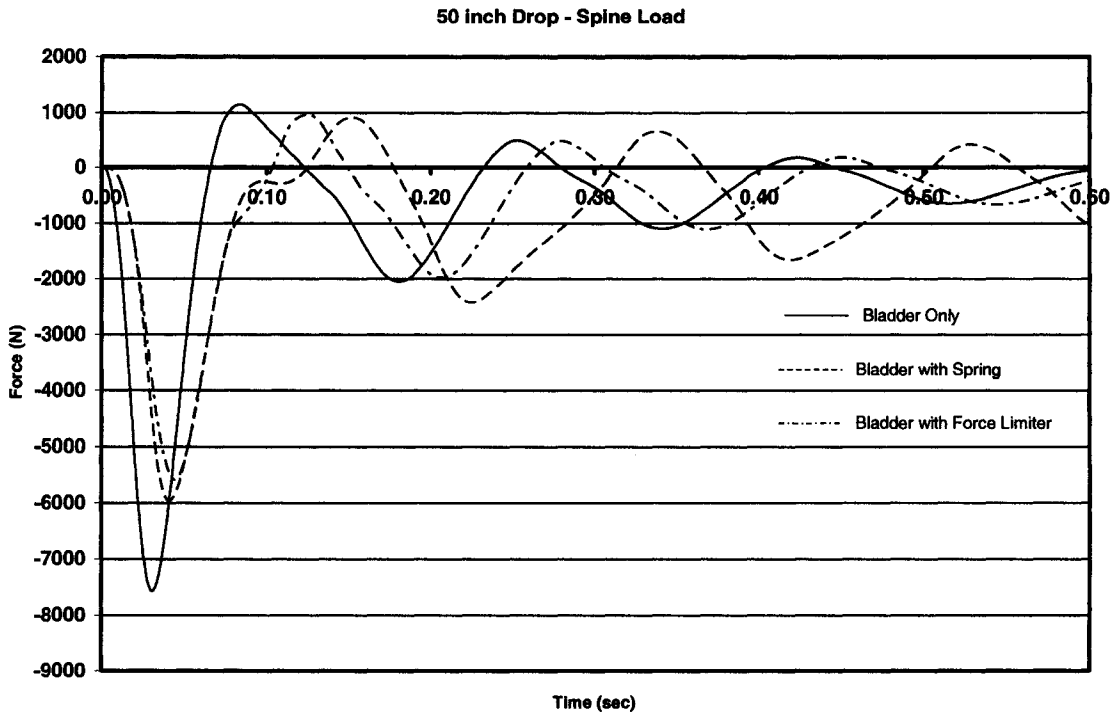
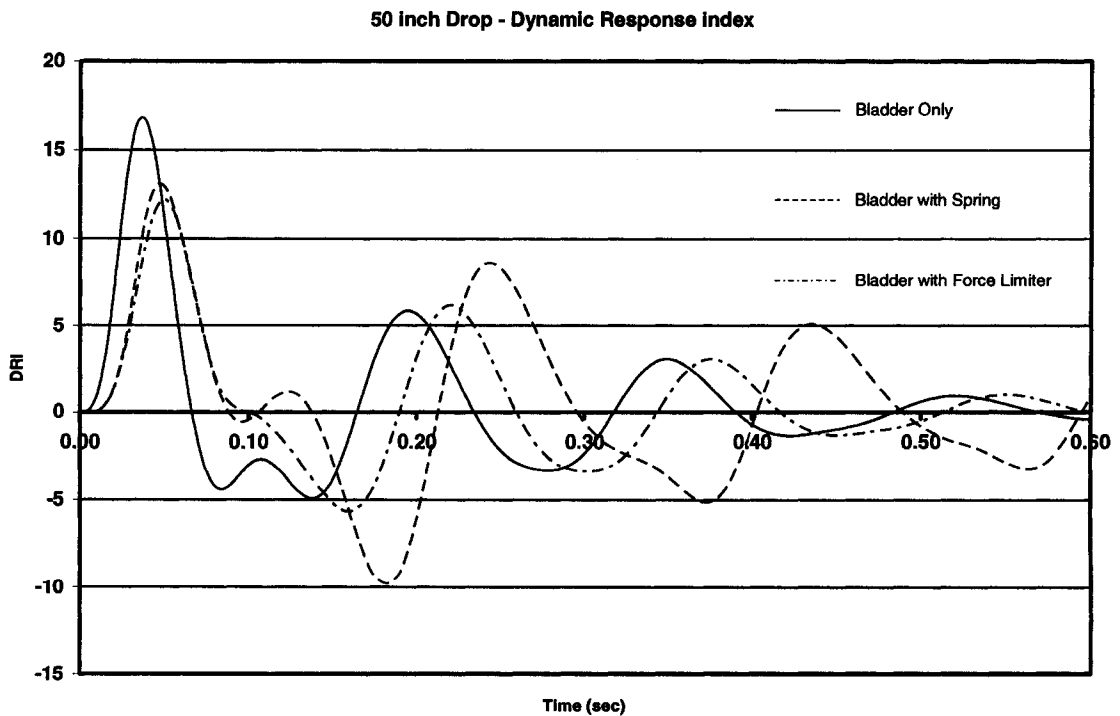


Figure A4-4 Dynamic Response Index, 80% Occupant Weight





**Figure A4-7 Spine Load, 120% Occupant Weight**



**Figure A4-8 Dynamic Response, 120% Occupant Weight**

## APPENDIX 5

### DERVIATION OF DYNAMIC RESPONSE INDEX

The Dynamic Response Index is based on the response of a single degree of freedom, mass-spring-damper system to a base input. Figure A5 is a diagram of the system.

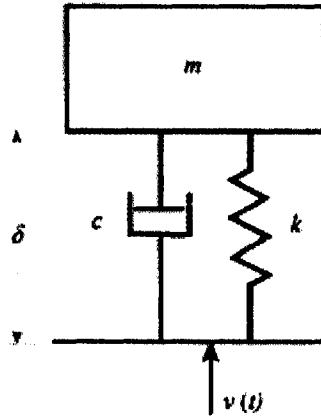


**Figure A5** Dynamic Response Index Diagram

If  $z_2$  is defined as the position of the mass and  $z_1$  is the position of the base, the force balance equation for this system can be written:

$$\sum F_z = M \ddot{z}_2 + C (\dot{z}_2 - \dot{z}_1) + K (z_2 - z_1) = 0 \quad (\text{A5-1})$$

Let  $\delta$  be equal to the difference between  $z_2$  and  $z_1$  so that:

$$\delta = (z_2 - z_1) \quad (\text{A5-2})$$

$$\dot{\delta} = (\dot{z}_2 - \dot{z}_1) \quad (\text{A5-3})$$

$$\ddot{\delta} = (\ddot{z}_2 - \ddot{z}_1) \quad (\text{A5-4})$$

Dividing Equation A5-1 by M and substituting Equations A5-2 through A5-4 gives:

$$\ddot{\delta} + \frac{C}{M} * (\dot{\delta}) + \frac{K}{M} * (\delta) = \ddot{z}_1 \quad (\text{A5-5})$$

The equations for resonant frequency and damping ratio are:

$$\omega_n = \sqrt{\frac{K}{M}} \quad (\text{A5-6})$$

$$\zeta = \frac{C}{M * 2 * \omega_n} \quad (\text{A5-7})$$

Substituting Equation A5-7 into A5-5 gives the familiar form of the DRI equation:

$$\ddot{\delta} + 2\zeta\omega_n * (\dot{\delta}) + \omega_n^2 * (\delta) = \ddot{z}_1 \quad (\text{A5-8})$$

In this equation,  $\omega_n$  is given a value of 52.9 rad/sec and  $\zeta$  is defined as 0.229.

## VITA

Graduate College  
University of Nevada, Las Vegas

Erik J. Wolf

### Home Address:

7191 Cypress Gardens Lane  
Las Vegas, Nevada 89119

### Degrees:

Bachelor of Science in Engineering, 2000  
University of Nevada, Las Vegas

Master of Science in Engineering, 2004  
University of Nevada, Las Vegas

### Publications:

Wolf, E., Reynolds, D.D., "Issues to be Considered in the Revision of ISO 10819",  
10<sup>th</sup> International Conference on Hand-Arm Vibration, 2004

Reynolds, Douglas D., Wolf, E, "Evaluation of Antivibration Glove Test Protocols  
Associated with the Revision of ISO 10819", Industrial Health, 2005, vol. 43

Dissertation Title: Development of Seat Shock Isolation Systems

### Dissertation Examination Committee:

Chairperson, Dr. Douglas Reynolds, Ph.D.  
Committee Member, Dr. Brian Landsberger, Ph.D.  
Committee Member, Dr. Brendan OToole, Ph.D.  
Committee Member, Dr. Woosoon Yim, Ph.D.  
Graduate Faculty Representative, Dr. Samaan Ladkany, Ph.D.